

Kinetic analysis of neuronal SNARE protein interactions

Dissertation
for the award of the degree
“Doctor of Philosophy (PhD)”
Division of Mathematics and Natural Sciences
of the Georg-August-Universität Göttingen

within the doctoral program Neuroscience
of the Georg-August University School of Science (GAUSS)

Submitted by
SONJA PRIBIĆEVIĆ

from
Belgrade, Serbia

Göttingen, 2021

Thesis Advisory Committee:

Prof. Dr. Reinhard Jahn

Laboratory of Neurobiology
Max Planck Institute for Biophysical Chemistry

Prof. Dr. Tobias Moser

Institute for Auditory Neuroscience & InnerEarLab
University Medical Center Göttingen

Prof. Dr. Marina Rodnina

Department of Physical Biochemistry
Max Planck Institute for Biophysical Chemistry

Extended Examination Committee:

(in alphabetical order)

Dr. Alexander Stein

Research Group Membrane Protein Biochemistry
Max Planck Institute for Biophysical Chemistry

Prof. Dr. Kai Tittmann

Department of Molecular Enzymology
Georg-August University Göttingen

Prof. Dr. Luis A. Pardo

Department of Molecular Biology of Neuronal Signals
Max Planck Institute for Experimental Medicine

Date of oral examination: 03.11.2021.

Herewith I declare, that I prepared this Doctoral Thesis, entitled "*Kinetic analysis of neuronal SNARE protein interactions*", on my own and with no other sources and aids than quoted.

Göttingen, 2021

Sonja Pribićević

Table of contents

ACKNOWLEDGEMENTS

ABSTRACT

1	INTRODUCTION	1
1.1	THE NEURON.....	1
1.2	THE SYNAPSE.....	2
1.2.1	Electrical synapse.....	2
1.2.2	Chemical synapse	3
1.3	THE PRESYNAPSE.....	4
1.3.1	The synaptic vesicle cycle.....	5
1.3.2	Factors that influence membrane fusion	6
1.4	THE SNARE PROTEINS	10
1.4.1	The neuronal SNAREs	13
1.4.1.1	Syntaxin-1.....	13
1.4.1.2	SNAP25.....	14
1.4.1.3	Synaptobrevin 2.....	16
1.5	THE MECHANISM OF THE NEURONAL SNARE ZIPPERING	17
1.5.1	Open questions	18
1.5.1.1	The molecular mechanism of SNARE assembly	18
1.5.1.2	The guidance of the SNARE assembly	19
1.5.1.3	The speed of the SNARE assembly.....	20
1.5.2	Experimental approaches for studying the SNARE assembly	22
1.6	THE AIM OF THIS PHD THESIS.....	24
2	MATERIALS AND METHODS.....	25
2.1	MATERIALS.....	25
2.1.1	Chemicals	25
2.1.2	Protein constructs.....	26
2.1.3	Buffers and media	28
2.2	METHODS.....	30
2.2.1	Methods for sample preparation.....	30
2.2.1.1	QuikChange Lightning Multi Site-Directed Mutagenesis.....	30
2.2.1.2	Midi-prep.....	33
2.2.1.3	Bacterial transformation for protein purification.....	34
2.2.1.4	Protein expression.....	34
2.2.1.5	Affinity purification	34
2.2.1.5.1	Syntaxin purification.....	35
2.2.1.6	Ion-exchange chromatography.....	36
2.2.1.7	Protein labeling.....	36
2.2.1.7.1	The fluorescent dyes	36
2.2.1.7.2	The labeling procedure	37
2.2.1.8	Size exclusion chromatography	37
2.2.1.9	SDS-PAGE and Coomassie Brilliant Blue Staining.....	38
2.2.2	Experimental methods	38
2.2.2.1	Stopped-flow experiments.....	38
2.2.2.1.1	Stopped-flow spectrophotometer.....	38

2.2.2.1.2	The settings and the general experimental procedure	39
2.2.2.1.3	Fitting of the acquired traces	40
2.2.2.2	Size exclusion experiments	40
3	RESULTS	42
3.1	PART I – INTERACTION BETWEEN COMBINATIONS OF TWO SNARE PROTEINS.....	42
3.1.1	Syntaxin and synaptobrevin	42
3.1.2	SNAP25 and synaptobrevin	44
3.1.3	Syntaxin and SNAP25	46
3.1.3.1	Syntaxin and SN1-SN2 domains of SNAP25	59
3.2	PART II - INTERACTIONS INVOLVING ALL THREE SNARE PROTEINS	60
3.2.1	SNAP25 titration	60
3.2.2	Syntaxin titration	64
3.2.3	Synaptobrevin titration	69
3.2.4	Testing for stable subcomplexes	76
3.3	SUMMARY OF THE DATA	79
3.3.1	Model 1 of the soluble SNARE complex formation	80
3.3.2	Model 2 of the soluble SNARE complex formation	81
4	DISCUSSION	83
	BIBLIOGRAPHY	88
	CURRICULUM VITAE	100

Acknowledgements

I would like to thank Prof. Dr. Reinhard Jahn for giving me an opportunity and the means to conduct the research presented in this PhD thesis. I am also very thankful for several long discussions during which I learned more about the SNARE field and biochemistry than during all of my reading sessions combined.

I would like to thank my direct supervisor Dr. Ángel Pérez-Lara for doing his best to be a good supervisor, for teaching me how to think when designing an experiment, for respecting my opinion and for creating a friendly atmosphere in which I always felt that I could say whatever was on my mind.

I would like to thank my TAC members Prof. Dr. Tobias Moser and Prof. Dr. Marina Rodnina for listening to the progress of my thesis and always offering useful advice. I would additionally like to thank Prof. Dr. Marina Rodnina for meeting with me to discuss kinetics whenever I asked for it, and Dr. Evan Mercier for introducing me to transient kinetics, teaching me how to properly use the KinTek software and for kinetics discussions.

I would like to thank the IMPRS Neuroscience office, especially Sandra Drube, for an incredible organization, for an impressive, Herculean effort to meet every student's needs, for friendliness and approachability and for making everything possible. Thank you.

I would like to express my immeasurable gratitude to Ursula Welscher-Altschäffel whose excellent technical support was instrumental in evading a complete burnout and whose kindness (and cakes ☺) could fix even the most difficult days.

I would like to thank Bekir for being the first person to patiently teach me how to work in a lab and for showing me that doing experiments is actually exciting and fun. It was this experience that persuaded me to stay and complete the PhD part of the IMPRS Neuroscience program. I would also like to thank Dr. Hiroshi Kawabe for giving me an opportunity to do a Master's thesis in his group and for writing an excellent recommendation letter (so I've been told) that convinced Prof. Dr. Jahn to offer me a PhD position.

I would like to thank Dr. Predrag Vujovic for his inspiring lectures that used to always revive my interest in science and remind me how amazing biology is, and for simply being a good, decent person that are so rarely found at Belgrade's Faculty for Biology.

In order to love your work, two conditions need to be met: the work needs to be interesting and, more importantly, you need to be surrounded by good people. I would therefore like to thank: Brigitte Barg-Kues, for making sure that the lab runs smoothly; Heike Löffler, for maintaining a steady supply of media and clean lab equipment; Peter Mienkus, for fixing the broken essentials, including the coffee machine and keeping the liquid nitrogen tank full; Dr. Hans Dieter Schmitt for his friendliness and willingness to help; Marcelo, for keeping the party going. I would also like to thank lab ex-members Agata, for sharing with me her encyclopedic knowledge of the synapse, Vedran and Claudia for always interesting

on-corridor and lunch conversations, for their scientific input and for being the glue that used to unify the labs of the first floor of Tower 6.

No matter how good a day gets, it can always be improved when shared with friends. On this note, I would like to thank my lab mates Rashi, Linda, Delane and my lab-and-building neighbor Katarina, for getting into the PhD boat with me, for countless conversations and scientific discussions over coffee (or beer), for advice that helped me look at things from a different perspective, for laughs and friendship that made this experience better in every sense. I would like to thank my friends from Serbia, Milica and Tamara, for their support and proving that distance is not important when the friendship is true.

I would like to thank my grumpy Alejandro, for always being there, for putting up with me on bad days, for laughing with me the rest of the days, for listening (or at least pretending to listen) to my problems and providing comfort and support.

Lastly, I would like to thank my parents, Lidija and Miodrag, for their unconditional love and support, for letting me choose my future and making me the person I am today. Finally, to my brother Ivan: thank you for everything, you are my best friend, my confidant, my mentor. It was awesome growing up with you and I am very lucky to have you in my life.

Abstract

When an action potential arrives at the axon terminal, it causes a local and transient increase in the Ca^{2+} concentration that starts a cascade of molecular interactions eventually leading to the fusion of synaptic vesicles with the plasma membrane. The key proteins in this process – syntaxin-1A, SNAP25 and synaptobrevin 2 – assemble into a SNARE complex that directly drives the membrane fusion. The interaction of the SNARE proteins and mechanism by which this interaction mediates membrane fusion is intensively investigated. Despite numerous studies, the answers to the core questions regarding the molecular mechanism, the guidance and the speed of SNARE complex formation remain unclear. In this work, I address one of these core questions, namely, the molecular mechanism of SNARE assembly as it represents a fundamental problem that underlies the understanding of any other process regarding SNARE-mediated fusion. Using purified, soluble SNARE proteins and kinetic measurements under different conditions, I identified some of the most likely intermediates of the SNARE assembly reaction and estimated the rate constants of their formation. Accordingly, I confirmed that the syntaxin-1A-SNAP25 interaction represents the first of the SNARE complex assembly reaction. Size exclusion chromatography experiments provided further details on the possible intermediates by showing that stable complexes can form between syntaxin-1A, synaptobrevin 2 and the individual SNARE domains of SNAP25. I conclude that SNARE complex formation occurs in at least two steps, and is initiated by the interaction between syntaxin-1A and SNAP25. The results and the experimental approach developed in this work represent a backbone for elucidating the complicated interactions that control synaptic vesicle fusion.

1 INTRODUCTION

1.1 THE NEURON

The nervous system arose with the appearance of multicellularity and the need for coordinated and harmonious functioning of all the cells that comprise a multicellular organism. The nervous system integrates the information received from the environment with the proprioceptive information to produce an appropriate response in the form of physiological change or a change in motion.

The main functional unit of the nervous system is a neuron. Neurons exist in a variety of shapes and sizes (first described by Ramón y Cajal, 1888) that accompany their distinct functions inside the nervous system. Despite this variability, all neurons have the same underlying structure that encapsulates their role in the information transfer.

Neurons typically possess two types of specialized processes that emanate from the cell body (soma) – an immense number of highly branched, thin dendrites and one axon (Figure 1.1).

Dendrites function as the main input center of the neuron. Their extensive branching and the presence of small protrusions – the dendritic spines – can greatly increase the surface through which a neuron establishes contacts with the other neurons. The number of these contacts is highly variable and dynamic, and sometimes can be astounding, as in the case of Purkinje neurons of the cerebellum that have up to 100 000 contacts (Hirano, 2018).

The axon is a process specialized for signal conduction. The length of the axon can vary depending on the type of the neuron. In contrast to dendrites, the branching of the axon occurs at its very end. The branched part of the axon, or telodendrion, ends in structures called axon terminals which establish contact with other neurons or effector cells.

The flow of information in the neuron is unidirectional, from the dendrites and the cell body to the axon. The electrotonic changes in the membrane potential of the dendrites that occur in a certain time frame are summed and, under the right circumstances, result in an action potential. The action potential is a specific change in the membrane potential that originates at the initial segment of the axon and propagates along its length. The propagation of the action potential occurs without decrement from the initial segment to the axon terminal. Upon reaching the axonal terminal, the action potential causes a cascade of molecular changes that eventually lead to the transfer of information to the next cell in line.

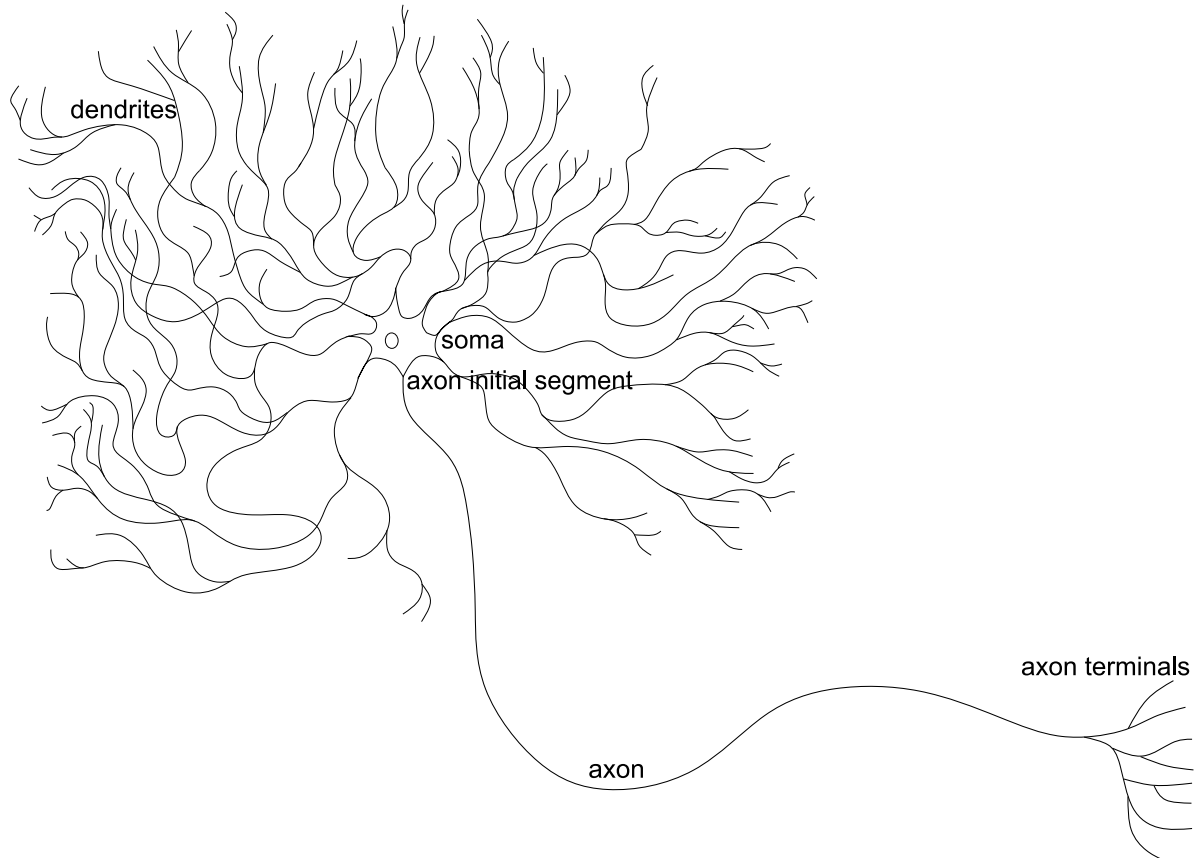


Figure 1.1. Neuron. *The illustration shows a single vertebrate motoneuron. The cell body or soma gives two types of processes: multiple, highly branched dendrites that receive information from other neurons and a long axon that sends the information further to the next cell in line.*

1.2 THE SYNAPSE

Neurotransmission is a process of information transfer between two neurons or a neuron and an effector cell. Neurotransmission occurs at specialized contact sites called synapses. There are two main types of synapses, electrical and chemical, that differ in their organization and means of action.

1.2.1 Electrical synapse

Electrical synapses were thought to be common in invertebrates and non-mammalian vertebrates, and only rarely found in mammals. Research in the last few decades showed that, although less numerous, electrical synapses are in fact widely distributed in the mammalian brain (Connors and Long, 2004; Nagy et al., 2018). The defining feature of the electrical synapse is a direct contact between neurons and continuity of their cytoplasm

that is mediated by gap junctions. This continuity allows for uninterrupted and bidirectional spread of electrotonic changes that influence neuronal excitability and lead to coordinated action potential firing (Bennett and Zukin, 2004; Pereda, 2014). Due to the structural organization of the electrical synapse, there is no possibility for signal amplification and modulation. Despite this limitation, electrical synapses are highly dynamic, plastic and are essential for the functioning of the nervous system (O'Brien, 2019).

1.2.2 Chemical synapse

Chemical synapses can have an array of different morphologies (Cowan et al., 2003). There are, however, two characteristic properties that are common for all of them: the lack of direct contact between the communicating neurons (Figure 1.2) and, consequently, the conversion of an electrical signal into a chemical one and vice versa. Due to these properties, chemical synapses are almost strictly unidirectional and functionally asymmetrical (Cowan et al., 2003). The neuron that sends the information, the presynaptic neuron, is at the synapse morphologically different from the neuron that receives the information, the postsynaptic neuron (Figure 1.2). The presynapse can be identified by the presence of neurotransmitter filled synaptic vesicles which, upon the arrival of the action potential, fuse with the plasma membrane (conversion from the electrical to the chemical signal). In contrast, the postsynapse contains high number of neurotransmitter binding receptors that, after binding, cause electrotonic changes in the postsynaptic neuron (conversion from the chemical to the electrical signal).

The presynaptic neuron is separated from the postsynaptic neuron by the synaptic cleft. The average width of the synaptic cleft in the central nervous system is 20 nm, but it varies in different types of synapses (Eccles and Jaeger, 1957). The synaptic cleft is a space filled with proteins whose role is to position pre- and postsynapse in the right orientation and maintain uniform distance (Biederer et al., 2017). The volume of the synaptic cleft is $0,5-8 \times 10^{-3} \mu\text{m}^3$, which allows for an efficient diffusion of neurotransmitters (Harris and Sultan, 1995). Additionally, the presence of enzymes that cleave neurotransmitters, e.g. acetylcholinesterase, changes the duration of neurotransmitter stimulation, giving the synaptic cleft an active role in neurotransmission (Soreq and Seidman, 2001).

As a consequence of their mechanism of action, chemical synapses are markedly slower than electrical synapses (Pereda, 2014). However, when considering the possibility for amplification, modulation and adaptation of the synaptic signal, chemical synapses far surpass the abilities of electrical synapses. These features and the abundance of chemical synapses lead to their intensive studying and better understanding compared to electrical synapses.

Given that this work focuses on the events that cause the synaptic vesicles to fuse with the plasma membrane, the following sections will address the presynapse in more detail.

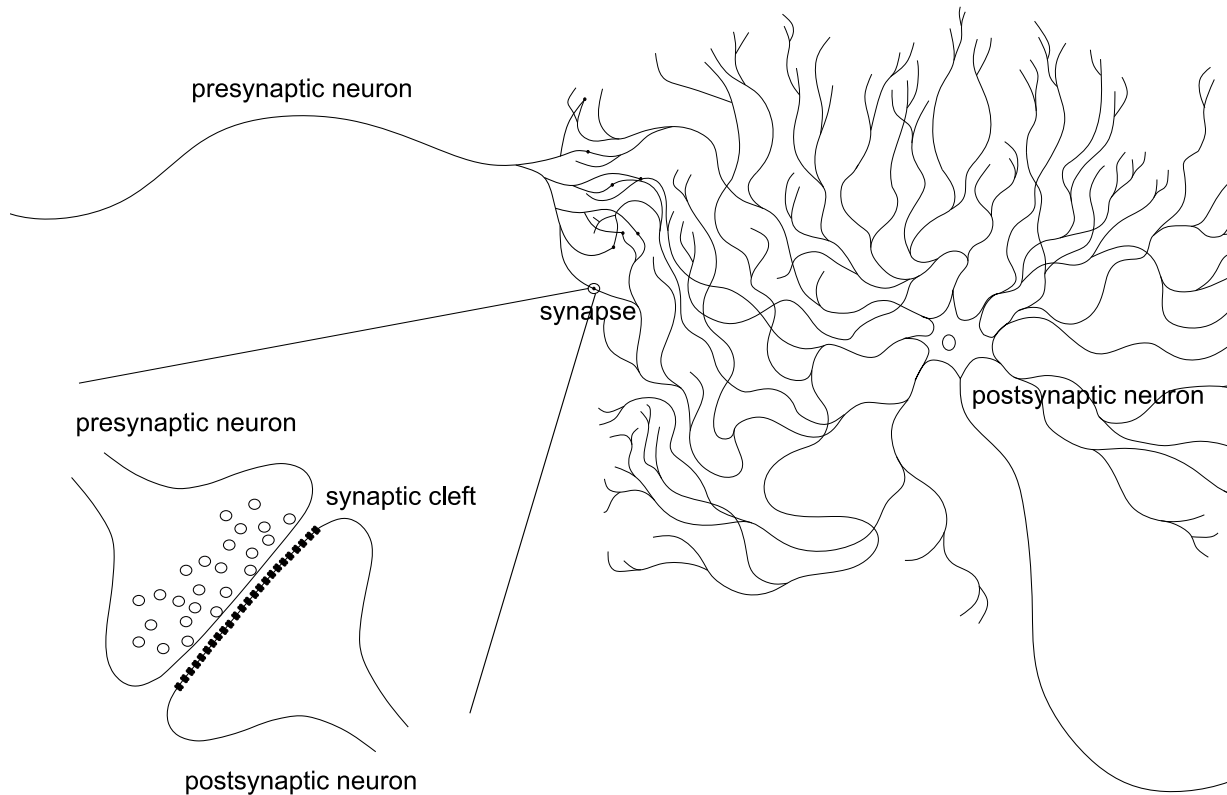


Figure 1.2. Chemical synapse. The axon of the presynaptic neuron branches near its end and forms synapses with the dendrites of the postsynaptic neuron. The enlarged view of the synapse shows an axon terminal of a presynaptic and a dendritic spine of a postsynaptic neuron in close apposition. The presynaptic neuron contains a large number of neurotransmitter-filled synaptic vesicles. The postsynaptic neuron shows an abundant presence of neurotransmitter binding channels on its surface. The presynapse and the postsynapse are separated by the synaptic cleft.

1.3 THE PRESYNAPSE

The most characteristic feature of the presynapse is the presence of numerous synaptic vesicles. Synaptic vesicles are rounded organelles with an average diameter of ~40 nm (Harris and Sultan, 1995; Takamori et al., 2006). The function of synaptic vesicles is to concentrate a large number of neurotransmitter molecules and to release them in a controlled manner into the synaptic cleft.

1.3.1 The synaptic vesicle cycle

When an action potential reaches the axon terminal, voltage dependent Ca^{2+} channels open. Due to the large difference in the concentration of Ca^{2+} ions between the outside and the inside of the neuron, the opening of the voltage gated Ca^{2+} channels causes Ca^{2+} influx (Berridge et al., 2000; Catterall, 2011). Inside the cell, Ca^{2+} ions have a role of signaling molecules that put in motion protein interactions that lead to the fusion of synaptic vesicles with the plasma membrane and the subsequent release of the neurotransmitter molecules into the synaptic cleft. The neurotransmitter release occurs in the restricted area of the presynapse dubbed the active zone (Figure 1.3). This electron dense area contains large number of proteins whose role is to concentrate synaptic vesicles, dock them to the plasma membrane, prime them for fusion and execute the fusion process itself (Südhof, 2012).

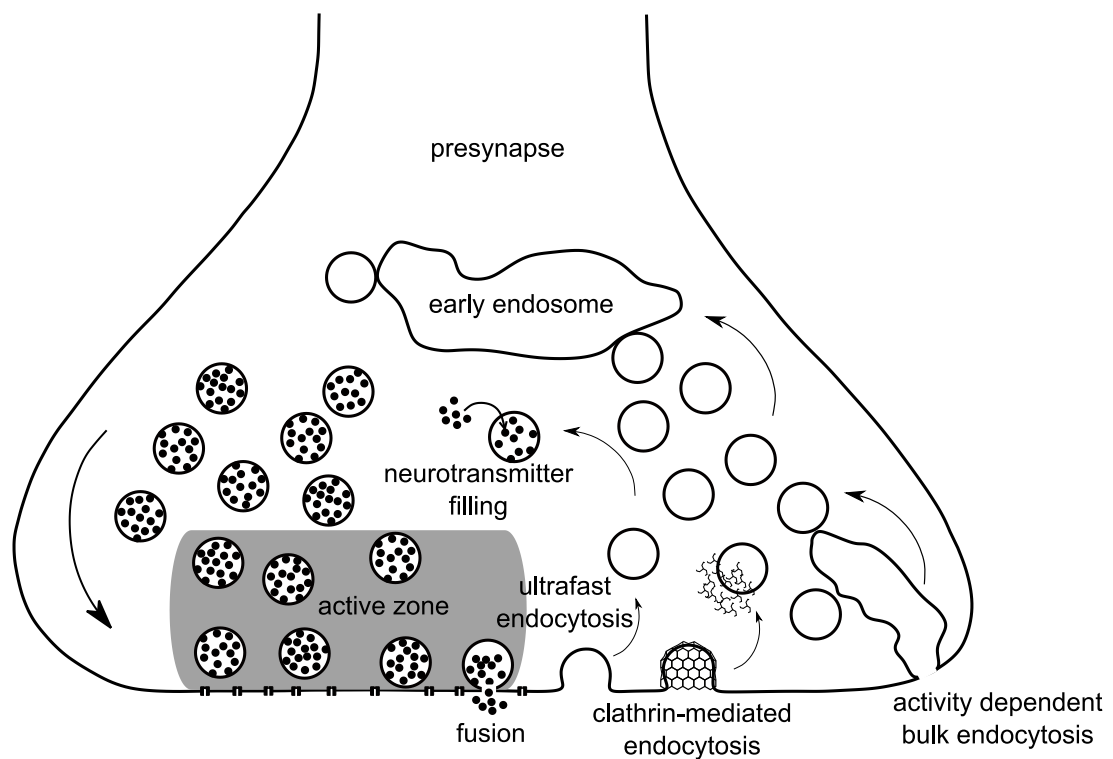


Figure 1.3. Synaptic vesicle cycle. Neurotransmitter loaded synaptic vesicles enter the active zone (gray square). The active zone contains a multitude of proteins that concentrate and prepare synaptic vesicles for fusion, as well as execute the fusion process itself. Membranes and proteins that end up at the presynaptic plasma membrane after synaptic vesicle fusion get endocytosed by clathrin-mediated, ultrafast or activity dependent bulk endocytosis. The retrieved vesicles get refilled with neurotransmitter molecules and again participate in the fusion reaction.

With the fusion, the plasma membrane expands. To maintain the size and functionality of the synapse, a compensatory endocytotic process re-forms the vesicles and retrieves lipids and proteins from the plasma membrane (Saheki and De Camilli, 2012). There is more than one pathway for the local regeneration of synaptic vesicles. The clathrin-mediated pathway requires formation of the clathrin coat around the budding vesicle that gets disassembled shortly after fission (Kaksonen and Roux, 2018). This process is considered to be slow and unable to adequately respond to the increased rate of vesicle fusion during prolonged stimulation (Mueller et al., 2004). Vesicle retrieval during high intensity fusion is thought to be mediated by fast (activity dependent bulk endocytosis) and ultrafast endocytosis that are both clathrin independent (Watanabe and Boucrot, 2017). The retrieved vesicles get either directly refilled with the neurotransmitter molecules (Murthy and Stevens, 1998), or fuse with the early endosome from which new synaptic vesicles originate (Watanabe et al., 2014). After refilling, the vesicles again participate in the fusion event. This process of synaptic vesicle fusion and recycling is called the synaptic vesicle cycle (Figure 1.3).

Due to the high level of exo- and endocytosis, the presynaptic plasma membrane is specialized to continuously undergo membrane remodeling. Membrane fusion and fission represent the basis of neuronal communication and are, therefore, very tightly controlled.

1.3.2 Factors that influence membrane fusion

The joining of the two lipid bilayers is influenced by factors such as charge, curvature, lipid composition, and by specific proteins present on the membrane surface. There are several recognized stages that characterize fusion: (i) docking; (ii) dehydration; (iii) hemifusion stalk formation; (iv) pore opening and expansion (Hernández and Podbilewicz, 2017; Witkowska et al., 2020, 2021; Yavuz et al., 2018). These stages are accompanied by corresponding energy barriers that need to be overcome in order for fusion to occur. Where exactly the energy barriers lie and how high they are, is still a matter of debate.

Docking refers to the anchoring of the two membranes at a close distance (Verhage and Sørensen, 2008). The distance at which the two membranes are considered to be docked is not firmly established as authors take different values (ranging anywhere from 0 nm to 50 nm) justified by different sample preparation and definitions of docking (Broadie et al., 1995; Hess et al., 1993; Imig et al., 2014; Richmond et al., 1999). Generally, docking is considered to go through two consecutive stages called loose and tight docking. Loosely docked state entails some distance between the two membranes and is reversible, while irreversible tight docking refers to a state in which the membranes are in direct contact (Witkowska et al., 2021; Yavuz et al., 2018).

For two apposing membranes to approach each other, the water molecules that lay between them need to be displaced. At considerably short distances, the polar heads of the two

Introduction

membranes are separated by a very thin layer of water. The phospholipid polar heads form hydrogen bonds with these water molecules that resist displacement. This leads to the generation of a strong repulsive force called the hydration barrier (Leikin et al., 1993). The hydration barrier can be reduced with different chemicals (such as ethylene glycol) and multivalent ions (such as Ca^{2+}) that dehydrate the phospholipid heads (Mondal Roy and Sarkar, 2011).

According to the widely accepted model, membrane fusion proceeds through a stalk intermediate (Markin et al., 1984). Local perturbations in the closely positioned membranes lead to the joining of the proximal monolayers into an hour-glass shaped stalk (Figure 1.4). The stalk expands to form a hemifusion diaphragm and, finally, the fusion of the distal monolayers forms a fusion pore (Chernomordik and Kozlov, 2008).

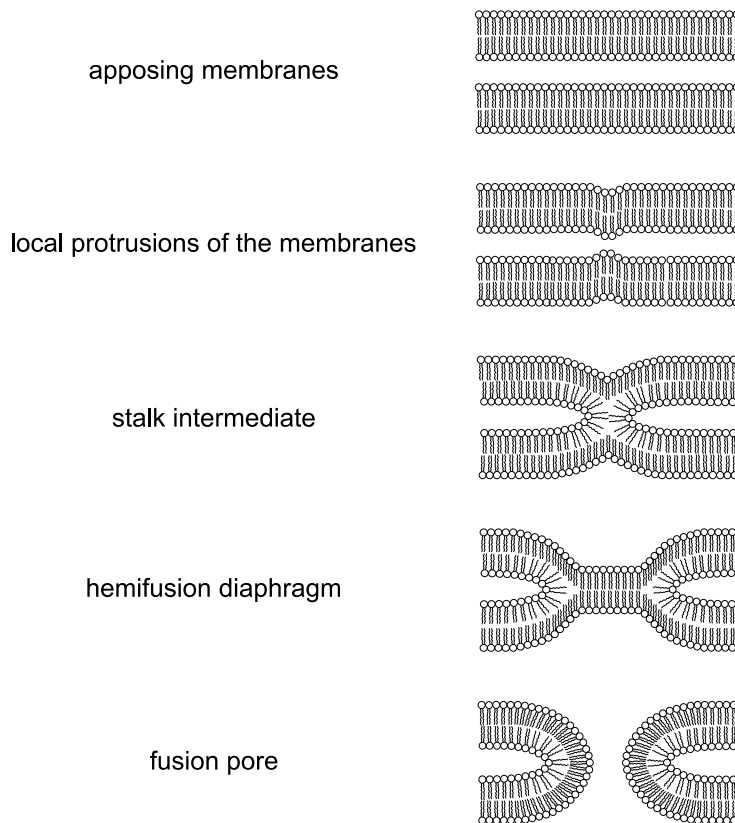


Figure 1.4. The stalk model of membrane fusion. As the two apposing membranes approach each other, local protrusions lead to the fusion of the proximal monolayers and formation of the stalk intermediate. The stalk intermediate expands to form a hemifusion diaphragm which progresses to the fusion pore with the fusion of the distal monolayers. This Figure was based on Figure 1 from (Chernomordik et al., 1985) and Figure 1 from (Chernomordik and Kozlov, 2008).

The bending of the membranes, necessary for the stalk and the fusion pore formation, is influenced by their lipid composition and correlates with their ability to form structures different from the bilayer structure (Binotti et al., 2021; Hamm and Kozlov, 1998).

Phospholipid molecules can have different shapes that are determined by the relative size of their polar head and hydrophobic tail (Sprong et al., 2001). The shape of lipids affects their packaging. If that shape is conical or of an inverted cone, the membrane will spontaneously tend to curve away from (negative spontaneous curvature) or towards (positive spontaneous curvature) the aqueous solution, respectively (Figure 1.5a,c). If the lipid molecules are cylindrical, the membrane will tend to stay flat, or have a slightly negative spontaneous curvature (Chernomordik and Kozlov, 2003) (Figure 1.5b). Membranes contain various types of lipids and this variety affects the spontaneous curvature and bending elasticity of the membrane, which consequently affects their ability to support the high curvature required for the stalk and pore formation.

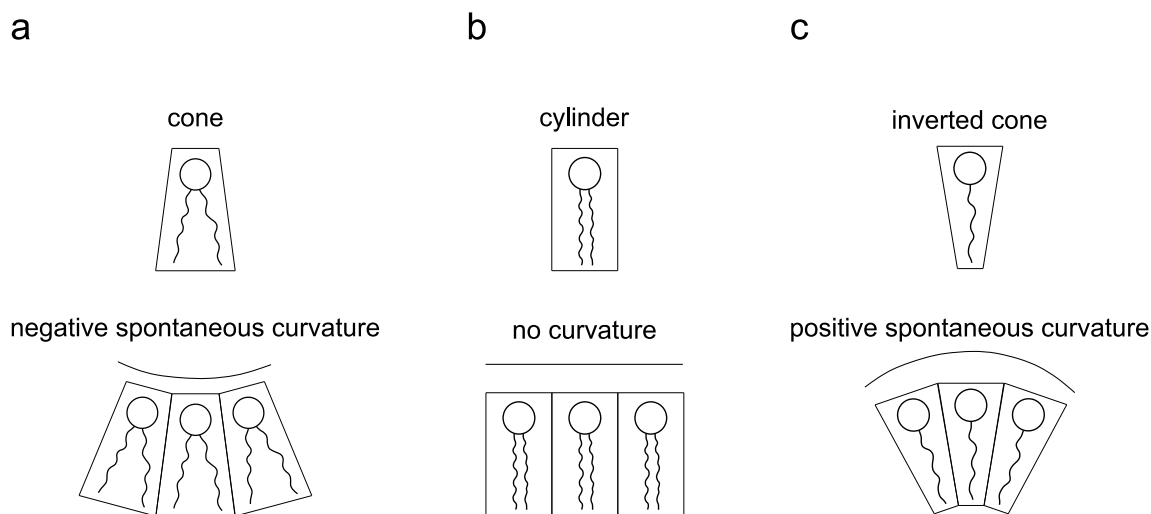


Figure 1.5. The shape of lipid molecules. Lipid molecules can have different shapes that are determined by the relative size of their polar head and hydrophobic tail. The shape of the lipid molecules affects their packaging into membranes. Membranes composed of lipid molecules that have a conical shape will tend to curve away from the aqueous solution and produce negative spontaneous curvature (**a**). Cylindrical lipids give planar membranes (**b**), while lipids that have the shape of an inverted cone will make membranes that tend to curve towards the aqueous solution and cause positive spontaneous curvature (**c**). This Figure was based on Figure 5 from (Sprong et al., 2001) and Figure 1b from (Chernomordik and Kozlov, 2008).

Although preceding the membrane fusion, the formation of the stalk does not guarantee it. Depending on the value for spontaneous curvature of the interacting monolayers, the stalk can either expand and lead to the formation of the hemifusion diaphragm or it can retract and reestablish the independence of the two membranes (Leikin et al., 1987).

The original estimations for the energy of the membrane fusion settled at ~ 40 $k_B T$ (Kozlovsky and Kozlov, 2002). This value was obtained for uncharged, purely lipid membranes with the assumption that high energy is required for the bending of the membrane that is generated by the formation of the stalk. The estimations did not consider the versatility of lipids in the membrane and their mobility. Membranes can respond to bending by positioning the lipids with negative spontaneous curvature at the neck of the stalk stabilizing it. Furthermore, it was shown that in the dehydrating condition, membranes made only of lipids with negative spontaneous curvature readily form stalks that are in fact very stable (Yang and Huang, 2002). This experimental observation confirmed the existence of the stalk intermediate, but placed it at the bottom of the energy landscape for fusion, in contrast to what was previously assumed.

Phospholipids that form biological membranes are in many cases negatively charged leading to the overall negative charge of the membrane. This negative charge opposes approaching of the two apposed membranes and, in addition to the hydration barrier, limits the initial distance between the membranes to an estimated 10-12 nm (Chernomordik and Kozlov, 2003). Compared to 2-3 nm for uncharged membranes, biological membranes most likely require higher energy investment than the calculated ~ 40 $k_B T$ making the spontaneous fusion a highly unlikely event.

In contrast to model membranes, biological membranes are not made only of lipids, but also contain a high number of proteins. The spatial organization of the membrane proteins is mediated by electrostatic and hydrophobic protein-protein and protein-lipid interactions (Bernardino de la Serna et al., 2016). Additionally, the position of the transmembrane proteins is determined by the length of their transmembrane domain that needs to fit the thickness of the hydrophobic core of the membrane (Milovanovic et al., 2015). Transmembrane and membrane associated proteins perform diverse functions. When it comes to fusion, proteins can influence the fusogenic properties of the membrane indirectly, by rearranging the lipid composition, or directly, by bringing apposing membranes closer together and generating force that introduces curvature, destabilizes membranes and promotes fusion (Kozlov et al., 2010).

1.4 THE SNARE PROTEINS

Identification of proteins involved in the neurotransmitter release was made possible by the genetic screens (Brenner, 1974; Novick et al., 1980) and development of cell-free *in vitro* fusion system (Balch et al., 1984). These experiments allowed for the discovery of the active zone SNARE (soluble *N*-ethylmaleimide-sensitive factor attachment protein receptor) proteins as sufficient and necessary for driving synaptic vesicle fusion (Weber et al., 1998).

SNARE proteins were first identified in the 1980's in the genetic screening experiments in *Saccharomyces cerevisiae* (Novick et al., 1980). In humans, they make up a superfamily of 36 small proteins whose role is to mediate vesicle fusion in the secretory pathways (Jahn and Scheller, 2006).

The majority of SNARE proteins are transmembrane proteins that contain a single transmembrane domain at their C-terminus. The exceptions that do not contain a transmembrane domain, such as SNAP25 (synaptosome-associated protein of 25 kDa), are docked to the membrane by attachment of acyl-chains. Some SNARE proteins have additional N-terminal α -helical domains (Dietrich et al., 2003).

The defining property of the SNARE proteins is an evolutionary conserved stretch of 60-70 amino acids called the SNARE domain that is connected to the transmembrane domain via flexible linker. The most characteristic feature of the SNARE domain is the repetition of hydrophobic residues in a heptad pattern. When unbound, the SNARE domain is unstructured. During binding, the SNARE domain folds into an α -helix in a way that positions all of the repeated hydrophobic residues on one side. This layer of hydrophobic residues represents interaction surfaces that lead to the formation of a parallel, intertwined four-helix bundle called the SNARE complex (Antonin et al., 2002).

The interacting residues at the center of the SNARE complex form 16 layers that are labeled with numbers from -7 to +8 (Figure 1.6a). All of the amino acids of the interacting layers are hydrophobic, except for the 0th layer amino acids that are hydrophilic and made up of 3 glutamine (Q) and one arginine (R) residues (Figure 1.6b). Based on the amino acid present at the 0th layer and the position they occupy in the SNARE complex, the SNARE proteins are classified into 4 groups: Qa, Qb, Qc and R SNAREs (Fasshauer et al., 1998a).

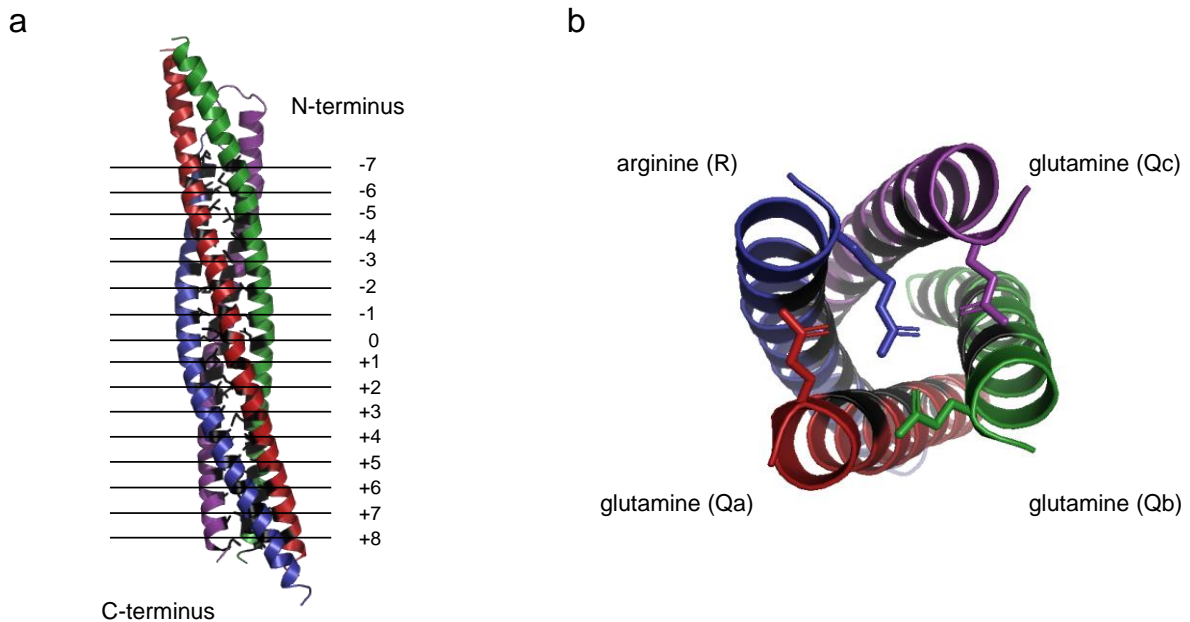


Figure 1.6. Interaction layers of the SNARE complex. The crystal structure of the neuronal core SNARE complex is plotted as an example for the coiled-coil bundle and shows four parallel, intertwined α -helices. The helices belong to the SNARE domain of Qa (red), Qb (green), Qc (purple) and R (blue) SNARE proteins. Interacting amino acids (black) form 16 layers that are indicated by 16 horizontal lines and labeled with numbers from N-terminal -7 to C-terminal +8 (a). Cross section of the four-helix bundle at the 0th layer shows the only hydrophilic layer of the SNARE core complex made up of three glutamines (Qa, Qb and Qc) and one arginine (R) that represents basis for QR-classification of SNARE proteins (b). Data from (Sutton et al., 1998) was used for construction of PyMol plots.

To be able to mediate the fusion, the set of interacting SNARE proteins needs to be in *trans*, meaning that they have to be distributed between the two fusing membranes (Nichols et al., 1997). The interaction starts at the N-terminus when the apposing membranes are ~ 8 nm apart, proceeds in a zipping-fashion towards the C-terminus that also extends into the transmembrane domains (Hanson et al., 1997; Li et al., 2007; Pobbati et al., 2006; Sørensen et al., 2006; Stein et al., 2009). It is thought that the SNARE proteins drive vesicle fusion by coupling the conformational change and the release of energy that accompanies the zipping to the energy required for overcoming the barriers for fusion (section 1.3.2). The most accepted model states that zippering of the SNARE proteins brings membranes very close and that the stiffness of the linker domain causes additional deformation of the lipid bilayers that makes the formation of the stalk easier and promotes fusion (Jahn and Scheller, 2006). Experiments performed with reconstituted proteoliposomes showed that an arrest of the SNARE zippering at specific points causes a comparable arrest at defined fusion intermediates, further demonstrating the contribution

of SNARE complex formation in different stages of fusion (Hernandez et al., 2012; Witkowska et al., 2020; Yavuz et al., 2018).

Once formed, the SNARE complex is very stable (Fasshauer et al., 2002). Disassembly of the SNARE complex requires the activity of the AAA+ (ATPases associated with various cellular activities) enzyme called NSF (*N*-ethylmaleimide-sensitive factor). With the help of the adaptor proteins SNAPs (soluble NSF attachment proteins) and with the expenditure of ATP, NSF unwinds the SNARE complex and releases the SNARE proteins. The free SNARE proteins, now present in the same membrane, are redistributed to their corresponding membranes from where they can drive a new round of fusion (Figure 1.7).

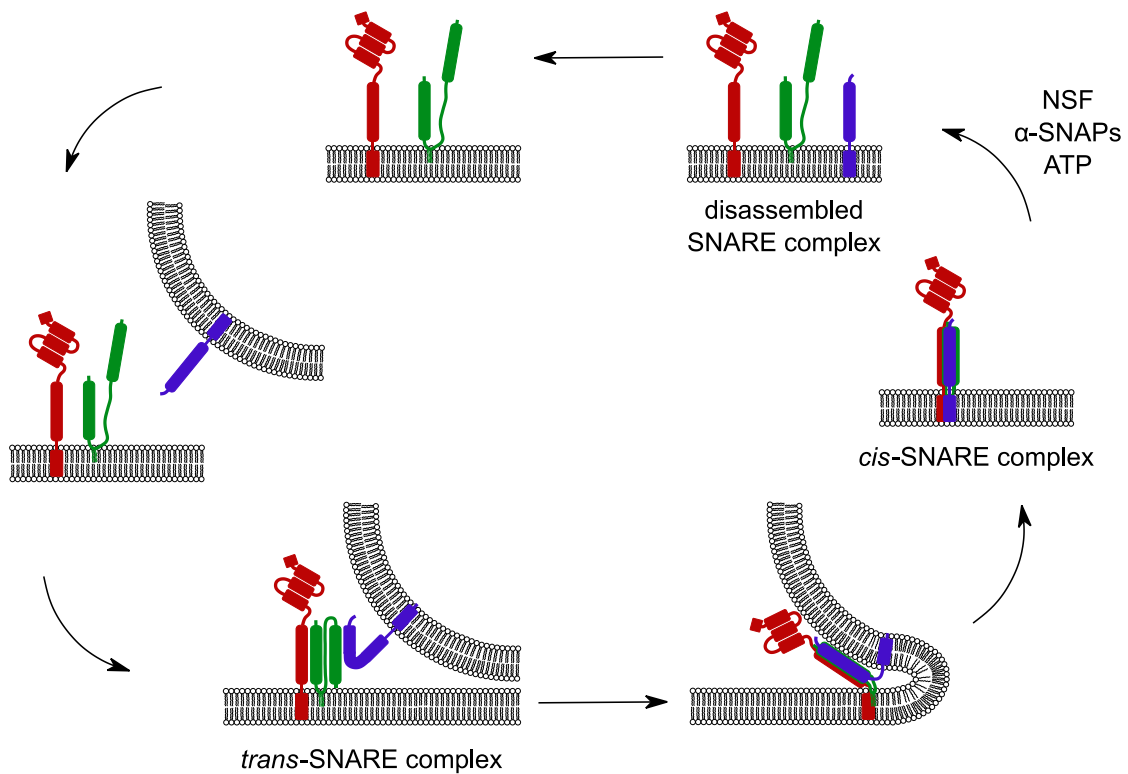


Figure 1.7. The SNARE assembly and disassembly cycle. Synaptobrevin 2 located at the synaptic vesicle interacts with the plasma membrane SNARE proteins syntaxin-1 and SNAP25. At the beginning, this interaction occurs in trans, meaning that the proteins are still in different membranes. As the zippering proceeds, the forming SNARE complex strains the membranes and pushes them upon each other leading to fusion. After fusion the completely zippered cis-SNARE complex is located in the plasma membrane. The cis-SNARE complex is disassembled by AAA+ ATPase NSF with the help of adaptor proteins, SNAPs, and with hydrolysis of ATP. The disassembled SNAREs are separated and redistributed to their corresponding membranes and participate in a new fusion cycle. This Figure was based on Figure 3 from (Jahn and Scheller, 2006).

1.4.1 The neuronal SNAREs

The three SNARE proteins that are located in the presynapse and that power synaptic vesicle fusion are syntaxin-1, SNAP25 and synaptobrevin 2 (or VAMP2 for vesicle-associated membrane protein 2).

1.4.1.1 *Syntaxin-1*

Syntaxin-1 is a transmembrane Qa SNARE protein situated at the presynaptic plasma membrane with a single pass transmembrane domain at its C-terminus. In addition to the SNARE and the transmembrane domain, syntaxin 1 has α -helical Habc domain and N-peptide.

The Habc domain and the SNARE domain of syntaxin-1 can interact, forming the so-called closed conformation of syntaxin-1. In the closed conformation, syntaxin-1 cannot interact with the other SNARE proteins and, thus, cannot participate in the SNARE complex formation (Chen et al., 2008; Dulubova et al., 1999). The open and closed conformations are in dynamic equilibrium, with the closed conformation occupying only 15-30% of the total amount of syntaxin-1 (Dawidowski and Cafiso, 2013; Margittai et al., 2003). Additionally, the Habc domain and the N-peptide are required for binding of SM (Sec1/Munc18-related) protein Munc18 (mammalian uncoordinated 18) to syntaxin-1 (Burkhardt et al., 2008). By interacting with the N-peptide, the Habc domain and the SNARE domain, Munc18-1 binds with high affinity to syntaxin-1 and stabilizes the closed conformation negatively affecting formation of the SNARE complex.

Alongside interactions between the different domains, syntaxin-1 molecules can also homooligomerize to form dimers and tetramers through their SNARE domains (Lerman et al., 2000; Margittai et al., 2001; Misura et al., 2001a). Dimers of syntaxin-1 were found to be in parallel orientation, while conflicting results were reported for tetramers. Crystal structure showed an antiparallel arrangement of the two dimers present in the tetramer with the phenylalanine at position 217 posing a steric hindrance to parallel binding (Misura et al., 2001a). In contrast, EPR analysis indicated parallel orientation of all four syntaxin-1 molecules in the tetramer (Margittai et al., 2001).

There are two isoforms of syntaxin-1 expressed in neurons, syntaxin-1A and syntaxin-1B. These two isoforms are 84% identical and are considered to be functionally redundant (Bennett et al., 1992). Consequently, the deletion of one syntaxin-1 isoform has little effect due to the compensatory effect of the second isoform. In contrast, the constitutive deletion of both isoforms is prenatally lethal (Vardar et al., 2016). Experiments using conditional double knock-out mice for syntaxin-1A/B showed that, in addition to vesicle docking, priming and fusion, syntaxin-1 has an important role in neuronal maintenance throughout neuronal lifetime (Imig et al., 2014; Vardar et al., 2016).

Syntaxin-1 molecules are not dispersed in the plasma membrane, but organized into 50-60 nm clusters with the average density of 19,6 clusters/ μm^2 (Sieber et al., 2007). Each cluster contains ~ 90 molecules of syntaxin-1. The densest part of the cluster is its center, and this density gradually decreases towards the periphery. Proteins in the cluster are in dynamic equilibrium with the freely diffusing proteins that surround the cluster (Bar-On et al., 2012; Sieber et al., 2007). This organization of syntaxin-1 is thought to be mediated by syntaxin-1 homooligomerization and by its interaction with the phosphatidyl inositol phosphates (PIPs). A stretch of positive amino acids adjacent to the transmembrane domain of syntaxin 1 interacts with negatively charged phosphates that most likely belong to PI(3,4,5) P_3 (Bogaart et al., 2013; Khuong et al., 2013). In addition to PI(3,4,5) P_3 , it was also shown that presence of syntaxin-1 clusters is stabilized by cholesterol (Lang et al., 2001).

1.4.1.2 SNAP25

SNAP25 is the founding member of the SNAP25 subfamily. An interesting feature of SNAP25 that is specific among the SNARE proteins, and shared only with the other members of SNAP25 subfamily, is the presence of two SNARE domains on one molecule (Kádková et al., 2019). The SNARE domains SN1 and SN2 belong to the Qb and Qc SNAREs, respectively, and are connected to each other via a flexible linker. The important role of the interhelical linker is the targeting and attachment to the plasma membrane since SNAP25 lacks a transmembrane domain (Gonzalo et al., 1999). Closer to the SN1 domain, the linker contains four cysteine molecules that are very closely positioned. Cysteine residues are dynamically palmitoylated in the cell by DHHC (aspartate-histidine-histidine-cysteine) palmitoyl transferases (Huang et al., 2004; Veit et al., 1996). Considering that SNAP25 is synthesized as a soluble protein and DHHP palmitoyl transferases are membrane proteins, palmitoylation requires prior association of SNAP25 to the membrane. This membrane association of the soluble SNAP25 is mediated by the basic residues in the cysteine rich domain that interact with phosphatidyl inositol phosphates, and QPARV motif adjacent to the cysteine rich region that interacts with DHHP enzymes (Gonzalo et al., 1999; Greaves et al., 2009; Weber et al., 2017). Although palmitoylation is deemed important for stable attachment of SNAP25 to the presynaptic plasma membrane, surprisingly, depalmitoylation does not cause its release (Gonzalo and Linder, 1997). It is not clear whether all of the cysteines need to be palmitoylated for SNAP25 to associate with the plasma membrane or there can exist various levels of palmitoylation with particular influence on docking, turnover and interaction kinetics with the other SNARE proteins. It has been shown, however, that the absence of cysteines or their palmitoylation slows down the fusion rate, but it does not influence the stability of the SNARE complex (Nagy et al., 2008; Washbourne et al., 2001).

The exact positions of cysteines in the linker domain depend on the isoform of SNAP25. There are two isoforms, SNAP25a and SNAP25b. The two isoforms differ in 9 amino acids

and result in SNAP25a having two additional charged amino acids on its surface (Bark, 1993). The expressed isoform is determined by alternative splicing of the exon 5. In mice, SNAP25a dominates in neurons during embryonic and early postnatal development and its level remains unchanged in the adult neurons. By contrast, the expression of SNAP25b increases approximately 40-fold postnatally and is a predominant form in the adult neurons (Bark et al., 1995). The highest increase in SNAP25b expression interestingly coincides with cortical synaptic maturation (Aghajanian and Bloom, 1967; Bark et al., 1995). It was shown in mice that replacing exon 5b, that leads to expression of SNAP25b, with exon 5a, that leads to expression of SNAP25a, causes defect in spatial learning, higher anxiety and pathological changes in *stratum lucidum* of the hippocampus (Johansson et al., 2008). The importance of this developmental switch from SNAP25a to SNAP25b in the neurons is quite interesting considering the small difference between these two isoforms and the fact that both of them are able to drive vesicle fusion. Biophysical characterization of SNAP25a and SNAP25b is largely missing, hence the influence of the isoform on the synaptic vesicle fusion and the importance of the postnatal switch is not well understood. It is important to mention that SNAP25a in mice corresponds to SNAP25b in rats and vice versa, and one needs to take caution when comparing data from different work.

Uncomplexed SNAP25 is largely unstructured. During the SNARE complex formation, α -helices form at the SNARE domains, while the linker remains unstructured and flexible (Sutton et al., 1998). Interestingly, helicity of the SNARE domains of SNAP25 increases with the increasing amount of NaCl, MgCl₂ and CaCl₂ (Fasshauer et al., 1997a). It is, however, not known if the increased helicity has any effect on the specificity or kinetics of SNAP25 interactions with the other proteins, although it was observed that in high NaCl concentration SNAP25 is able to form oligomers (Fasshauer et al., 1997a)

SNAP25 binds to syntaxin-1. This interaction has been intensively studied and proven to be truly complicated. Convincing evidence points to the formation of the 2:1 complex, in which two syntaxin molecules are bound to one SNAP25 molecule (Fasshauer and Margittai, 2004; Fasshauer et al., 1997b; Wiederhold and Fasshauer, 2009; Xiao et al., 2001). The SNARE domains of syntaxin-1 and SNAP25 in the 2:1 complex appear to be in parallel orientation, resembling the SNARE complex (Margittai et al., 2001; Xiao et al., 2001). The 2:1 complex is predominantly considered to be an off pathway that is either disassembled by NSF and α -SNAP or prevented to assemble in the first place by the activity of accessory proteins in the active zone (Baker and Hughson, 2016; Ma et al., 2013; Pobbati et al., 2006; Weber et al., 2000; Wiederhold and Fasshauer, 2009).

On the presynaptic plasma membrane SNAP25 molecules are organized in clusters that are closely positioned to syntaxin-1 clusters (Lang et al., 2001; Rickman et al., 2010). SNAP25 clusters are elliptical and the majority of them were found to cover ~28% bigger area compared to syntaxin-1 clusters (Bar-On et al., 2012). Similar to syntaxin-1, SNAP25 clusters have the highest density of proteins in the center that then gradually decreases

towards the periphery (Bar-On et al., 2012). Individual SNAP25 molecules surround the periphery of the cluster and interact with the syntaxin-1 molecules that surround the syntaxin-1 clusters (Rickman et al., 2010). It has been suggested by Rickman et al. that the clusters serve as a reserve pool of syntaxin-1 and SNAP25 from which reactive proteins isolate to form the syntaxin-SNAP25 complex (Rickman et al., 2010).

Cleavage of SNAP25 by botulinum toxins A and E effectively prevents synaptic vesicle fusion, directly demonstrating the role of SNAP25 in the neurotransmitter release (Blasi et al., 1993; Schiavo et al., 1993). In addition to synaptic vesicle fusion, it has been shown that SNAP25 knockout neurons have impaired vesicle docking (Imig et al., 2014). Furthermore, deletion of SNAP25 strongly reduces neuronal survival and arborization (Delgado-Martínez et al., 2007).

1.4.1.3 *Synaptobrevin 2*

Synaptobrevin 2 is an R-SNARE protein with a single pass transmembrane domain at its C-terminus. Synaptobrevin 2 contains one SNARE domain that is connected to the transmembrane domain via linker. Unlike syntaxin 1 and SNAP25 which are located at the plasma membrane, synaptobrevin 2 is present on the synaptic vesicle. One synaptic vesicle contains an average of ~70 synaptobrevin 2 molecules (Takamori et al., 2006).

Synaptobrevin 2 belongs to a group of intrinsically disordered proteins. As SNAP25, the SNARE domain of synaptobrevin 2 folds into α -helix during the SNARE complex formation. Synaptobrevin 2 is, however, not completely flexible along its entire cytoplasmic length, but shows a trend of increasing rigidity towards the linker domain (Lakomek et al., 2019). The linker contains basic residues that were shown to bind to negatively charged head groups of lipid molecules (Williams et al., 2009). This binding tilts synaptobrevin 2 and moves the SNARE domain towards the synaptic vesicle. The SNARE domain transiently and dynamically binds to lipids with low affinity and this interaction correlates with a change in α -helicity (Brewer et al., 2011; Ellena et al., 2009; Lakomek et al., 2019; Liang et al., 2014). Additionally, it is considered that the binding of the C-terminal part of the SNARE domain to lipids, and formation of α -helices, lowers the energy barrier for fusion by increasing the rate of SNARE complex formation and by reducing the repulsive forces between the membranes (Lakomek et al., 2019; Liang et al., 2014).

Synaptobrevin 2 is cleaved by botulinum toxins B, D, F, and by tetanus neurotoxin (Schiavo et al., 1993). Cleavage of synaptobrevin 2 causes arrest in neurotransmitter exocytosis causing flaccid or spastic paralysis in the case of botulinum or tetanus toxin, respectively (Montecucco, 1986; Schiavo, 1992). Synaptobrevin 2 knockout mice die immediately after birth and electrophysiological recordings from the hippocampal embryonic neuron cultures of these mice showed 90% reduction in the fast, Ca^{2+} induced release (Schoch et al., 2001). Moreover, analysis of synaptobrevin 2 knockout neurons by electron tomography showed

a severe reduction in the synaptic vesicle docking and 25% increase in the synaptic vesicle volume (Imig et al., 2014).

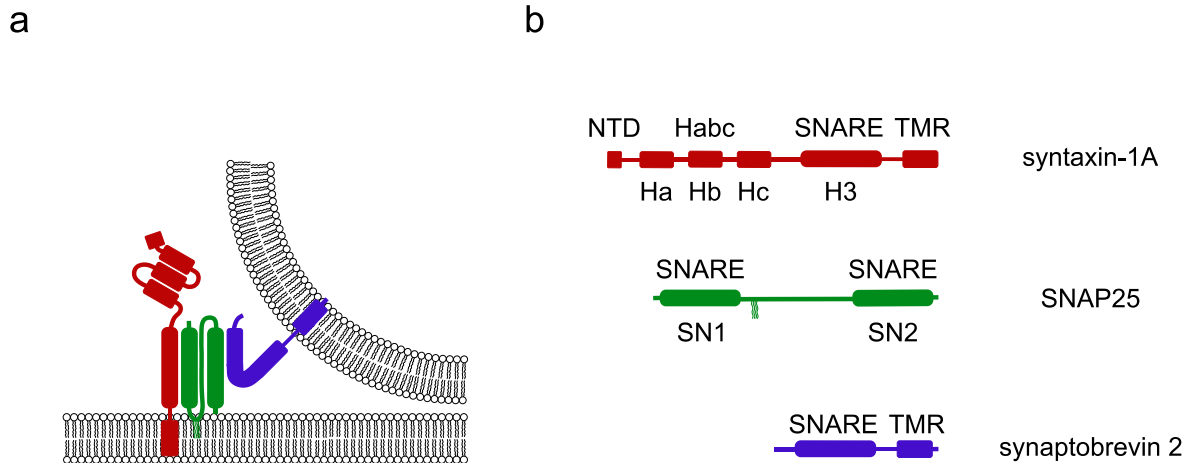


Figure 1.8. The location and the domain structure of neuronal SNARE proteins. Neuronal Q-SNARE proteins syntaxin-1 (red) and SNAP25 (green) are located on the presynaptic plasma membrane. Syntaxin is associated with the membrane via a transmembrane domain, while SNAP25 is docked through palmitoylated cysteines in the linker domain. Unlike syntaxin-1 and SNAP25, synaptobrevin 2 (blue) is an R-SNARE situated at the synaptic vesicle. The three SNARE proteins interact to form the SNARE complex and drive fusion of the synaptic vesicle to the plasma membrane (a). Syntaxin-1 and synaptobrevin 2 contribute with one SNARE domain each, while SNAP25 brings two SNARE domains, SN1 and SN2. In addition to the SNARE domain, syntaxin-1 contains α -helical Habc domain and N-terminal peptide (b). TMR-transmembrane region; NTD-N-terminal domain.

1.5 THE MECHANISM OF THE NEURONAL SNARE ZIPPERING

Understanding the mechanism of the neuronal SNARE zippering turned out to be a uniquely complicated problem.

As shortly mentioned in previous sections, SNARE proteins belong to the class of intrinsically disordered proteins and are mainly unstructured when they are outside of the SNARE complex (Snead and Eliezer, 2019). The SNARE assembly is coupled to the folding of the individual SNARE proteins into α -helix and their intertwining into a coiled-coil structure. Although the zippering appears to occur in an organized manner, the disorder of the free SNARE proteins makes the starting point of the interaction unknown. It is,

therefore, not easy to predict their motion and to precisely determine the range of molecular acrobatics that can occur during binding.

Syntaxin-1 and SNAP25 make up about 1% of total brain proteins (Walch-Solimena et al., 1995). Their abundance and the intrinsic disorder account for a certain stickiness that is evident especially for syntaxin-1 that has been reported to bind to multitude of ion channels and receptors (<https://www.uniprot.org/uniprot/Q16623.html>) (Jahn and Scheller, 2006).

The SNARE proteins also show a high level of promiscuity as SNARE proteins belonging to different pathways are able to form SNARE complexes (Yang et al., 1999). Since there is high specificity in fusion between the cargo carrying vesicles and their target site, it is evident that cell needs to employ additional mechanisms/proteins that ensure cognate SNARE interaction.

1.5.1 Open questions

There are three unanswered questions that are central to the SNARE zippering problem that concern the molecular mechanism, the guidance and the speed of the SNARE complex formation.

1.5.1.1 The molecular mechanism of SNARE assembly

The first central question that remains unanswered regards the molecular mechanism of the SNARE zippering. Namely, it is still uncertain in which order the different SNAREs enter the reaction. The predominant view is that syntaxin-1 and SNAP25 first interact to form an intermediate that creates a binding site for synaptobrevin 2. This sequence of events seems the most plausible for several reasons: (i) syntaxin-1 and SNAP25 are both located at the plasma membrane; (ii) syntaxin-1 and SNAP25 clusters in the plasma membrane are in proximity and in some places overlap; (iii) syntaxin-1 and SNAP25 bind to each other and form a stable complex; (iv) preformed syntaxin-1-SNAP25 complex reconstituted in liposomes seems to accelerate fusion with synaptobrevin 2 liposome *in vitro* (Pobbati et al., 2006). As explained in section 1.4.1.2, SNAP25 contains two SNARE domains, SN1 and SN2. Available evidence suggests that, out of these two domains, SN1 most likely binds first to syntaxin-1 (Fasshauer et al., 1998; Misura et al., 2001b). The question remains whether SN2 binds subsequently to synaxin-1-SN1 complex and is then followed by synaptobrevin 2 or is it the other way around.

Recently, a different reaction pathway is being suggested. Evidence from fungal vacuolar fusion indicates that SM protein Vps33 mediates the formation of a template complex between the Qa and R SNAREs, to which Qb and Qc SNAREs bind (Baker et al., 2015). Given that the synaptic vesicle fusion is a specialized form of intracellular fusion and taking into account the similarities between the SNAREs and SM proteins involved in these processes, it was postulated that neuronal SNAREs have the exact same pathway. Namely, it was proposed that Munc18 organizes formation of the template complex

between syntaxin-1 and synaptobrevin 2 to which SNAP25 binds. It is known that Munc18, contains a synaptobrevin (R) binding site (Parisotto et al., 2014; Sitarska et al., 2017; Xu et al., 2010). According to the template complex hypothesis, when Munc18 is in complex with the closed syntaxin-1, the binding site for synaptobrevin 2 is covered and, thus, synaptobrevin 2 cannot bind. In order for the template complex to form, synaptobrevin 2 binding site needs to be uncovered, which means that syntaxin-1 needs to be in a somewhat open conformation (Baker and Hughson, 2016). Optical tweezer experiments that use the constitutively open LE mutant of syntaxin-1 seem to support this hypothesis (Jiao et al., 2018). Furthermore, there have been occasional reports showing an interaction between syntaxin-1 and synaptobrevin 2 that also suggested that synaptobrevin 2 can only bind to the SNARE domain of syntaxin-1 when it is not “blocked” by Habc, or in other words, when syntaxin-1 is in an open conformation (Calakos et al.; Fasshauer et al., 1998b; Hazzard et al., 1999). It is possible that Munc18 stabilizes this interaction, but it is not clear how it would transition from the high affinity complex with the closed syntaxin-1 to the transient template complex. This hypothesis also directly opposes experiments that describe a complex between Munc18, syntaxin-1 and SNAP25 as an intermediate in the SNARE assembly (Dawidowski and Cafiso, 2013; Jakhanwal et al., 2017; Shen et al., 2007; Zhang et al., 2016). Unlike the template complex, the complex between Munc18, syntaxin-1 and SNAP25 was stable enough to be isolated and tested *in vitro* where it showed accelerated synaptobrevin 2 binding (Jakhanwal et al., 2017).

Another open question that relates to the mechanism and kinetics of SNARE assembly concerns the irreversibility of the SNARE zippering. Specifically, it is known and accepted that the SNARE complex is exceptionally stable and that it does not spontaneously dissociate to its components in a biologically relevant timeframe, meaning that the SNARE assembly reaction is practically irreversible (Fasshauer et al., 2002). However, the assembly reaction occurs in multiple steps, but it is not clear at which point exactly it becomes irreversible. Unfortunately, not enough attention is paid to this problem as many authors either report the dissociation constant of the irreversible SNARE assembly or ignore the likely reversible intermediate steps.

1.5.1.2 The guidance of the SNARE assembly

The second central question concerns the energy content of the free SNARE proteins. As mentioned, SNARE proteins in their disordered state store a high amount of energy that is released with the formation of the SNARE complex. It was proposed that one SNARE complex is enough to drive synaptic vesicle fusion (Bogaart et al., 2010). For this to be true, the entire energy released from the assembly of one SNARE complex needs to be channeled towards overcoming the energy barrier for synaptic vesicle fusion. This can only be achieved, presumably, by the proper assembly of the SNARE complex. Misfolded, unproductive complexes observed in solution would therefore lead to useless dissipation of energy that can no longer be employed for fusion. It is generally accepted that in neurons

accessory proteins help to align and guide SNAREs towards the correct assembly pathway. The prime candidate protein for this role is the aforementioned Munc18.

Munc18 has an absolutely essential role in neurotransmission as it was shown that Munc18 knockout neurons have completely abrogated fusion (Verhage et al., 2000). Munc18 was mentioned in section 1.4.1.1 as an SM protein that locks syntaxin-1 in a closed conformation in which it is not able to participate in the SNARE complex formation. Nevertheless, Munc18 was found to also bind to the SNARE complex, an interaction that seems to be crucially dependent on N-terminal peptide of syntaxin-1 (Burkhardt et al., 2008; Dulubova et al., 2007; Khvotchev et al., 2007; Shen et al., 2007). It is not quite clear how does the transition from the closed Munc18-syntaxin-1 complex to the Munc18-SNARE complex occur. Generally accepted explanation involves CATCHR (complexes associated with tethering containing helical rods) tethering protein Munc13 that would open syntaxin-1 in Munc18-syntaxin-1 complex and accelerate its transition into the SNARE complex (Ma et al., 2011; Richmond et al., 2001; Yang et al., 2015). On the other hand, it was suggested that arachidonic acid, released from the plasma membrane by the activity of lipases, promotes SNARE complex formation by changing the conformation of syntaxin-1 in Munc18-syntaxin-1 complex or by revealing additional binding sites on Munc18 (Connell et al., 2007; Latham et al., 2007).

Through its close interaction with syntaxin-1 and through interactions with other SNAREs, it is accepted that Munc18 is able to nucleate and closely control SNARE assembly, although it is still not known how exactly is this achieved.

In addition to SNARE aligning and nucleating the SNARE assembly, Munc18 is suggested to have another role in assuring the fusion of cognate SNAREs and thereby preventing the crosstalk that would arise from the before mentioned SNARE promiscuity (Shen et al., 2007).

1.5.1.3 The speed of the SNARE assembly

The third central problem of the neuronal SNARE field considers the apparent speed at which the SNARE complex forms. The vesicle fusion driven by the SNARE proteins *in vitro* can take hours to complete and it seems, therefore, incompatible with the millisecond synaptic vesicle fusion observed *in vivo* (Katz and Miledi 1965). Most of the work regarding the SNARE complex formation revolves around understanding the underlying cause of this incompatibility.

Multiple reasons have been put forward as an explanation for the slow *in vitro* assembly of the neuronal SNARE proteins. Some of the most prominent ones are: oligomerization and open-closed conformations of syntaxin-1 observed in solution (section 1.4.1.1), formation of the unproductive 2:1 complex between syntaxin-1 and SNAP25 (section 1.4.1.2), and misfolding of the SNARE complex in solution such as formation of the anti-parallel bundle (Weninger et al., 2003).

The dominant and widely accepted hypothesis that tries to reconcile the slow kinetics observed *in vitro* with the fast kinetics observed *in vivo*, is that the zippering of the SNARE proteins proceeds in two phases. The first phase includes nucleation and zippering of the N-terminal part, while the second phase corresponds to the zippering of the C-terminal part of the SNARE complex. According to this hypothesis, between the ending of the first phase and the beginning of the second phase there is a pause in zippering (Gao et al., 2012; Li et al., 2016). This kinetic pause is then exploited in neurons for the arrest of the SNARE assembly *in trans*. The arrest is presumably stabilized by the accessory proteins that maintain the partially zippered *trans*-SNARE complex until the arrival of Ca^{2+} when the block is removed, and the SNARE zippering is allowed to proceed. The leading candidate proteins in charge of maintaining the partially assembled SNAREs are synaptotagmins and complexins.

Synaptotagmins are considered to be the main Ca^{2+} sensor in fast synaptic vesicle fusion. The neuronal synaptotagmins are single pass transmembrane proteins located at the synaptic vesicle membrane. They characteristically possess two C2-domains, C2A and C2B, that bind the total of five Ca^{2+} molecules. Additionally, C2B domain contains a polybasic motif that interacts with acidic phospholipids present at the presynaptic plasma membrane, that are especially enriched in syntaxin-1 and SNAP25 clusters (sections 1.4.1.1 and 1.4.1.2) (Perin et al., 1990). Synaptotagmin-1 has also been reported to bind to syntaxin-1, SNAP25 and their dimer, as well as to the zippered SNARE complex (Bennett et al., 1992; Kee and Scheller, 1996; Rickman and Davletov, 2003). Binding of Ca^{2+} changes conformation of synaptotagmins affecting their interactions with both proteins and lipids (Chapman et al., 1995).

Complexins are small soluble proteins that were shown to bind to the neuronal SNARE complex at the groove formed by syntaxin-1 and synaptobrevin 2 (Chen et al., 2002). Complexins are therefore placed downstream of the initiation of the SNARE assembly. Their role in the SNARE zippering is considered to be dual, stimulatory and inhibitory (Trimbuch and Rosenmund, 2016). The stimulatory role is accomplished by stabilizing and advancing the zippering, and by interacting with synaptotagmin which then sensitizes the partially zippered SNARE complex to the arrival of Ca^{2+} (Xue et al., 2010; Yoon et al., 2008). The inhibitory role is achieved by serving as a clamp that gets inserted into the advancing SNARE complex locking it in a partially zippered state (Schaub et al., 2006).

Synaptotagmins and complexins are thought to be acting in concert to achieve synchronous, Ca^{2+} -dependent neurotransmitter release. Recent crystal structure obtained for this synaptotagmin-complexin-SNARE complex proposed that, in the primed state, two synaptotagmin molecules bind to the SNARE complex on the opposite sides and in antiparallel orientation (Zhou et al., 2017). One synaptotagmin molecule seems to bind only to the SNARE complex, while the second one forms a tripartite complex with complexin and the SNAREs (Zhou et al., 2017).

The clamped, partially zippered *trans*-SNARE model offers explanation for the fast and synchronous *in vivo* fusion. The evidence for this model is indirect as the *trans*-SNARE complex has never been captured. In addition, it has been calculated that the disassembly of the SNARE complex requires 10 ATP molecules indicating that the SNARE proteins are highly energized in their disordered form (Shah et al., 2014). This means that there exists a steep energy gradient between the free and the zippered SNARE proteins, leading to a conclusion that by stopping the SNARE complex zippering, the majority of that energy would be dissipated and not utilized for overcoming the energy barrier for fusion. However, the energy landscape for vesicle fusion is rather rugged. It is then possible that the energy of the SNARE zippering is released in portions that are used to overcome different hills of the energy landscape. It was already mentioned that the stalk is most likely in the energy valley (section 1.3.2) which means the first considerable energy must precede the stalk formation. It was also experimentally shown that tightly docked vesicles that do not yet have proximal monolayers fused, present another energy valley (Yavuz et al., 2018). The energy released from the formation of the half-zippered SNARE complex could possibly be directed at overcoming the barrier required for establishing contact between the apposing membranes. The docked and primed synaptic vesicles are very close to the plasma membrane and these states can presumably be a result of the half-zippered SNARE complex (Imig et al., 2014). Shrinking of the neuronal membrane by the application of hypertonic sucrose solution leads to fusion of the primed synaptic vesicles, suggesting that the energy barrier for the final step of fusion might not be too high (Rosenmund and Stevens, 1996). It is, therefore, plausible that the C-terminal SNARE zippering provides enough energy to complete the fusion. Another possibility can be that the accessory proteins in some way store that energy and direct it to the vesicle fusion when the time is right, however, direct evidence for this proposition is lacking.

1.5.2 Experimental approaches for studying the SNARE assembly

The field of neuronal SNARE assembly and synaptic vesicle fusion is more than mildly chaotic. For almost every finding there is data that supports either the exact opposite or something completely different. After more than 30 years of active research there are very few concepts that are considered to be a proven fact. This complexity arises undoubtedly from the complicated interactions between the proteins and lipids involved in fusion, but also from the experimental approaches themselves.

By far the most common way for studying SNARE mediated synaptic vesicle fusion is by employing lipid mixing and content mixing assays.

In the lipid mixing assays, liposomes are usually labeled with one or two fluorescent dyes that change their fluorescence upon fusion. Generally, a dye and a quencher are

reconstituted into one liposome that gets diluted after fusion with the unlabeled liposome. This separation by dilution leads to unquenching and to an increase in fluorescence that can be monitored (Hoekstra and Düzgüneş, 1993). The content mixing assay works by the same principle with the difference that the lumen of the liposomes is labeled with dyes, commonly a FRET pair, that change their fluorescence upon fusion (Hoekstra and Düzgüneş, 1993; Yu et al., 2019). Fusion of artificial liposomes with reconstituted proteins can be leaky and additional measures need to be taken in the case of content mixing to avoid artefacts coming from the leaked contents.

The lipid mixing and content mixing assays are very useful and have contributed valuable information to the field. However, one has to keep in mind that these assays monitor liposome fusion, not protein interactions. This is very often forgotten and these assays are used for reconstruction of interaction sequence of minimum three proteins. When using accessory proteins, these assays cannot distinguish whether the change that the examined proteins cause is due to their effect on the SNARE complex or on the liposomes directly. Furthermore, if there is a limiting step that arises from the fusion process itself, it can be erroneously attributed to protein interactions.

Proteins can be reconstituted into liposomes using a few different methods. All of them at some point contain detergent that needs to be removed for the liposomes to form. The removal of the detergent is not always complete or consistent, and the potential residual detergent can contribute to variability in the data (Rizo and Südhof, 2012). The data can also vary depending on the protein-lipid ratio used for reconstitution as well as with the size of the liposomes and, therefore, their curvature. Reconstituted proteins are not evenly distributed between different liposomes, meaning that the liposomes can contain different number of proteins or can even be empty. Proteins in the liposomes are, in addition, not evenly distributed along the liposome surface, but are in patches that result in high local protein concentration.

Docking of liposomes is by its virtue very similar to aggregation making it difficult to distinguish between the two processes. Liposomes tend to aggregate on their own and this can be a problem, especially in the experiments where liposomes are fluorescently labeled. The aggregation can cause light scattering that leads to unspecific fluorescence increase.

It is quite clear that the proteoliposome system is very heterogeneous and complex. Some of the caveats of proteoliposome system stand for other study systems as well. The inconsistencies in the data present in the field most likely arise as a consequence of the multiple variables existing in these systems whose influence is unknown and, therefore, uncontrollable. Variables such as lipid composition, bilayer curvature and charge, etc. have an influence on individual SNAREs (section 1.4.1) and consequently influence the rate and their ability to form the SNARE complex. Additionally, combinations of these variables appear to also have a synergistic effect that is difficult to understand and untangle.

Lately, optical tweezer approach for studying the SNARE zippering is gaining in popularity. In these experiments a single SNARE complex is attached by two ends to polystyrene beads that are optically trapped. Beads are moved with light in a way that stretches the SNARE complex and causes its disassembly. This approach can measure small changes in force-extension or extension-time curves that can be used to calculate the unfolding and folding energies in real time (Zhang and Hughson, 2021). The biggest value of optical tweezers is that it allows access to details in folding that are impossible to obtain with other methods. However, to be able to do multiple cycles of pulling and relaxing in these experiments, SNARE proteins are fused. Fusing two or three proteins into one protein changes the molecularity of the reaction making the SNARE zippering an intramolecular reaction from the intermolecular one. It is well established that intramolecular reactions are entropically favored and occur significantly faster than the intermolecular reactions (Fersht, 2017). Therefore, in most cases, the optical tweezer experiments can provide information only on processes downstream of the nucleation of the SNARE zippering.

1.6 THE AIM OF THIS PHD THESIS

Out of the three open questions addressed in section 1.5.1, the problem regarding the molecular mechanism of the SNARE assembly is the most basic one as it underlies the problems of the speed of the SNARE zippering and the necessity for its regulation. Understanding the mechanism of zippering and its kinetics is profoundly important for understanding the way in which accessory proteins are able to modulate and control this interaction and how the interplay between SNAREs and accessory proteins translates into fast synaptic vesicle fusion. Therefore, the aim of this PhD thesis is to determine the order in which the SNARE proteins syntaxin-1, SNAP25 and synaptobrevin 2 enter the SNARE assembly reaction.

2 MATERIALS AND METHODS

2.1 MATERIALS

2.1.1 Chemicals

All of the chemicals used in this work are presented in the following table:

Table 2.1. Chemicals. All of the chemicals used in this work are listed in the table in the column on the left. The middle left column represents the CAS RN (Chemical Abstracts Service Registry Number) for each chemical, the middle right column the catalogue number, while the column on the right shows the name of the company that produces the chemical. The names of the chemicals are organized in an alphabetical order.

Name	CAS RN	Catalogue number	Company
2-propanol	67-63-0	1.09634.2511	Merck
Acetic acid	64-19-7	1.00063.2511	Merck
Acrylamide Solution (30%)	79-06-1, 110-26-9	A4983,0500	AppliChem GmbH
Alexa Fluor™ 488 C ₅ maleimide	500004-82-0	A10254	Thermo Fisher Scientific
Alexa Fluor™ 647 C ₂ maleimide	-	A20347	Thermo Fisher Scientific
Ammonium sulfate	7783-20-2	1.01217.1000	Merck
APS	7727-54-0	A3678-100g	Sigma-Aldrich
BD Bacto™ agar	9002-18-0	214010	BD
Benzamidine hydrochloride hydrate	206752-36-5	B6506-25g	Sigma-Aldrich
Bromophenol Blue (BPB)	34725-61-6	B6131	Sigma-Aldrich
Chitin beads	-	S6651L	New England Biolabs
Coomassie Brilliant Blue	6104-58-1	A3480,0025	AppliChem GmbH
DMSO	67-68-5	472301-100ML	Sigma-Aldrich
DNase	9003-98-9	A3778,0500	AppliChem GmbH
DTT	3483-12-3	19733320	Molekula
EDTA	6381-92-6	1.08418.1000	Merck
Ethanol	64-17-5	1.00983.1011	Merck

Materials and Methods

Glycerol	56-81-5	24388.320	VWR Chemicals
HEPES	7365-45-9	9105.3	Carl Roth GmbH
Imidazole	288-32-4	56750-1KG	Sigma-Aldrich
IPTG	367-93-1	IPTG025	Formedium
KCl	7447-40-7	1.04936.1000	Merck
Methanol	67-56-1	1.06009.2511	Merck
MgCl ₂	7791-18-6	1.05833.1000	Merck
NaCl	7647-14-5	1.06404.5000	Merck
Ni ²⁺ beads	-	88222	Thermo Fischer Scientific
Ortho-phosphoric acid	7664-38-2	1.00573.1000	Merck
PMSF	329-98-6	6367.3	Carl Roth GmbH
SDS	151-21-3	20765.03	SERVA Electrophoresis
Tcep	51805-45-9	C4706-10G	Sigma-Aldrich
TEMED	110-18-9	T9281-25ML	Sigma-Aldrich
Thrombin	9002-04-4	154163	MP Biomedicals, LLC
Tricine	5704-04-1	A1085,1000	AppliChem GmbH
Tris	77-86-1	103156X	VWR Chemicals
Trypsin inhibitor	9035-81-8	T9253-1G	Sigma-Aldrich
Tryptone/Peptone	91079-40-2	8952.1	Carl Roth GmbH
Urea	57-13-6	1.08487.5000	Merck
Yeast Extract	8013-01-2	2363.2	Carl Roth GmbH

2.1.2 Protein constructs

Five protein constructs were used in this work. All of the protein constructs were derived from *Rattus norvegicus*. Syntaxin-1A, SNAP25a and synaptobrevin 2 were mutated to contain one cysteine in their SNARE domain, close to their 0th layer (see Introduction, section 1.4). Figure 2.1 shows the positions of the mutated amino acids in the crystal structure of the neuronal SNARE complex (Sutton et al., 1998). Syntaxin-1A and synaptobrevin 2 constructs did not contain the transmembrane domain. All of the constructs, except syntaxin-1A, were cloned into pET28a vectors that carries His₆-tag, N-terminal thrombin cleavage site and kanamycin resistance. Syntaxin-1A contains a thrombin cleavage site at its N-terminus. Using pET28a vector and thrombin for syntaxin-1A purification would lead to the removal of the first nine amino acids of the protein (Burkhardt et al., 2008). For that reason, I used pTXB1 vector for syntaxin-1A. The pTXB1

vector carries C-terminal intein-CBD (chitin binding domain) tag and ampicillin resistance. Intein is a self-cleavable protein sequence whose cleavage is induced by the presence of a strong reducing agent, such as DTT (Xu and Evans, 2001).

The plasmids were bought from Novagen (pET28a) and New England Biolabs (pTXB1). The detailed plasmid sequences can be found on:

- (i) [https://www.snapgene.com/resources/plasmid-files/?set=pET_and_duet_vectors\(novagen\)&plasmid=pET-28a\(%2B\)](https://www.snapgene.com/resources/plasmid-files/?set=pET_and_duet_vectors(novagen)&plasmid=pET-28a(%2B))
– for pET28a
- (ii) https://www.snapgene.com/resources/plasmid-files/?set=basic_cloning_vectors&plasmid=pTXB1
– for pTXB1

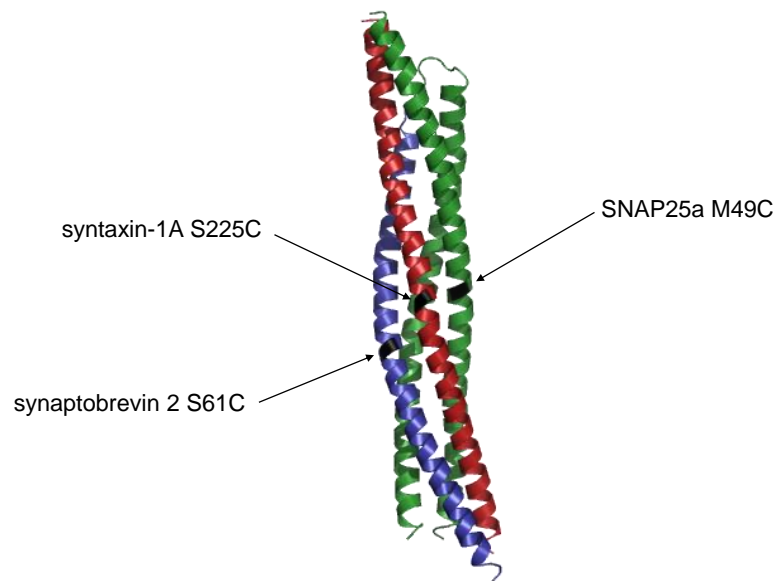


Figure 2.1. Positions of the mutated amino acids in the crystal structure of the neuronal SNARE complex. The mutated amino acids of syntaxin-1A (red), synaptobrevin 2 (blue) and SNAP25a (green) are located near the 0th interaction layer of the SNARE complex. All of the selected amino acids were changed into cysteine for later labeling with the cysteine specific fluorescent dyes. S225C – serine at the position 225 was mutated into cysteine; S61C – serine at the position 61 was mutated into cysteine; M49C – methionine at position 49 was mutated into cysteine.

The following table summarizes the employed protein constructs:

Table 2.2. Protein constructs. All of the protein constructs used in this work are listed in the column on the far-right (Protein). Each row contains protein name, the residues that the protein construct consists of, and the introduced amino acid mutations. The second column (Vector) shows the name of the plasmid that carries the protein gene. The third column (Cloning sites) contains restriction sites that were used for cloning of the protein sequence into the expression vector. Finally, the work in which the protein construct was made is listed in the far-left column (Publication).

Protein	Vector	Cloning sites	Publication
Syntaxin-1A (1-265); C145A, S225C	pTXB1	NdeI/SapI	(Yavuz, 2014); this work
SNAP25a (1-206); M49C	pET28a	NheI/XhoI	(Margittai et al., 2001)
SN1 (1-83)	pET28a	NheI/XhoI	(Fasshauer and Margittai, 2004)
SN2 (120-206)	pET28a	NheI/XhoI	(Fasshauer and Margittai, 2004)
Synaptobrevin 2 (1-96); S61C	pET28a	NdeI/XhoI	(Margittai et al., 2001)

For simplicity, syntaxin-1A, SNAP25a, and synaptobrevin 2 will be further on referred to only as syntaxin, SNAP25 and synaptobrevin, respectively.

2.1.3 Buffers and media

The buffers used in this work were all prepared in the same way. The components were, in the calculated volumes, mixed in a measuring cylinder. The MilliQ water (filtered through Millipak® Express 40; MPGP04001; Merck) was added until just below the final volume. At that point, the pH was adjusted while stirring with the magnetic rod. The volume of the buffer was then finalized using a volumetric flask. In the final step, the buffer was filtered through 0,2 µm cellulose acetate membrane filter (11107--50-----N; Sartorius) with the help of the vacuum pump (N820.3 FT18; KNF Laboport). The list of the buffers and their composition is shown in Table 2.3.

The stocks and some of the buffers (labeled with “*” in in the Table 2.3) were made and maintained by Ursula Welscher-Altschäffel. Media and salts for bacterial growth were made and autoclaved by Heike Löffler (labeled with “**” in the Table 2.3). The SOC medium was purchased from New England Biolabs (B9020SVIAL).

Table 2.3. Buffers. The table shows the name of the buffers and media used in this work (far-left column, Name), together with their composition (middle left column, Composition),

Materials and Methods

concentration of each of the components (middle right column, Concentration) and the pH value (far-right column, pH). The buffers in the table are arranged in an alphabetical order.

Name	Composition	Concentration	pH
ÄKTA A	HEPES	20 mM	~7,4
	EDTA	1 mM	
	Tcep	0,1 mM	
ÄKTA B	HEPES	20 mM	~7,4
	NaCl	1000 mM	
	EDTA	1 mM	
	Tcep	0,1 mM	
	Tris	200 mM	
	Tris	100 mM	
Cathode buffer *	Tricine	100 mM	-
	SDS	0,1 %	
	Methanol	50% v/v	
Coomassie Brilliant Blue stain *	Acetic Acid	10% v/v	-
	Coomassie Brilliant Blue R-250	0,2% w/v	
	Acetic acid	10% v/v	
Destaining buffer *	Isopropanol	20% v/v	-
	HEPES	20 mM	
Dialysis buffer	NaCl	150 mM	~7,4
	EDTA	1 mM	
	Tcep	0,1 mM	
	HEPES	20 mM	
Elution buffer 1	NaCl	500 mM	~7,4
	Imidazole	400 mM	
	HEPES	20 mM	
Elution buffer 2	NaCl	500 mM	~8,5
	DTT	50 mM	
	HEPES	20 mM	
Experiment buffer	KCl	150 mM	~7,4
	Tcep	0,1 mM	
	Tris	3 M	
Gel buffer *	SDS	0,3%	8,5
	Tryptone	1% w/v	
	Yeast extract	0,5% w/v	
LB (Luria broth) medium **	NaCl	1% w/v	-
	LB medium	500 ml	
	BD Bacto Agar	1,5% w/v	
LB-agar medium **	HEPES	20 mM	~7,4
	NaCl	500 mM	
	NaCl	137 mM	
Lysis buffer	KCl	27 mM	~7,4
	Na ₂ HPO ₄	10 mM	
	KH ₂ PO ₄	1,8 mM	
	NaCl	137 mM	
PBS *	KCl	27 mM	~7,4
	Na ₂ HPO ₄	10 mM	
	KH ₂ PO ₄	1,8 mM	
	NaCl	137 mM	

Materials and Methods

Resolving gel (10%) (for two mini-gels)	Acrylamide Solution	3,5 ml	
	Gel buffer	3,4 ml	
	MilliQ	1 ml	
	50% Glycerol	2,1 ml	-
	TEMED	7 µl	
	10% APS	50 µl	
Salts **	K ₂ HPO ₄ x 3H ₂ O	720 mM	
	KH ₂ PO ₄	170 mM	-
Sample buffer (5x) *	Tris (1M, pH=6,8)	20% v/v	
	SDS (20%)	25% v/v	
	DTT	38,5% w/v	-
	Glycerol	37,5% v/v	
	BPB (1% in ethanol)	1,5% v/v	
	Acrylamide Solution	525 µl	
Stacking gel (for two mini-gels)	Gel buffer	1,05 ml	
	MilliQ	4,8 ml	-
	TEMED	5,25 µl	
	10% APS	27 µl	
	Tryptone	1,3% w/v	
TB (Terrific Broth) medium **	Yeast extract	2,7% w/v	-
	Glycerol	0,44% w/v	
	HEPES	20 mM	
Wash buffer 1	NaCl	500 mM	~7,4
	Imidazole	40 mM	
	HEPES	20 mM	
Wash buffer 2	NaCl	500 mM	~8,5
	Tcep	0,1 mM	

2.2 METHODS

2.2.1 Methods for sample preparation

2.2.1.1 QuikChange Lightning Multi Site-Directed Mutagenesis

Mutations in the pTXB1-syntaxin construct and a deletion of the transmembrane domain (residues 265-288) were introduced with QuikChange Lightning Multi Site-Directed Mutagenesis kit following the manufacturer's instructions (Agilent Technologies, Inc.).

QuikChange Lightning Multi Site-Directed Mutagenesis kit introduces a mutation via single mutagenic primer. Using multiple primers that anneal to the same strand, it is possible to introduce multiple mutations at once. The primers were designed according to the Primer Design Guidelines in the manual (Agilent Technologies, 2011) and ordered from Eurofins Genomics. Table 2.4 shows the primer sequences and their characteristics.

The mutagenesis kit was also used for deletion of 69 base pairs that comprise the transmembrane domain of syntaxin (amino acids 266-288). For this purpose, both forward and reverse primers were used. The primers for deletion were designed to align perfectly with the sequences that surround the sequence that encodes the transmembrane domain.

Table 2.4. Primers and their characteristics. The primer sequence and its length (in bp – base pairs) is shown in the column on the far-left (Primer). The subsequent columns from left to right show: the GC content of the primer (GC (%)), the melting temperature (T_m (°C)) and what was the primer used for (Purpose). All of the primers were designed according to the Primer Design Guidelines in the manual (Agilent Technologies, 2011) and were ordered from Eurofins Genomics. The melting temperature was calculated according to the formula provided in the manual ($T_m = 81,5 + 0,41(\%GC) - \frac{675}{N} - \%mismatch$; %GC – GC content, N – primer length, %mismatch – number of base pairs that are different from the DNA template).

Primer	GC (%)	T_m (°C)	Purpose
5'-actaccgagaacgcagcaaagggcgcatc-3' (29 bp)	58,6	82,3	Mutation of cysteine at position 145 of syntaxin to serine
5'-catgctggtggagtgccagggggagat-3' (27 bp)	63	82,3	Mutation of serine at position 225 of syntaxin to cysteine
5'-aggaagaagtgcatacgggagatgcactagttgcctacc-3' (41 bp)	53,7	>75	Deletion of the transmembrane domain of syntaxin
5'-cgtgatgcacttcttctgcgtgccttgctctggtactt-3' (39 bp)	53,8	74,7	Deletion of the transmembrane domain of syntaxin

The PCR mix was calculated and prepared according to the protocol provided in the manual (Agilent Technologies, 2011):

Reaction component	Volume
10xQuikChange Lightning Multi rection buffer	2,5 µl

Materials and Methods

Double-distilled H ₂ O	X µl (for the final volume of 25 µl)
QuikSolution	0,7 µl
DNA-template	X µl (100 ng)
Mutagenic primers	X µl (100 ng for each primer)
dNTP mix	1 µl
QuikChange Lightening Multi enzyme blend	1 µl
Total	25 µl

Considering that the pTXB1 vector contains 6 706 base pairs, the following PCR protocol was used (Agilent Technologies, 2011):

Segment	Cycles	Temperature	Time
1	1	95 °C	2 minutes
2	30	95 °C	20 seconds
		55 °C	30 seconds
		65 °C	3 minutes
3	1	65 °C	5 minutes

Upon completion of the PCR protocol, the tube containing the PCR products was cooled down to <37 °C and 1 µl of the Dpn I endonuclease was added (provided with the kit). The Dpn I endonuclease cleaves the hemimethylated parental strain, leaving only mutated plasmids. To ensure proper cleavage, the PCR sample was incubated with the Dpn I for 1 hour at 37 °C. Nearing the end of the incubation time, XL-10-Gold Ultracompetent cells (provided with the kit) were gently thawed on ice. After thawing, the cells (~45 µl) were transferred to a 14-ml Falcon® polystyrene Test Tube with the round bottom (BD) and β-mercaptoethanol (2 µl; provided with the kit) was added. The cells were then incubated for 10 minutes on ice, with gentle tapping every 2 minutes.

The PCR products, treated with the Dpn I, were carefully added (1,5 µl) to the cells and the obtained transformation mix was incubated on ice for another 30 minutes. The incubation was followed by a heat-shock for exactly 30 seconds at 42 °C and further incubation on ice for 2 minutes. The SOC medium, pre-heated to 42 °C, was added (500 µl) to the treated cells that were then incubated at 37 °C with shaking at 250 rpm (Thermomixer compact; Eppendorf®). After 1 hour of incubation, the cells were centrifuged for 1 min at 4000 rpm (Centrifuge 5702 R, Eppendorf®). The centrifugation caused the cells to move to the bottom of the tube, leaving the clear medium on the top. To concentrate the cells, the medium was discarded by decanting until ~70 µl was left in the tube. The cells were resuspended by pipetting and plated on the LB-agar plates (664160; Greiner Bio-One GmbH) supplemented with ampicillin (pTXB1 plasmid carries ampicillin resistance,

section 2.1.2). The cells were spread on the plate with a sterilized metal rod and incubated for minimum of 16 hours at 37°C (BD 115; Binder GmbH). The single colonies that formed were selected, individually expanded overnight in LB-ampicillin medium (100 ml) and used for the isolation of the mutated plasmid.

2.2.1.2 *Midi-prep*

Plasmid purification was performed using Plasmid DNA Purification kit (Macherey-Nagel) and following the instructions from the User Manual (Macherey-Nagel, 2011). The protocol is described in the next paragraph.

The overnight-grown 100 ml bacterial culture (section 2.2.1.1) was centrifuged at 4400 rpm (Centrifuge 5702 R, Eppendorf®) and 4°C. The cleared medium was discarded and the bacterial pellet was resuspended in the Resuspension Buffer RES supplemented with RNase A. The Lysis Buffer LYS was added to the resuspended cells. The mixture was gently inverted 5 times and the cells were left to lyse at room temperature. The Lysis Buffer LYS breaks down the cells by sodium hydroxide/SDS treatment which can also damage the plasmid DNA during prolonged exposure (Macherey-Nagel, 2011). The lysis was, therefore, stopped after 5 minutes with the Neutralization Buffer NEU that contains potassium acetate. The mixture was inverted 10-15 times (until colorless) and the cellular debris was pelleted by short centrifugation. The supernatant was further cleared by passing through a NucleoBond® Xtra Column Filter previously soaked with the Equilibration Buffer EQU. The cleared supernatant was then passed through the NucleoBond® Xtra Column that contains filters that capture the plasmid DNA. The column with the DNA was washed with 8 ml of the Wash Buffer WASH and then eluted with 12 ml of the Elution Buffer ELU pre-heated to 50°C. The plasmid was precipitated from the eluate with 8,4 ml of isopropanol and vigorous vortexing. The precipitate was pelleted by a 1h centrifugation at 4°C and 4400 rpm (Centrifuge 5702 R, Eppendorf®). The pellet was washed with 70% ethanol, dried and resuspended in filtered and autoclaved MilliQ water.

Plasmid concentration and purity were measured using Nanodrop spectrophotometer (NanoDrop ND-1000, UV/Vis Spectrophotometer; Thermo Fischer Scientific). The sequence of the purified plasmid was determined by Sanger Cycle Sequencing/Capillary Electrophoresis method (performed by SeqLab-Microsynth GmbH).

The volumes of the Resuspension, Lysis and Neutralization Buffer are not stated in the protocol description. The used volume depended on the optical density of the starting bacterial culture and was calculated with the formula provided in the User Manual: $V\text{ (ml)} = \frac{400}{OD_{600}}$; where V – Volume, and OD_{600} – optical density at 600 nm.

2.2.1.3 Bacterial transformation for protein purification

Heat competent BL21 (DE3) strain of *Escherichia coli* was purchased from New England BioLabs (C2527H) and transformed with the corresponding plasmid construct (Table 2.2). The transformation protocol was based on Hanahan, 1983.

Bacterial cells were thawed on ice for 10 min and 1.5 μ l of the plasmid was added to the thawed cells. The mixture was incubated on ice for 30 min. In the meantime, the water bath was heated to exactly 42°C and SOC medium was thawed and preheated in the water bath. After the incubation time, the mixture of cells and plasmid was heat shocked in the water bath for exactly 45 seconds and incubated for another 2 min on ice. Heat shock shortly disrupts the *E. coli* membrane and allows the plasmid to enter the cells. Finally, 500 μ l of the heated SOC medium was added and the now transformed cells were incubated for 1h in Thermomixer (Thermomixer compact; Eppendorf®) at 37°C and 400 rpm. The cells were concentrated by short centrifugation for 1 min at 4000 rpm (Centrifuge 5415 D with F45-24-11 rotor; Eppendorf®), the excess SOC medium was disposed of by decantation. 30 μ l of the concentrated, transformed cells was plated on kanamycin/ampicillin-LB-agar plates and incubated for minimum of 16 h at 37°C (BD 115; Binder GmbH). The formed colonies were picked and resuspended in 100 ml of LB medium that was used as a preculture for protein expression.

2.2.1.4 Protein expression

The preculture was prepared by inoculating a single bacterial colony in 100 ml of LB-kanamycin/ampicillin medium, and incubating at 37°C with 120 rpm shaking (Multitron; Infors HT) overnight. 10 ml of the preculture was inoculated to 450 ml of the TB medium supplemented with 50 ml of the salts (Table 2.3) and the cells were grown at 37°C and 120 rpm shaking (Multitron; Infors HT) until the OD₆₀₀ reached approximately 0.9. At that moment, the protein expression was induced with 0.25 mM IPTG (isopropyl β -D-1-thiogalactopyranoside). The induced cultures were further incubated at 22°C and 120 rpm shaking overnight. The following day, the cultures were centrifuged for 30 min at 4°C and 4000 rpm (Sorvall centrifuge RC 12BP+, Thermo Fischer Scientific). The formed bacterial cell pellet was washed with ice-cold PBS and stored at -20°C.

2.2.1.5 Affinity purification

Proteins that were cloned into the pET28a vector were all purified in a similar fashion. The following protocol is based on the standard Ni²⁺-NTA protein purification protocol (Petty, 1996) and optimization introduced by Ursel Ries and Dr. Ángel Pérez-Lara.

The bacterial pellet was resuspended in the Lysis buffer supplemented with protease inhibitors (0,5 mM trypsin inhibitor, 10 mM benzamidine hydrochloride, 1 mM PMSF – final concentrations), DNase (tip of spatula) and MgCl₂ (1 mM). Breaking of the cells was done either by sonication (Branson Sonifier W-450, Marshall Scientific) or by microfluidizer (M-110L Microfluidizer® Materials Processor, Microfluidics Inc.). In case of sonication, flat probe was used, strength was set to 8, cycles set to 50%. The cells were

sonicated on ice 6 times for 40 sec with 40 second breaks between each sonication round. In case of lysis by microfluidizer, the resuspended pellet was first homogenized with 10 strokes by Dounce homogenizer and then ran through microfluidizer machine twice at the pressure of 17 000 psi. The prepared homogenate was adjusted to 6M urea and incubated with stirring at room temperature for 15 min. Urea unfolds proteins which would cause the dissociation of all the other proteins that might be bound to the protein of interest. The homogenate was afterwards centrifugated at 13 000 rpm at 4°C for one hour (Sorvall RC 6+ Centrifuge; Thermo Fischer Scientific). The supernatant was incubated with Ni²⁺-NTA beads (3 ml of equilibrated beads per 1 l of culture) previously equilibrated with the Lysis buffer. After 3h of incubation, the flowthrough was collected, volume was measured, and the beads were washed with the same volume of the Wash buffer 1. The protein was then eluted from the beads with 50 ml of the Elution buffer 1 by gravity flow. The speed of elution was adjusted to approximately one drop per second using a valve (1-Way Stopcock, D100 455980, Discofix®). To cleave off the His-tag, 5 mg of thrombin in 50% glycerol was added, as well as Tcep (0.1 mM final concentration) to prevent formation of disulfide bridges. The eluate was then loaded into the dialysis bag (Spectra/Por® 1 Dialysis Tubing 6-8 kD 50mm 100ft; 132665; Repligen) previously soaked in the Dialysis buffer, and dialysed at 4°C with stirring overnight. The next day, the eluate was taken out of the dialysis bag, filtered through 0.2 µm filter (FP 30/0.2 CA-s, Whatman®) and further purified using ion-exchange chromatography.

2.2.1.5.1 Syntaxin purification

As mentioned in section 2.1.2, unlike the other proteins used in this study, syntaxin was cloned in the pTXB1 vector which utilizes the intein-CBD system. The purification protocol was based on the IMPACT Kit Instruction Manual (New England Biolabs, 2020) and was slightly different than previously described. Those differences are stressed in the following paragraph.

After breakage of the bacterial cells with the sonicator (Branson Sonifier W-450, Marshall Scientific), urea was added until the final concentration of 2 M. Higher concentration was avoided as it would interfere with binding of syntaxin to the chitin beads (New England Biolabs, 2020). The protein was incubated with the beads (10 ml of chitin beads per 1l of culture) overnight at 4°C on a rotator (Test-tube-rotator 34528; Schütt labortechnik). Following the washing with the Wash buffer 2, the beads with the protein were quickly washed by gravity flow with one column volume (~50 ml) of the Elution buffer 2. After that, 50 ml of the Elution buffer 2 was added and left to induce cleavage ON at 4°C on a rotator. The next day, the eluate was collected, put in previously soaked dialysis bag and dialyzed in Dialysis buffer overnight at 4°C that was stirred with the magnetic rod. Even after elution there would still be high amount of protein bound to the beads. To retrieve this protein, second overnight cleavage with 50 ml of the Elution buffer 2 and dialysis were performed. As before, the dialyzed protein was filtered with 0.2 µm filter (FP 30/0.2 CA-s, Whatman®) and further purified with ion-exchange chromatography.

2.2.1.6 Ion-exchange chromatography

The ion-exchange chromatography columns were attached to the ÄKTA system (GE Pharmacia ÄKTA Purifier 10 UPC) and equilibrated with ÄKTA A and ÄKTA B buffers in the following order: ÄKTA A – 3 column volumes, ÄKTA B – 3 column volumes, ÄKTA A – 3 column volumes. Depending on the isoelectric point of the protein of interest and the pH of the buffers, two types of columns were used: anionic exchanger MonoQ™ 10/100 GL (17-5167-01; Cytiva) – for syntaxin, SNAP25, SN1, SN2, and cationic exchanger MonoS™ 10/100 GL (17-5169-01; Cytiva) – for synaptobrevin. Previously filtered protein (0.2 µm filter – (FP 30/0.2 CA-s, Whatman®)) was loaded onto the equilibrated column with the flow of 1.5 ml/min. After loading and additional washing with the ÄKTA A buffer, the protein was eluted with gradient elution (from 0% to 100% of ÄKTA B in 15 CV) at the flow of 2 ml/min. The fractions containing the peak of interest were collected, their concentration was measured using Nanodrop spectrophotometer (NanoDrop ND-1000, UV/Vis Spectrophotometer; Thermo Fischer Scientific) and 500 µl fractions were snap-frozen in liquid nitrogen and stored at -80°C.

2.2.1.7 Protein labeling

2.2.1.7.1 The fluorescent dyes

The stopped-flow titration experiments required labeling of proteins with fluorescent dyes that form a FRET (Förster resonance energy transfer) pair. FRET is a non-radiative energy transmission that occurs between the two fluorescent dyes, the donor and the acceptor dye, at a distance of <100 Å (Förster, 1946). For FRET to occur, the emission spectrum of the donor and the excitation spectrum of the acceptor dye need to have an overlapping region. The extent of the energy transfer will depend on the distance and the degree of spectral overlap between the dyes (Lakowicz, 2013).

The chosen fluorescent pair was Alexa Fluor™ 488 C₅ maleimide and Alexa Fluor™ 647 C₂ maleimide (Table 2.1, Figure 2.2) as the donor and the acceptor dye, respectively. The maleimide group of these fluorescent dyes interacts with cysteine residues and forms a stable thioether bond thereby labeling the proteins.

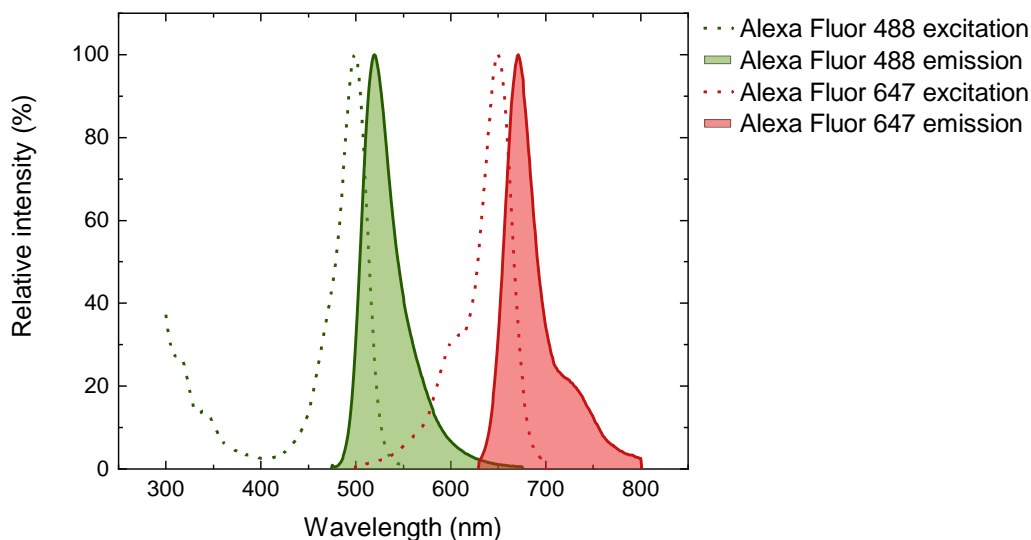


Figure 2.2. *The excitation and emission spectra of Alexa Fluor 488 and Alexa Fluor 647. The excitation spectra of both dyes are shown in dashed lines, while the emission spectra are shown in full-lines and colored surface area. The donor dye, Alexa Fluor 488, is in green, and the acceptor dye, Alexa Fluor 647, is in red.*

2.2.1.7.2 The labeling procedure

The 500 μ l ion-exchange protein fractions (section 2.2.1.6) were thawed and mixed with the corresponding dye previously dissolved in DMSO. The protein to dye molar ratio was 1:5. The mixture was wrapped in aluminum foil and incubated overnight at 4° on a rotator (Test-tube-rotator 34528; Schütt labortechnik). The next day the labeled protein was separated from the free dye using size exclusion chromatography.

2.2.1.8 Size exclusion chromatography

Before every experiment, the ion-exchange 500 μ l fractions were thawed, labeled with fluorescent dyes (section 2.2.1.7) if necessary, and finally purified using the size exclusion chromatography with Superdex75® 10/300 FPLC® (9738031; Pharmacia Biotech) column. The column was attached to the ÄKTA system (GE Pharmacia ÄKTA Purifier 10 UPC) and primarily equilibrated with 3 column volumes of the Experiment buffer at the flow of 0.5 ml/min. Before loading onto the column, the 500 μ l protein sample was centrifuged at 14 000 rpm (Fresco 21 Microcentrifuge; Heraeus; Thermo Fischer Scientific), 4°C for 10 min to pellet any aggregates. The loading and the run were also done at the flow of 0.5 ml/min. The fractions containing the peak of interest were collected, their concentration was measured using either by Nanodrop, BCA or Pierce660, depending on the protein sample, and the fractions were kept at 4°C on ice until the execution of the experiment.

2.2.1.9 SDS-PAGE and Coomassie Brilliant Blue Staining

During the protein purification, a sample was collected at each step of the process. The success of the purification was judged by the SDS-PAGE separation and Coomassie Brilliant Blue staining of the collected samples.

The polyacrylamide gels, the sample buffer, and the Anode and Cathode buffers were prepared according to the protocol by Schagger and von Jagow, 1987. The composition of each of these buffers is shown in Table 2.3. The SDS-PAGE separation was performed on Bio-Rad, Mini Protean II™ system at two successive voltages: 70 V – until the samples enter the separating gel and 100 V – until the separation is complete. The bands were subsequently visualized by Coomassie Brilliant Blue staining (composition in Table 2.3). The gel in the stain was boiled, incubated for 10 min with gentle rocking and then destained with the Destaining buffer.

2.2.2 Experimental methods

2.2.2.1 Stopped-flow experiments

2.2.2.1.1 Stopped-flow spectrophotometer

The stopped-flow experiments were performed on a SX20D Stopped-Flow Spectrophotometer (Applied Photophysics). The spectrophotometer contains two syringes in which the sample is stored and brought to the right temperature by a water bath. Upon triggering, equal volume of 60 µl is pushed by a drive ram from both syringes into the tubings of the stopped flow machine. In the tubings, the contents are mixed and eventually brought to the recording cell where the reaction is monitored. Three to four triggering events are required to prime the recording cell. The time it takes for the sample to reach the recording cell from the moment of triggering is called a dead-time of the machine. For the stopped-flow spectrophotometer, the dead-time amounts to ~2 ms, which makes this method specifically suitable for capturing the early stages of the reaction.

The photomultiplier tubes (PMTs) with the inserted optical filters were attached to the recording cell and connected to the computer. The stopped flow machine has a possibility of recording from two fluorescent channels simultaneously. The choice of the PMTs and the filters depends on the fluorescent dyes selected for the experiment. Given that I have chosen Alexa Fluor™ 488 C₅ maleimide and Alexa Fluor™ 647 C₂ maleimide for my experiments, I required two kinds of PMT tubes. The PMT 300-650 nm (Type R6095, Applied Photophysics) with the 534/30 bandpass filter (BrightLine HC, F39-533, AHF analysentechnik AG) recorded changes in Alexa Fluor™ 488 C₅ maleimide, while the near-infrared PMT 300-900 nm (Type R2228, Applied Photophysics) with 665 nm cut-on filter (RG665, Schott) recorded changes in the Alexa Fluor™ 647 C₂ maleimide. The donor dye, Alexa Fluor™ 488 C₅ maleimide, was stimulated with a SX LED Light Source PSU

(Applied Photophysics) and 470 nm optical cable (Applied Photophysics) that was also connected to the recording cell.

The schematic representation of the stopped-flow spectrophotometer is shown in Figure 2.3. Detailed description of the SX20MV Stopped-Flow Spectrophotometer and its operation can be found in the User Manual (Applied Photophysics, 2012).

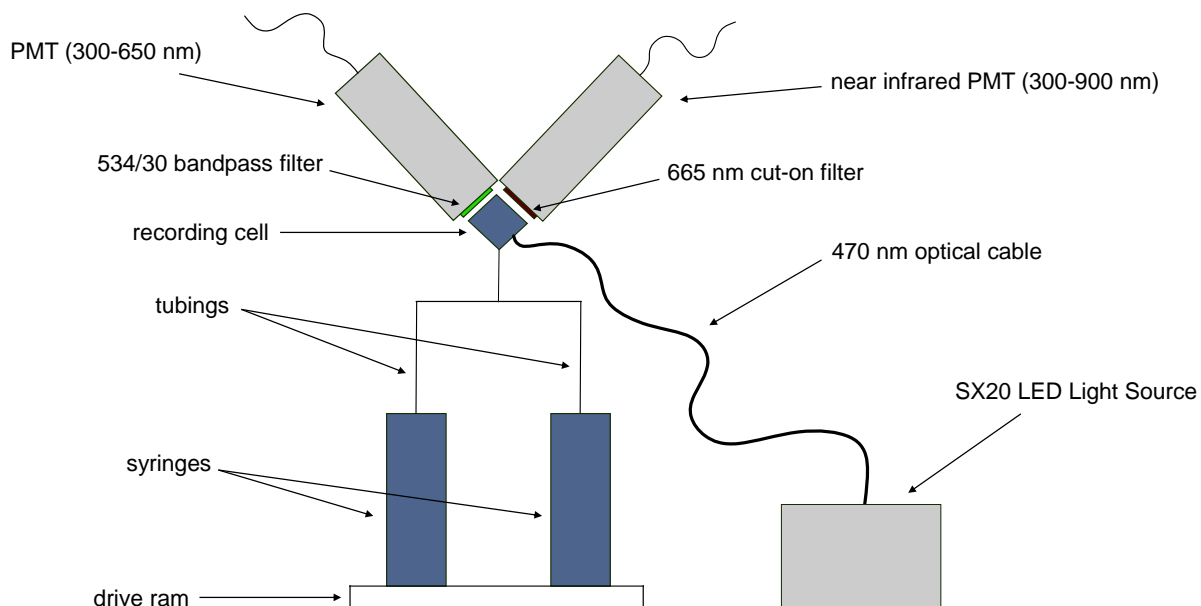


Figure 2.3. Schematic representation of the stopped-flow spectrophotometer. When the reaction is triggered, the drive ramp pushes out equal volume of the sample from the two syringes. The syringes are connected to the recording cell via tubings. The recording cell is illuminated by the SX20 LED Light Source and the 470 nm optical cable. Two PMTs with the corresponding filters (300-650 nm with the 534/30 bandpass filter, and 300-900 nm with the 665 nm cut-on filter) record the fluorescent changes in the recording cell.

2.2.2.1.2 The settings and the general experimental procedure

A detailed description of the content of both syringes for each experiment is done in the Results section.

The temperature of the water bath was set to 37°C (Ecoline steredition RE104, Lauda Dr. R. Wobser GmbH & Co. KG). The protein samples were loaded onto stopped flow syringes and incubated for 5 min to adjust to the temperature of the experiment. The intensity of the LED Light Source was set to 10 mA. To capture the changes in both Alexa Fluor™ 488 C₅ maleimide and Alexa Fluor™ 647 C₂ maleimide dyes, the “Dual fluorescence” option turned on. Additionally, the “Disable oversampling” option was turned on to avoid unequal smoothing of the trace during acquisition. The priming of the recording cell was done with

four triggering events. The 10 000 data points were recorded in a logarithmic timescale over 1500 seconds with two technical replicates.

2.2.2.1.3 Fitting of the acquired traces

In a reaction, the reactant and the product concentrations change over time in an exponential manner (Goodrich and Kugel, 2007). The reaction is, therefore, best described by the application of the exponential equations. Successful description of the reaction with an exponential equation(s) gives values for the rate constants. The rate constants describe the time it takes for molecules to bind or fall apart. Estimating the values for the rate constants can provide understanding of the reaction mechanism (Goodrich and Kugel, 2007).

To be able to extract rate constants, the titration traces were fit to a combination of exponential and exponential-linear equations. The fitting was performed with the KinTek Explorer (Professional version 6.3; KinTek Corporation) and the OriginPro (2019b; OriginLab Corporation) softwares. The selection of the equation was done based on the overall shape of the trace and on the evaluation of the goodness of the fit.

The fitting was assessed by the distribution of the residuals, on the confidence interval of the measured parameters and on the χ^2/DoF (KinTek Explorer) or R^2 (OriginPro) value. The residuals represent distances of the individual points from the fitted line and should be randomly distributed above and below the line (Motulsky and Christopoulos, 2004). χ^2 is the sum of individual probabilities that the datapoint is described by the selected equation, while the DoF (degrees of freedom) represents all of the individual datapoints. The better the fit, the χ^2/DoF is closer to 1 (Johnson, 2010). R^2 (coefficient of determination) is the proportion of the total variance of the dependent variable that can be predicted by the equation (Motulsky and Christopoulos, 2004). The value of R^2 lies between 0 and 1, with 1 meaning that the fit perfectly describes the data.

In summary, fitting was considered to be good if the residuals are randomly distributed around the fitted line, if the confidence intervals were low and if χ^2/DoF and R^2 values were close to 1. If multiple equations satisfied these criteria (e.g. monoexponential and biexponential), the one with less parameters was always chosen.

2.2.2.2 Size exclusion experiments

Proteins were mixed at 1:1 ratio in different combinations detailedly described in the Results section. Final concentration was 5 μM for each of the proteins and the final volume was 600 μl . The samples were incubated overnight at 4°C on a rotator (Test-tube-rotator 34528; Schütt labortechnik). The next day, before loading on the gel filtration column, the samples were centrifuged for 10 min at 14 000 rpm (Fresco 21 Microcentrifuge; Heraeus; Thermo Fischer Scientific) and 4°C to remove any aggregates that might have formed overnight. After centrifugation, 500 μl of every sample was separated on a Superdex™200 Increase

Materials and Methods

10/300 column (28-9909-44; Cytiva) at 4°C in the Experiment buffer (Table 2.3) with the flow of 0.5 ml/min. The separation was done on ÄKTA pure 25M (Cytiva). The fractions of 500 µl were collected and the peaks of interest were visualized on an SDS-PAGE Schagger gel (section 2.2.1.9).

3 RESULTS

Constructing a model of the SNARE complex assembly requires identification of the interaction steps and an estimation of their rate constants. To this end, I performed titration experiments of the SNARE proteins in different combinations.

The Results section of this work is split into Part I, which focuses on the interactions between combinations of two SNARE proteins, and Part II, in which the interplay of the three SNARE proteins is examined. In the following segments, the stopped-flow and gel filtration experiments are always performed at 37°C and 4°C, respectively. As described in the Materials and Methods section, donor dye refers to AlexaFluor 488 C5-maleimide, and the acceptor dye refers to AlexaFluor 647 C2-maleimide.

3.1 PART I – INTERACTION BETWEEN COMBINATIONS OF TWO SNARE PROTEINS

3.1.1 Syntaxin and synaptobrevin

Syntaxin, labeled with the donor dye, and synaptobrevin, labeled with the acceptor dye, were titrated in an equimolar fashion. This means that at every concentration tested, syntaxin and synaptobrevin were at 1:1 molar ratio. The experimental scheme is shown in Figure 3.1a.

The syntaxin-synaptobrevin interaction was examined at 5 different concentrations. The stopped-flow measurements showed no change in the acceptor fluorescence in the observed time frame of 1500 seconds (Figure 3.1b). Labeled synaptobrevin with unlabeled syntaxin (acceptor only) as well as labeled syntaxin with unlabeled synaptobrevin (donor only) controls did not differ from the titration traces (Figure 3.1c). Since the proteins were labeled with fluorescent dyes close to the 0th layer, this result demonstrates that syntaxin and synaptobrevin do not form a complex that would position their 0th layers close.

To exclude the possibility of a hypothetical interaction in which the 0th layers of syntaxin and synaptobrevin are distant while the proteins remain bound at some other region (e.g. N-terminus), I performed the size exclusion chromatography of the overnight-incubated syntaxin-synaptobrevin sample. The proteins were again in 1:1 molar ratio, 5 μ M concentration each, and the separation was done on Superdex200 Increase 10/300 (Figure 3.2). This experiment confirmed that there is no stable complex formation between syntaxin and synaptobrevin.

Results

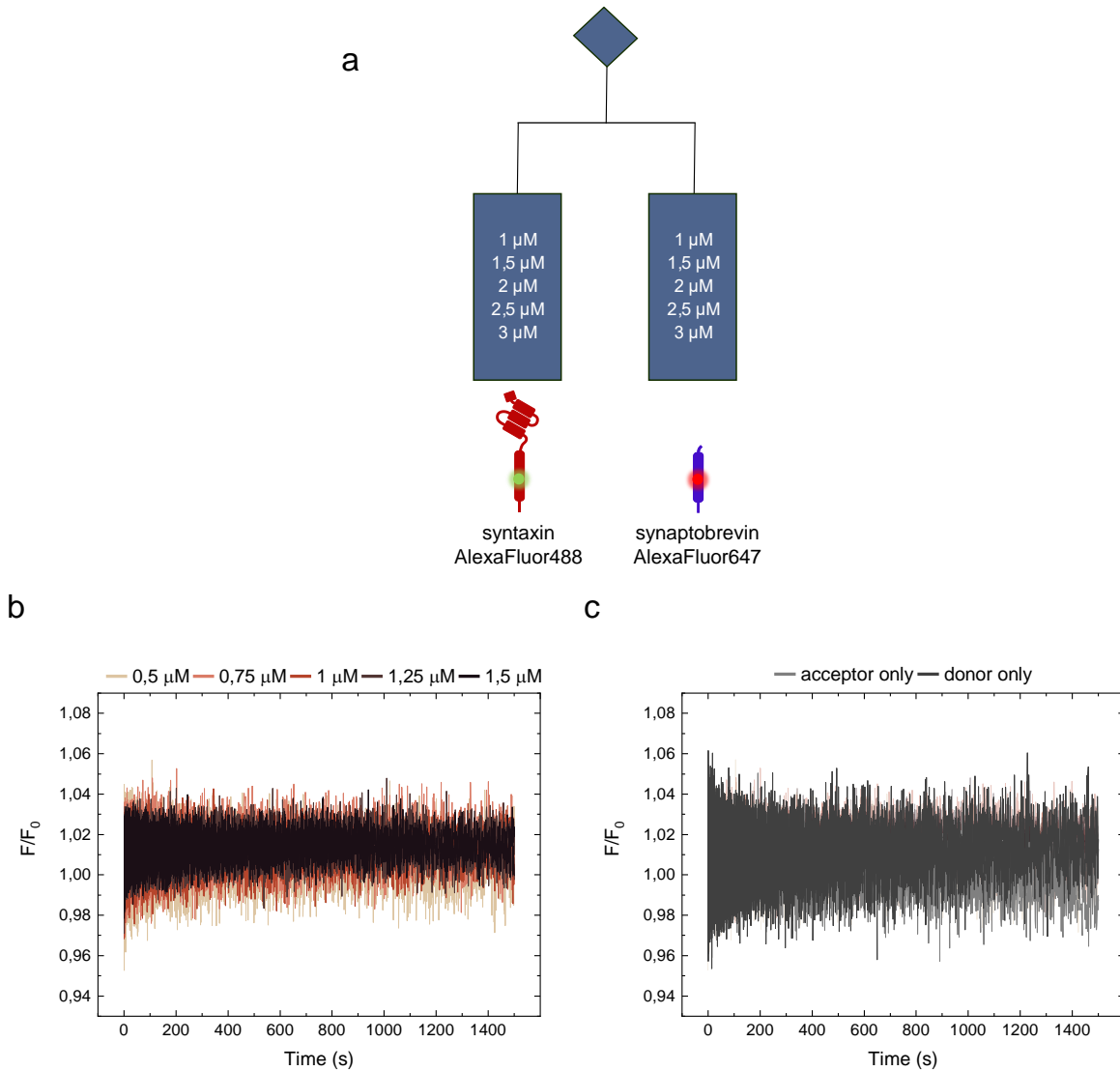


Figure 3.1. Equimolar titration of syntaxin and synaptobrevin. Schematic representation of the experimental design. Donor labeled syntaxin was placed in the lefthand syringe, while the acceptor labeled synaptobrevin was in the righthand one. The concentrations of syntaxin and synaptobrevin in the syringes are indicated on the scheme (**a**). The change in the acceptor fluorescence was observed for 1500 seconds at each concentration (**b**). The lack of increase and the indifference to the concentration change indicates an absence of syntaxin-synaptobrevin complex. Acceptor only (light grey) and donor only (dark grey) controls are not different from the titration traces (**c**). The relative fluorescence change (F/F_0) is a ratio between the measured fluorescence intensity (F) and the average fluorescence intensity of the first 100 data points (F_0).

Results

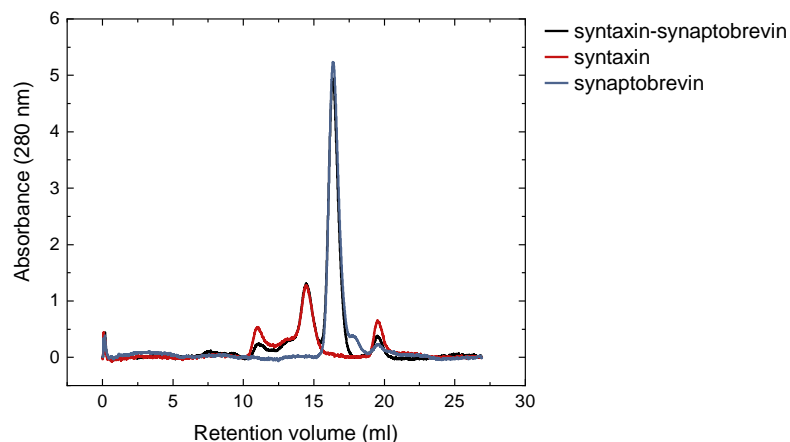


Figure 3.2. Size exclusion chromatogram of syntaxin-synaptobrevin complex. The overnight-incubated syntaxin (red), synaptobrevin (blue) and syntaxin-synaptobrevin (black) were separated on Superdex200 Increase 10/300. The protein concentrations were 5 μ M each. No syntaxin-synaptobrevin complex could be detected.

3.1.2 SNAP25 and synaptobrevin

The complex formation between SNAP25 and synaptobrevin was tested in the same manner as the interaction between syntaxin and synaptobrevin. Donor labeled SNAP25 and acceptor labeled synaptobrevin were titrated in an equimolar ratio (Figure 3.3), and the formation of the potential complex was monitored for 1500 seconds. Additionally, SNAP25 and synaptobrevin were incubated overnight and separated on Superdex200 Increase 10/300.

As in the case of syntaxin and synaptobrevin titration, SNAP25 and synaptobrevin also failed to form any detectable complex in both titration experiment (Figure 3.3) and the size exclusion chromatography (Figure 3.4).

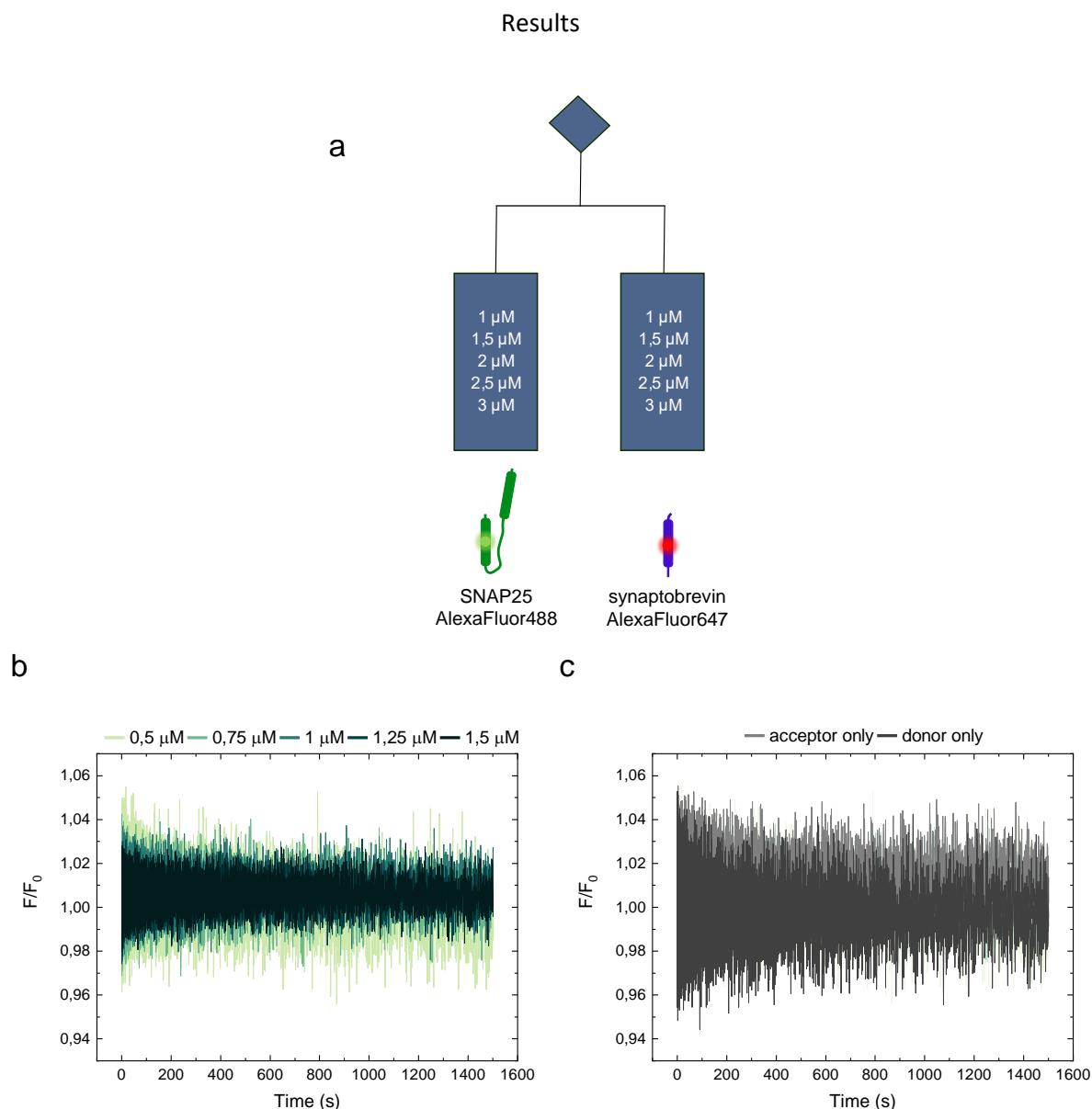


Figure 3.3. Equimolar titration of SNAP25 and synaptobrevin. Schematic representation of the stopped-flow experimental design (a). SNAP25 and synaptobrevin were placed at indicated concentrations in the lefthand and the righthand syringes, respectively (a). The titration traces show no change in the acceptor fluorescence in the observed time frame of 1500 seconds (b). Acceptor only (light grey) and donor only (dark grey) controls do not show any unspecific fluorescent change (c). The relative fluorescence change (F/F_0) is a ratio between the measured fluorescence intensity (F) and the average fluorescence intensity of the first 100 data points (F_0).

Results

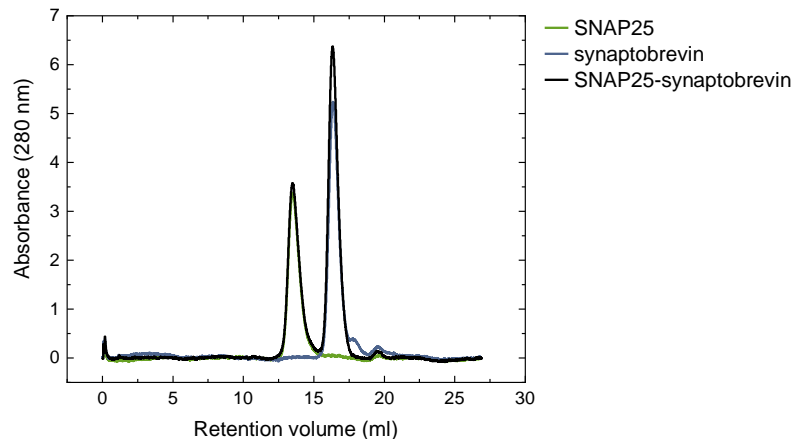


Figure 3.4. Size exclusion chromatogram of SNAP25-synaptobrevin complex. Overnight incubated SNAP25 (green), synaptobrevin (blue) and SNAP25-synaptobrevin (black) were separated on Superdex200 Increase 10/300. The displayed chromatogram shows no difference between individual proteins and the SNAP25-synaptobrevin sample, confirming that SNAP25 and synaptobrevin do not form a complex.

3.1.3 Syntaxin and SNAP25

Finally, the interaction between syntaxin and SNAP25 was examined. The experiments were performed in the same way as for the previously discussed pairs of SNARE proteins. For the titration experiment, syntaxin was labeled with the donor dye, and SNAP25 was labeled with the acceptor dye. The experimental setup and the titration traces are shown in Figure 3.5.

Unlike the syntaxin-synaptobrevin and SNAP25-synaptobrevin titrations, which showed no change in the acceptor fluorescence, syntaxin and SNAP25 manifested marked fluorescence increase in the acceptor channel (Figure 3.5b), indicating a complex formation. The amplitude increase followed the increase in the concentrations, and the plateau was reached after approximately 600 seconds. The acceptor only and donor only controls remained flat showing that the observed increase is indeed due to the syntaxin-SNAP25 interaction (Figure 3.5c).

Results

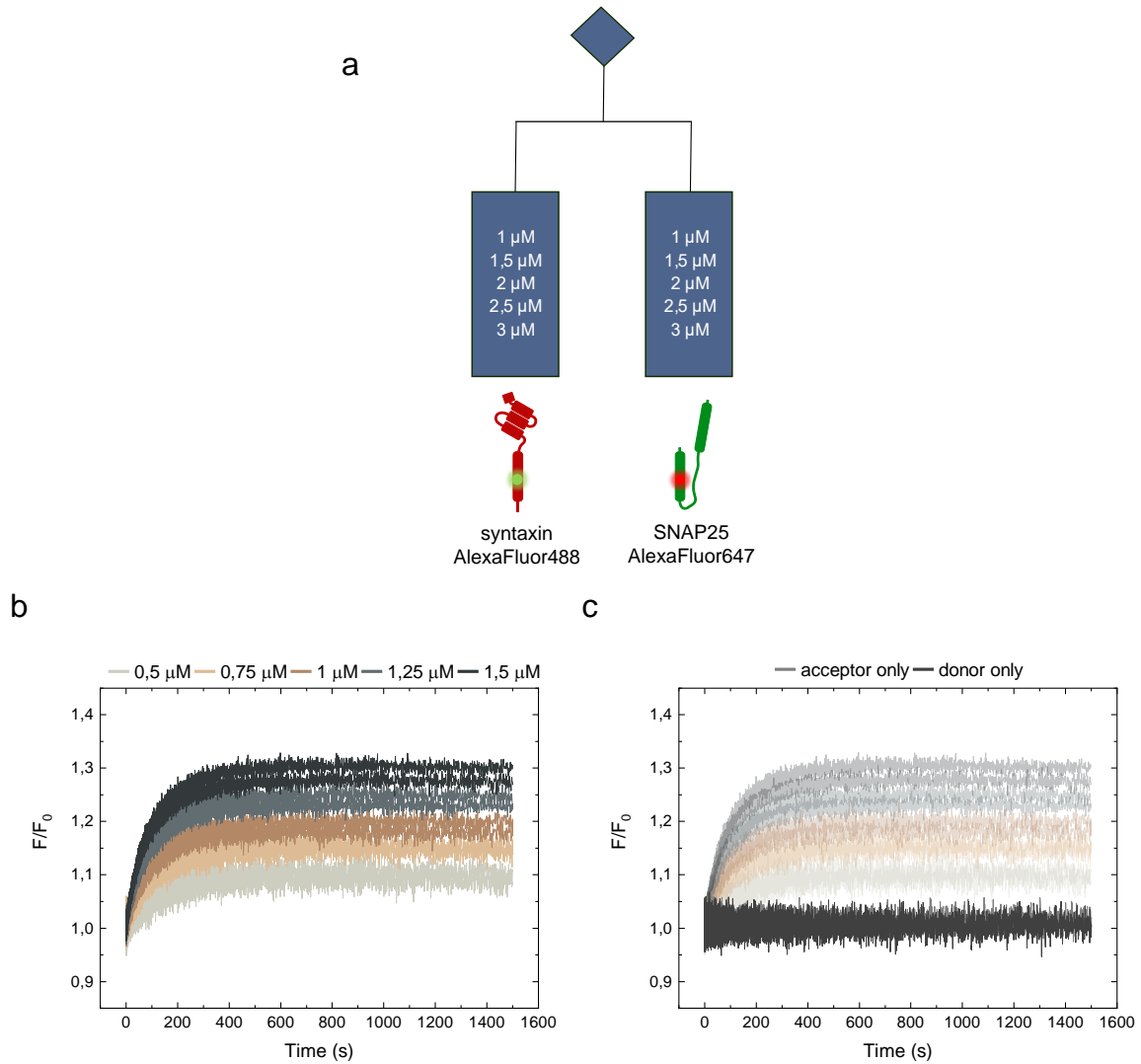


Figure 3.5. Equimolar titration of syntaxin and SNAP25. Schematic representation of the equimolar titration of donor labeled syntaxin and acceptor labeled SNAP25 (**a**). The syringe concentrations of syntaxin and synaptobrevin are indicated in the lefthand and righthand syringe, respectively. The fluorescence increase shows syntaxin-SNAP25 complex formation (**b**), while the acceptor only (light grey) and donor only (dark grey) controls remain flat (**c**). The relative fluorescence change (F/F_0) is a ratio between the measured fluorescence intensity (F) and the average fluorescence intensity of the first 100 data points (F_0).

The obtained raw titration traces were fit to a monoexponential equation (see Materials and Methods section 2.2.2.1.3):

$$y = Ae^{(-k_{obs}x)} + C \quad (1)$$

Results

where y corresponds to the recorded fluorescence intensity (F), A to the amplitude of the trace, k_{obs} to the observed rate constant, x to the time and C to the starting point of the fit (Figure 3.6). Fitting the titration traces gives the value for the observed rate constant(s) that can be used to extract of the real rate constants of the examined reaction.

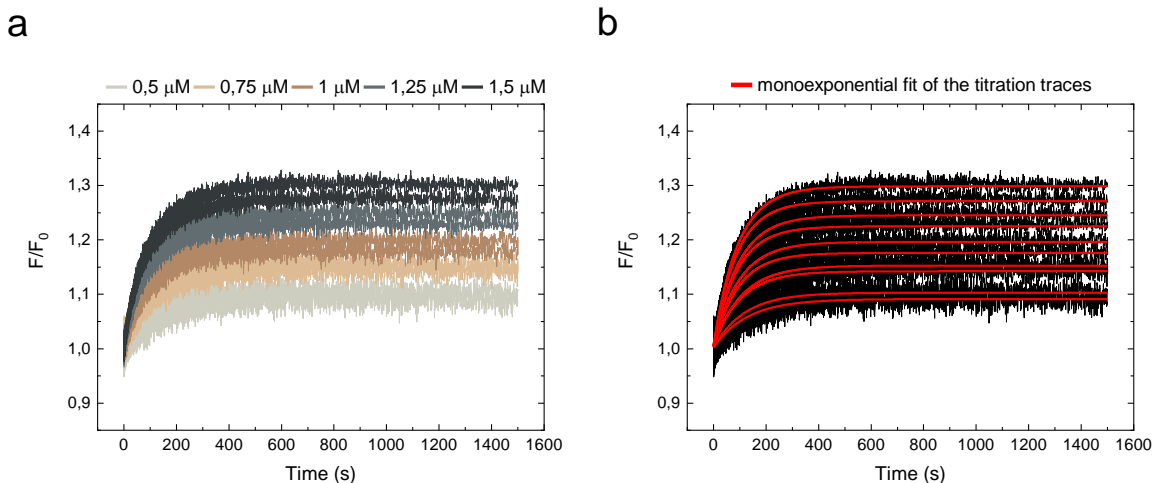


Figure 3.6. Fitting of the syntaxin-SNAP25 titration traces. The traces obtained from the equimolar titration of syntaxin and SNAP25 were fit to a monoexponential equation. The left part of the graph shows the titration traces (a). The right part of the graph shows the fitted traces (red) that are superimposed to the titration traces (now in black) (b). The relative fluorescence change (F/F_0) is a ratio between the measured fluorescence intensity (F) and the average fluorescence intensity of the first 100 data points (F_0).

In bimolecular equimolar titration experiments, the rate constants can be determined with the following linear equation:

$$k_{\text{obs}}^2 = 4k_1k_{-1}[A]_0 + (k_{-1})^2 \quad (2)$$

(modified from Bernasconi, 2012; Czerlinski, 1966)

Here, k_{obs} is the observed rate constant, k_1 the association rate constant, k_{-1} the dissociation rate constant and $[A]_0$ is the initial concentration of the titrant. Since the initial concentrations of syntaxin and SNAP25 are equal, $[\text{syntaxin}]_0 = [\text{SNAP25}]_0$, $[A]_0$ can refer to either one of them. However, the fit of the square of the obtained k_{obs} versus $[\text{syntaxin}]_0$ showed a slight departure from the linear dependence for all three biological replicates and a high variability between the slopes of the fitted lines (Figure 3.7). Additionally, the fit of the first and the second biological replicate gave a negative number for the intercept $(k_{-1})^2$, making the calculation of the k_{-1} and, consequently, k_1 impossible. The difficulties in determining k_1 and k_{-1} with equation (2) suggests that the interaction between syntaxin

Results

and SNAP25 does not occur in a simple single step, despite the monoexponential appearance of the titration traces (Figure 3.6).

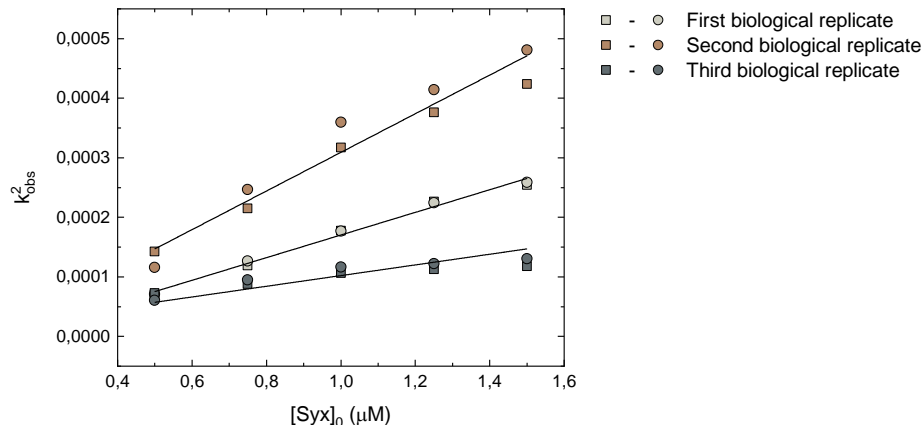


Figure 3.7. Concentration dependence of the k_{obs}^2 for the syntaxin-SNAP25 titration experiment. The square of the k_{obs} obtained from the monoexponential fit of the syntaxin-SNAP25 titration traces was plotted against the initial concentration of syntaxin. The plot shows three biological replicates (marked with different colors) and for each biological replicate there are two technical repeats (marked with squares for the first and circles for the second technical repeat). The data points for each biological replicate were fit to a linear equation. The data showed slight deviation from the linear dependence and a high variability in the slopes of the fitted traces. The intercept for the first and the second biological replicate was a negative number, making the determination of the k_1 and k_{-1} with this method impossible, thereby indicating that the syntaxin and SNAP25 interaction does not occur in a simple single step.

The size exclusion experiment supported the fluorescence data. The syntaxin-SNAP25 complex appears as a prominent peak at 11,3 ml (Figure 3.8a), and the peak fraction shows the presence of both proteins on the SDS-PAGE (Figure 3.8b) with the syntaxin band having higher intensity compared to the band of SNAP25. The syntaxin-SNAP25 sample also showed the peak of unbound SNAP25 in the chromatogram (Figure 3.8a, comparison between the green and the black trace). In contrast, the peak(s) of syntaxin seems to disappear completely (Figure 3.8a, comparison between the red and the black trace). These results support the notion that the syntaxin-SNAP25 complex has an unequal number of syntaxin and SNAP25 molecules, with syntaxin outnumbering SNAP25.

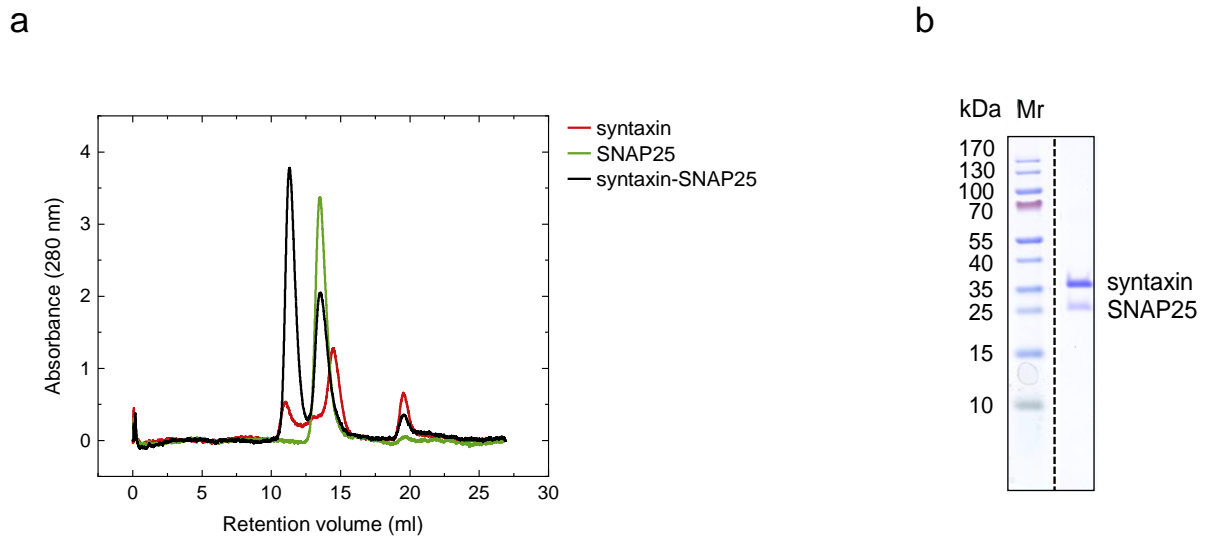


Figure 3.8. Size exclusion chromatography of syntaxin-SNAP25 complex. Size exclusion chromatography of syntaxin (red), SNAP25 (green) and syntaxin-SNAP25 complex (black) shows the presence of syntaxin-SNAP25 complex that elutes from the Superdex200 Increase 10/300 column at 11,3 ml (a). SDS-PAGE of the peak fraction of the syntaxin-SNAP25 sample shows the presence of both proteins with the syntaxin band having higher intensity compared to the SNAP25 band (b). The size exclusion experiment indicates the formation of the syntaxin-SNAP25 complex that contains an unequal number of syntaxin and SNAP25 molecules.

The possible candidate for the observed complex is a famous 2:1 complex in which two syntaxin molecules are bound to one SNAP25 molecule (Fasshauer et al., 1997b). The 2:1 complex has been reported to form between SNAP25 and the H3 domain of syntaxin (Fasshauer and Margittai, 2004; Margittai et al., 2001; Wiederhold and Fasshauer, 2009), as well as between SNAP25 and syntaxin that only lacks its transmembrane domain (Fasshauer et al., 1997b), such as the one used in this work. If this hypothesis is correct, that would signify that the formation of the syntaxin-SNAP25 complex must occur in at least two steps. The first step of the reaction could be either syntaxin dimerization or the formation of 1:1 syntaxin-SNAP25 complex.

Upon closer observation of the syntaxin size exclusion chromatogram, three peaks can be noticed and it is therefore evident that syntaxin alone is capable of forming oligomers (Figure 3.9a). The concentration of syntaxin is the highest for the peak that elutes at 14,5 ml (peak 3), and that most likely corresponds to syntaxin monomers. The two other peaks that elute at 11 ml (peak 1) and 13,1 ml (peak 2) could presumably correspond to syntaxin tetramers and dimers, respectively. The SDS-PAGE separation shows the presence of syntaxin in all three peaks (Figure 3.9b).

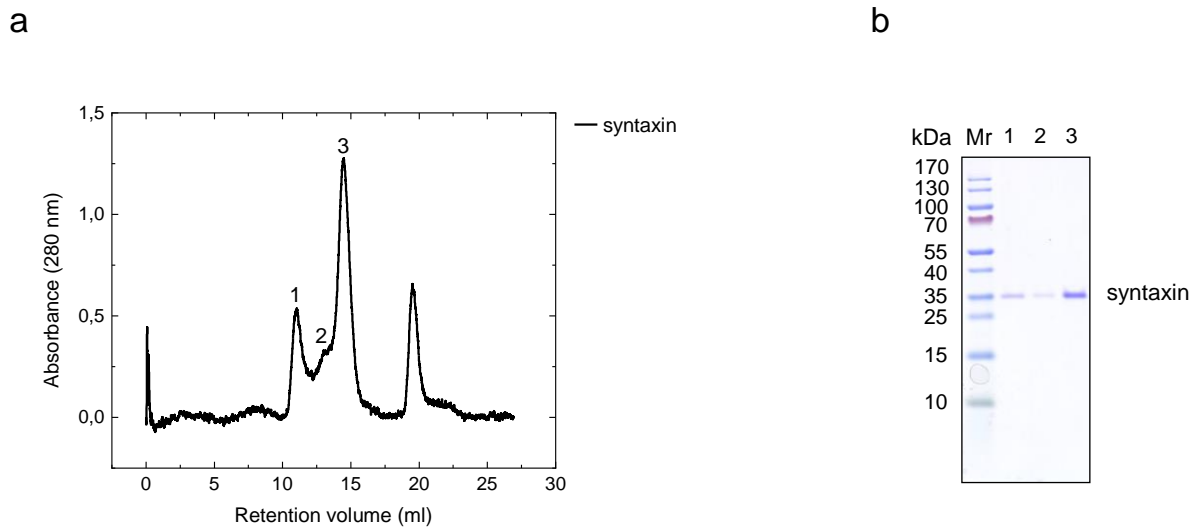


Figure 3.9. Size exclusion chromatography of syntaxin alone. Size exclusion chromatography was performed on 5 μ M syntaxin incubated overnight at 4°C. The chromatogram shows the presence of three distinct populations of syntaxin molecules that appear as three peaks at 11 ml (peak 1), 13,1 ml (peak 2) and 14,5 ml (peak 3) (a). All three peak fractions were separated on SDS-PAGE that was subsequently stained with Coomassie Brilliant Blue (b). Syntaxin was detected in all of the fractions at different concentrations that correspond to the different intensities of the bands.

Syntaxin dimers and tetramers have been reported for the H3 domain (Margittai et al., 2001; Misura et al., 2001a), as well as for the soluble full length syntaxin fragment (1-265) (Lerman et al., 2000) identical to the one used in this work. The rate constants of syntaxin dimerization and tetramerization are not known, however, measurements done using analytical equilibrium ultracentrifugation provided dissociation constant (K_d) values for the dimer and tetramer at 4°C ($K_{d-dimer} = 1,4 \pm 0,5 \mu$ M and $K_{d-tetramer} = 12 \pm 0,6 \mu$ M; Lerman et al., 2000). Values obtained for the dissociation constant depend on the temperature at which it was measured (van't Hoff equation). Considering that all the kinetic experiments in this work are done at 37°C, and that the enthalpy for the syntaxin oligomerization is not known, I unfortunately did not have direct use of the reported K_d values.

I made an attempt to monitor syntaxin oligomerization using the stopped-flow approach. For this purpose, syntaxin was labeled either with the donor or the acceptor dye. Differently labeled syntaxin molecules were placed in separate syringes (Figure 3.10a). The oligomer formation was detected as a change in the acceptor fluorescence, that was again monitored over 1500 seconds. Due to time constraints, this experiment was performed only once. Preliminary data (Figure 3.10b) shows that syntaxin oligomers start

Results

forming early, already after approximately 0,01 seconds. The traces show two very clearly separated phases. The two phases can presumably correspond to the dimer and the tetramer formation between the differently labeled syntaxin molecules. It is, however, not clear at this point which phase belongs to which process.

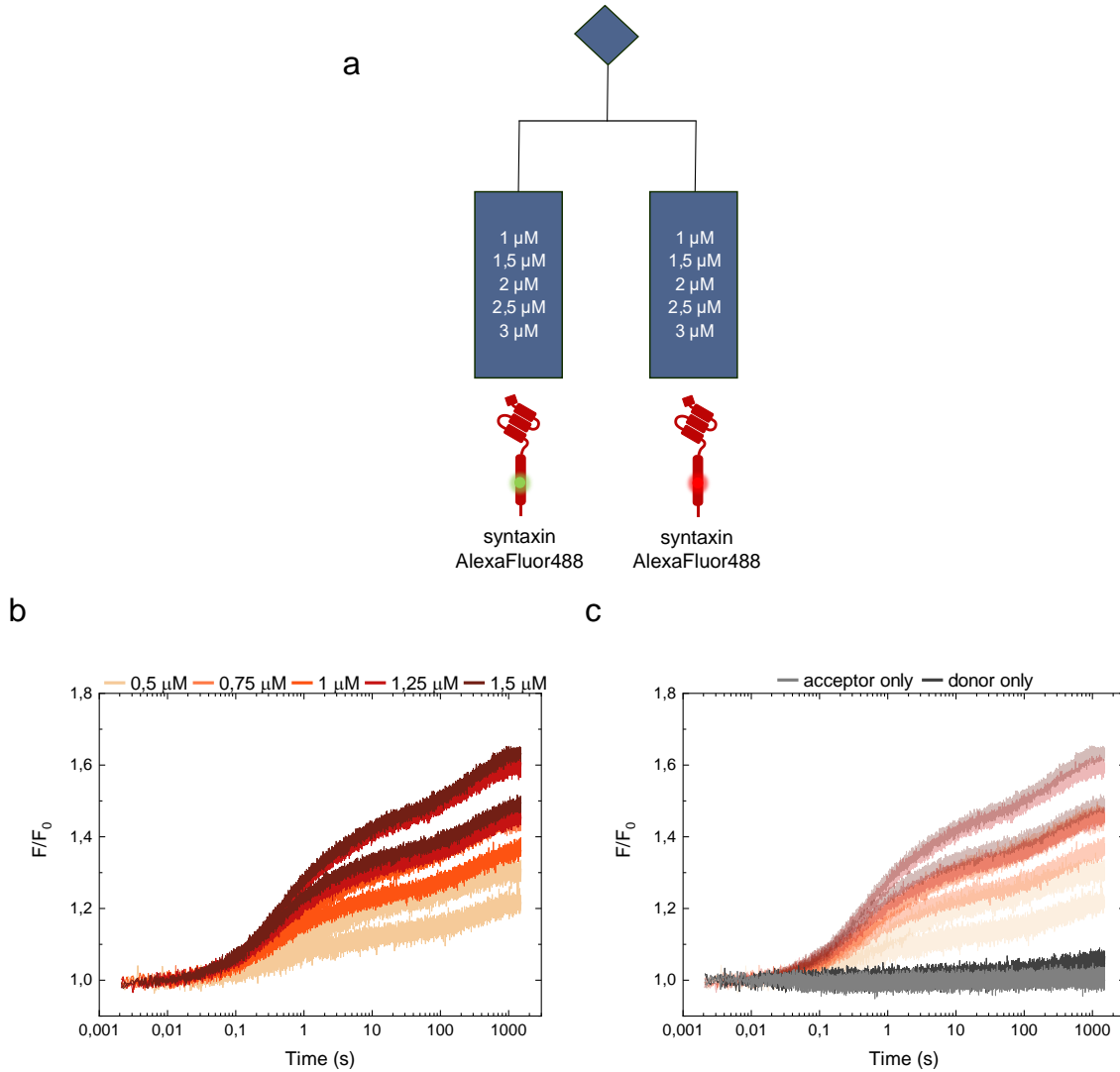


Figure 3.10. Syntaxin oligomerization. Donor and acceptor labeled syntaxin was loaded at the indicated concentrations to the lefthand and righthand syringes, respectively (a). The change in the acceptor fluorescence at different concentrations was monitored over 1500 seconds (b). The fluorescence increase occurs in two phases that could correspond to the dimer and the tetramer formation. The donor only control (dark grey) showed a very slight increase in fluorescence that started at approximately 100 seconds, while the acceptor only control (light grey) did not show any change in fluorescence (c). This experiment was done only once, and it is therefore preliminary data that still needs to be confirmed. The x-axis

showing the time was plotted in the logarithmic scale for better observation of the two phases. The relative fluorescence change (F/F_0) is a ratio between the measured fluorescence intensity (F) and the average fluorescence intensity of the first 100 data points (F_0).

Since the syntaxin oligomers form in the absence of SNAP25, it is conceivable that in the case of 2:1 complex formation, syntaxin dimerization is the first step and is followed by SNAP25 binding (Model 1 - Figure 3.11).

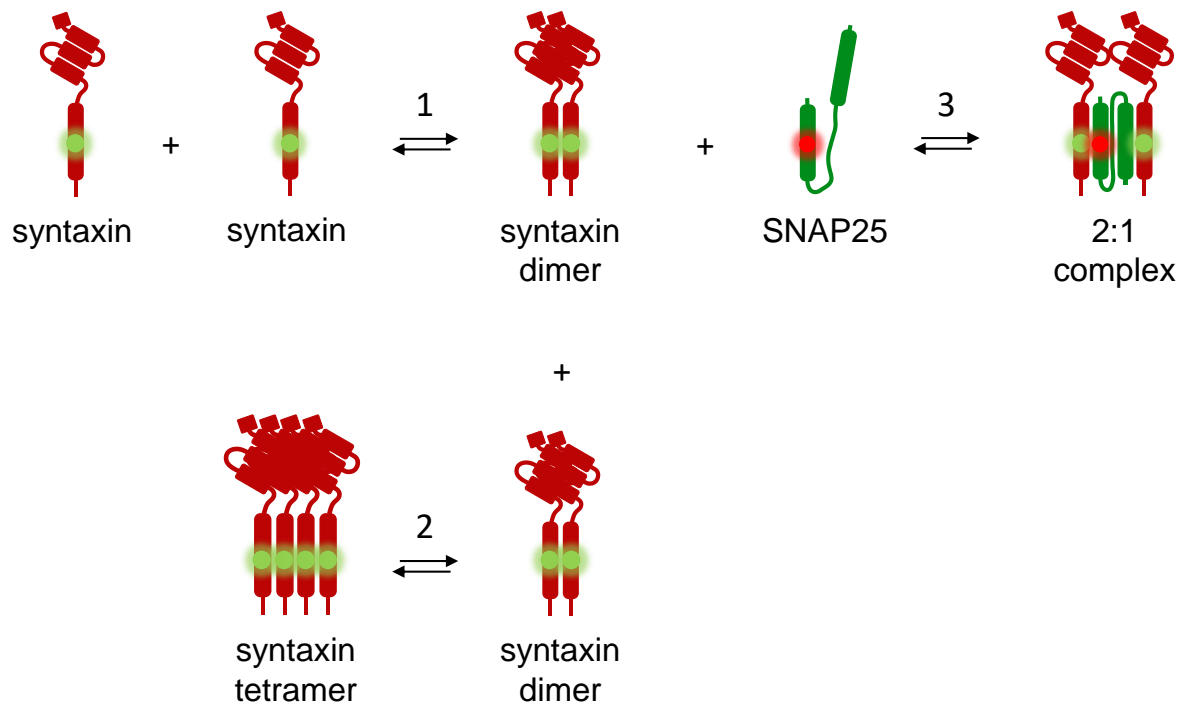


Figure 3.11. Model 1. Hypothetical model for syntaxin and SNAP25 interaction. The first step is the formation of the syntaxin dimer (1) which would then be followed either by syntaxin tetramerization (2) or binding of SNAP25 and formation of the 2:1 complex (3). Red and green dots stand for the acceptor and the donor dyes, respectively.

On the other hand, it has been reported that addition of the DPC detergent during syntaxin purification leads to their monomerization and increases the propensity for the open state (Liang et al., 2013; personal communication). Incubation of such “monomeric” syntaxin with SNAP25 leads to the formation of a stable 1:1 syntaxin-SNAP25 complex (Kreutzberger et al., 2016). Additionally, the binding of SNAP25 to the H3 domain of syntaxin and the formation of 2:1 complex was described even in cases where syntaxin oligomerization is estimated to be low (Margittai et al., 2001). It is, therefore, possible that

the 1:1 syntaxin-SNAP25 complex represents the first step of the reaction, which is then followed by the binding of the second syntaxin molecule (Model 2 – Figure 3.12).

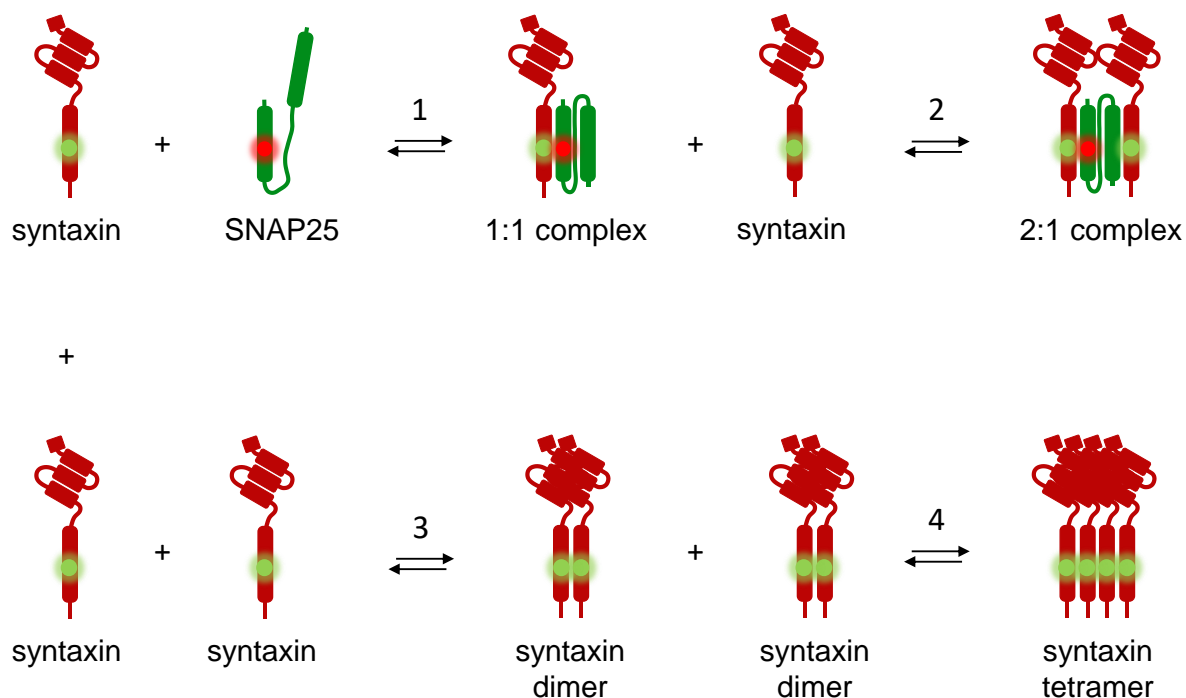


Figure 3.12. Model 2. Hypothetical model for syntaxin and SNAP25 interaction. In the first step of the reaction, syntaxin and SNAP25 interact to form a 1:1 syntaxin-SNAP25 complex (1). Second syntaxin molecule binds to the 1:1 complex and forms a 2:1 syntaxin-SNAP25 complex (2). In a side reaction, syntaxin molecules oligomerize forming dimers (3) and tetramers (4). Red and green dot stand for the acceptor and the donor dye, respectively.

Both models have three kinetic possibilities for the syntaxin-SNAP25 assembly: (i) the first step is much faster than the second step, (ii) the second step is much faster than the first step, and (iii) both steps occur at similar rates. For each one of these possibilities, the equations for determination of the rate constants will differ. One needs to also consider that due to syntaxin oligomerization, the starting concentrations of syntaxin and SNAP25 in the stopped flow experiment will not be exactly equimolar. The syringe containing syntaxin will not consist only of monomers, but most likely of monomers, dimers and tetramers in an unknown ratio. When mixing with SNAP25, syntaxin dimers would immediately be available for interaction with SNAP25 in the case of Model 1. This could possibly explain the monoexponential appearance of the titration traces (Figure 3.5, Figure 3.6) and the slight deviation from the perfect monoexponential fitting as syntaxin gets depleted (Figure 3.7). The same is true for Model 2, where binding of SNAP25 to syntaxin would also be affected by the reduced initial concentration of syntaxin monomers, the faster depletion of syntaxin monomers as two syntaxin molecules are required for every

Results

reaction, and the delay caused by the time it takes for syntaxin dimers and tetramers to dissociate to monomers.

To be able to estimate the relative rates of the steps in syntaxin-SNAP25 interaction and determine which equations would be the most appropriate, an attempt was made to determine $k_{1\text{obs}}$ and $k_{2\text{obs}}$ from the titration traces by fitting to a biexponential equation. As shown in Figure 3.13, fitting of the highest concentration improved slightly with the biexponential fit, while for the lower concentrations, fitting to the biexponential equation was possible in only one of the three biological replicates (in the sense that it gave reasonable results).

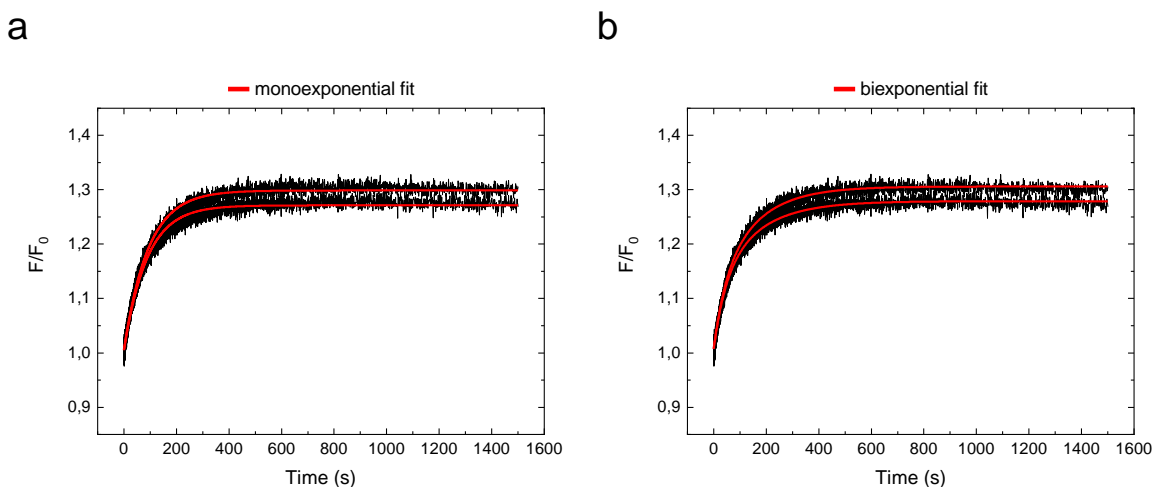


Figure 3.13. Comparison between a monoexponential and biexponential fit of the 1,5 μM titration traces from the syntaxin-SNAP25 titration experiment. The 1,5 μM titration traces were fit to a monoexponential (a) and biexponential (b) equation. The biexponential fit showed slightly improved fit. The relative fluorescence change (F/F_0) is a ratio between the measured fluorescence intensity (F) and the average fluorescence intensity of the first 100 data points (F_0).

Since all the necessary formulas for determination of the rate constants require the knowledge of the observable rate constants, and since it was not possible to obtain reliable values for $k_{1\text{obs}}$ and $k_{2\text{obs}}$, it was also not possible to calculate the values of the rate constants manually. In order to determine which of the two proposed models better describes the obtained data, I employed the KinTek Explorer software (Johnson et al., 2009b, 2009a). KinTek utilizes simulations to fit the data with multiple kinetic parameters according to a predefined model. The fitting in KinTek suggested that Model 1 (Figure 3.11), in which syntaxin dimerization is the first step of the syntaxin-SNAP25 assembly, only slightly better describes the data as judged by the χ^2/DoF values (see Materials and Methods, section 2.2.2.1.3). Interestingly, assuming a one-step reaction, the values for the

association rate constant obtained by fitting in KinTek ($k_{on} \sim 6000 \text{ M}^{-1}\text{s}^{-1}$) correspond to the published values (Fasshauer and Margittai, 2004).

Comparison between the $1,5 \mu\text{M}$ traces of the preliminary syntaxin-syntaxin titration and the titration of syntaxin and SNAP25 (Figure 3.14) shows that the syntaxin-SNAP25 traces are placed in between the two phases of syntaxin traces. The first phase occurs before the association of syntaxin and SNAP25 starts. Moreover, it reaches a plateau before the syntaxin-SNAP25 interaction makes any significant progress. If the first phase corresponds to the dimer formation, it would make a strong case for Model 1 (Figure 3.11). On the other hand, the second phase of syntaxin titration starts shortly before the syntaxin-SNAP25 traces reach a plateau. If the second phase corresponds to dimer formation, that would mean that the 2:1 complex assembly occurs by Model 2 (Figure 3.12).

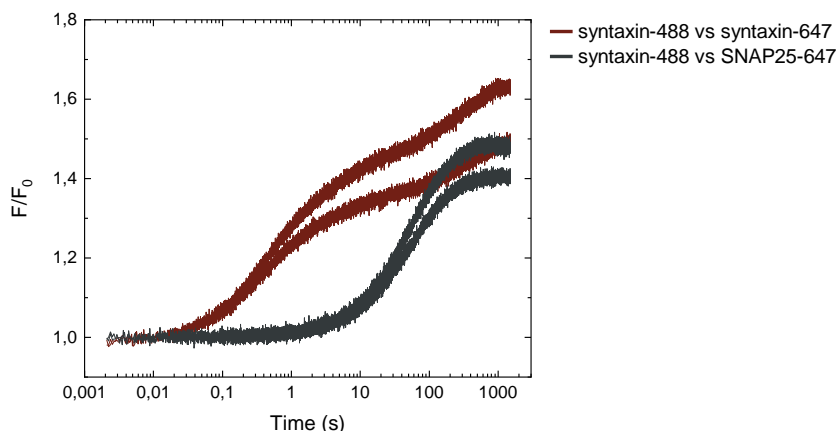


Figure 3.14. Comparison between the $1,5 \mu\text{M}$ titration traces of the syntaxin-syntaxin and the syntaxin-SNAP25 titration experiments. The first phase in the syntaxin-syntaxin titration traces reaches a plateau before the association between syntaxin and SNAP25 makes any significant progress. The second phase starts shortly before the syntaxin-SNAP25 traces reach a plateau. The x-axis showing the time was plotted in logarithmic scale for better observation of the differences between the traces from the two titration experiments. The relative fluorescence change (F/F_0) is a ratio between the measured fluorescence intensity (F) and the average fluorescence intensity of the first 100 data points (F_0).

To try to further clarify the syntaxin-SNAP25 interaction, I performed a dissociation experiment. Labeled syntaxin and SNAP25 were incubated for 10 minutes at 37°C to form the 2:1 complex. The preformed complex was subsequently mixed with the excess of unlabeled SNAP25 (Figure 3.15a) or unlabeled syntaxin (Figure 3.15b). In this experiment, as soon as the labeled components dissociate, their place in the complex would be taken by

Results

the unlabeled protein, leading to a decrease in fluorescence. This decrease will occur at the rate at which the tested protein dissociates from the complex.

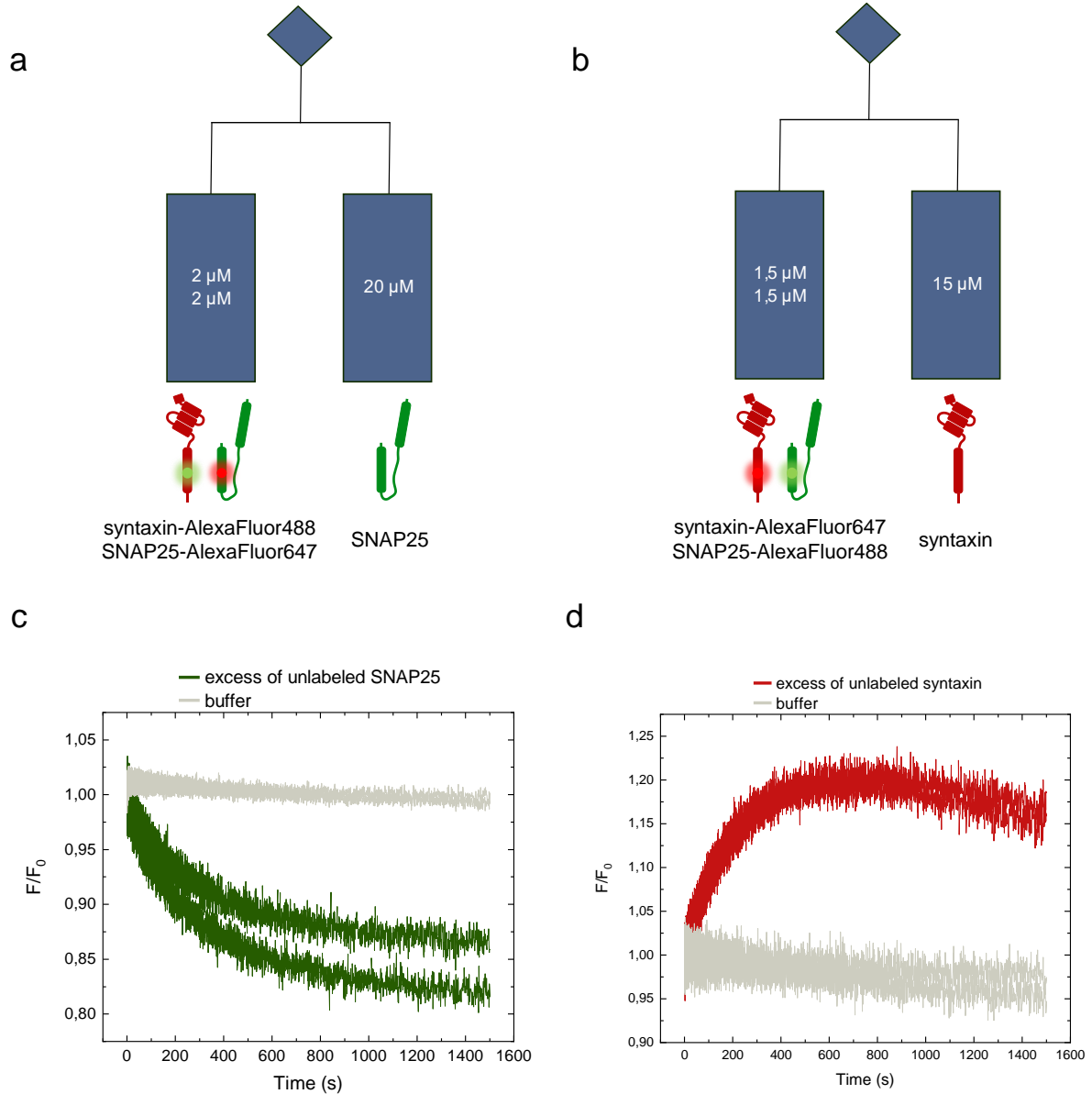


Figure 3.15. Dissociation of acceptor labeled SNAP25 and acceptor labeled syntaxin. Equimolar concentration of donor labeled syntaxin and acceptor labeled SNAP25 was placed in the left and syringe and preincubated to form the 2:1 syntaxin-SNAP25 complex. Excess concentration of unlabeled SNAP25 was placed in the righthand syringe (**a**). In the second experiment, equimolar concentration of donor labeled SNAP25 and acceptor labeled syntaxin was placed in the lefthand syringe and preincubated to form the 2:1 syntaxin-SNAP25 complex. Unlabeled syntaxin was placed in the righthand syringe

Results

at excess concentration **(b)**. In both experiments, the change in the acceptor channel was monitored. In the case of excess SNAP25, the acceptor fluorescence decreased over time and reached a plateau after approximately 1000 seconds **(c)**. The acceptor fluorescence in the case of excess syntaxin was surprisingly increasing in the first 600 seconds, after which it started decreasing **(d)**. The relative fluorescence change (F/F_0) is a ratio between the measured fluorescence intensity (F) and the average fluorescence intensity of the first 100 data points (F_0).

The SNAP25 dissociation experiment showed the expected decrease in the acceptor fluorescence (Figure 3.15c). Fitting of the titration traces to a monoexponential equation (1) provided the dissociation rate constant of $3,44 \times 10^{-3} \pm 0,02 \times 10^{-3} \text{ s}^{-1}$ (Figure 3.16).

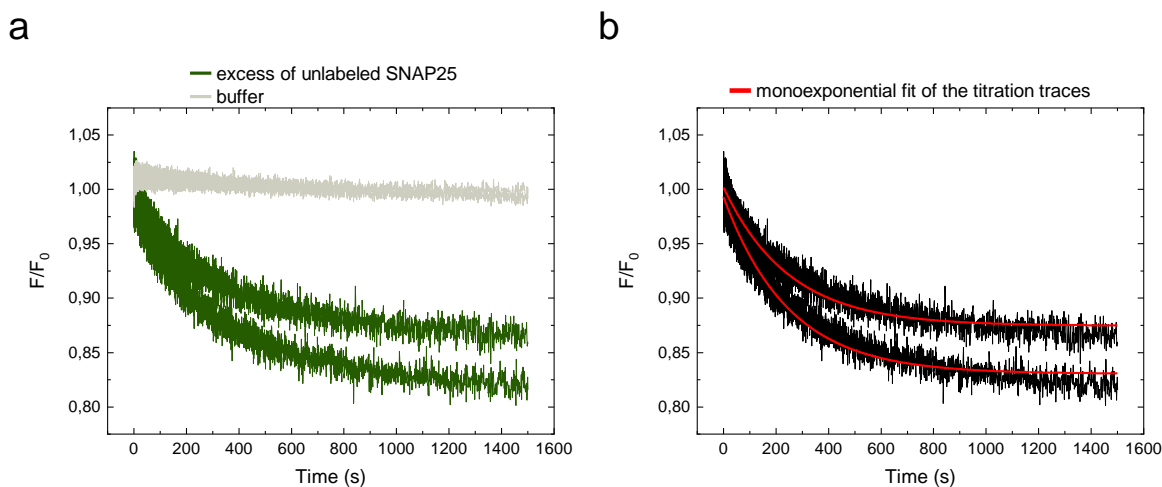


Figure 3.16. Fitting of the SNAP25 dissociation experiment. The obtained traces were fit to a monoexponential equation which provided the dissociation rate constant of $3,44 \times 10^{-3} \pm 0,02 \times 10^{-3}$. The relative fluorescence change (F/F_0) is a ratio between the measured fluorescence intensity (F) and the average fluorescence intensity of the first 100 data points (F_0).

In contrast to the SNAP25 dissociation, the syntaxin dissociation experiment showed an increase in the acceptor fluorescence for the first 600 seconds. The increase was initially very surprising and unexpected. However, it should be kept in mind that the labeled, preincubated sample contains free donor labeled SNAP25 because of the 2:1 ratio between syntaxin and SNAP25 in the complex. Additionally, if there is any labeled syntaxin that is not in the 2:1 complex, it can (in the case of Model 1) quickly interact with the unlabeled

syntaxin and then bind to the free, labeled SNAP25 causing the observed increase in the acceptor fluorescence.

3.1.3.1 Syntaxin and SN1-SN2 domains of SNAP25

Unlike syntaxin and synaptobrevin, SNAP25 possesses two SNARE domains, SN1 and SN2, that participate in the formation of the SNARE complex. When observing the syntaxin-SNAP25 complex, it is not clear whether only one or both SN1 and SN2 domains interact with syntaxin. To this end, I combined syntaxin with each of the two fragments of SNAP25 (SN1 (1-83) and SN2 (120-206)), as well as syntaxin with both of the SNAP25 fragments. The samples were incubated rolling overnight at 4°C and separated the next day on Superdex200 Increase 10/300 column.

Results of the size exclusion separation, presented in Figure 3.17, indicate that only the SN1 fragment of SNAP25 is able to form a complex with syntaxin when present alone. The complex between the H3 domain of syntaxin and the SN1 fragment of SNAP25 has been described before (Fasshauer et al., 1998b; Misura et al., 2001b). This experiment showed that, in addition to the H3 domain, a full soluble syntaxin that contains the H3, Habc and N-terminal domains, can form a complex with SN1 (Figure 3.17a, green trace).

In contrast to the syntaxin-SN1 sample, there was no difference between the chromatogram of syntaxin alone and in the presence of SN2, demonstrating that the SN2 fragment of SNAP25 alone cannot bind to syntaxin (Figure 3.17a, purple trace).

There was very little difference between the chromatograms of the syntaxin-SN1 and the syntaxin-SN1-SN2 samples, which can mean that a complex forms exclusively between syntaxin and the SN1 fragment of SNAP25. Chromatograms of SN1 and SN2 alone are not shown because both fragments lack amino acids that absorb light at 280 nm.

Peak fractions from the syntaxin-SN1 and syntaxin-SN1-SN2 samples were separated on an SDS-PAGE and visualized with Coomassie Brilliant Blue dye (Figure 3.17b). The band of SN1 in the syntaxin-SN1 peak fraction is noticeably weaker than the syntaxin band, which is to be expected considering the difference in the molecular mass, however, a different number of molecules in the complex is also not excluded. Unfortunately, SN1 and SN2 fragments have very similar sizes (9,6 kDa for SN1 and 9,8 kDa for SN2) and cannot be distinguished on the SDS-PAGE gel. It is therefore not clear from the size exclusion experiment if both SN1 and SN2, when present together, form a complex with syntaxin. A band that corresponds to both of them could be detected in the peak fraction on the gel together with the band of syntaxin. As with the syntaxin-SN1 sample, the band corresponding to SN1 and SN2 had weaker intensity when compared to the syntaxin band.

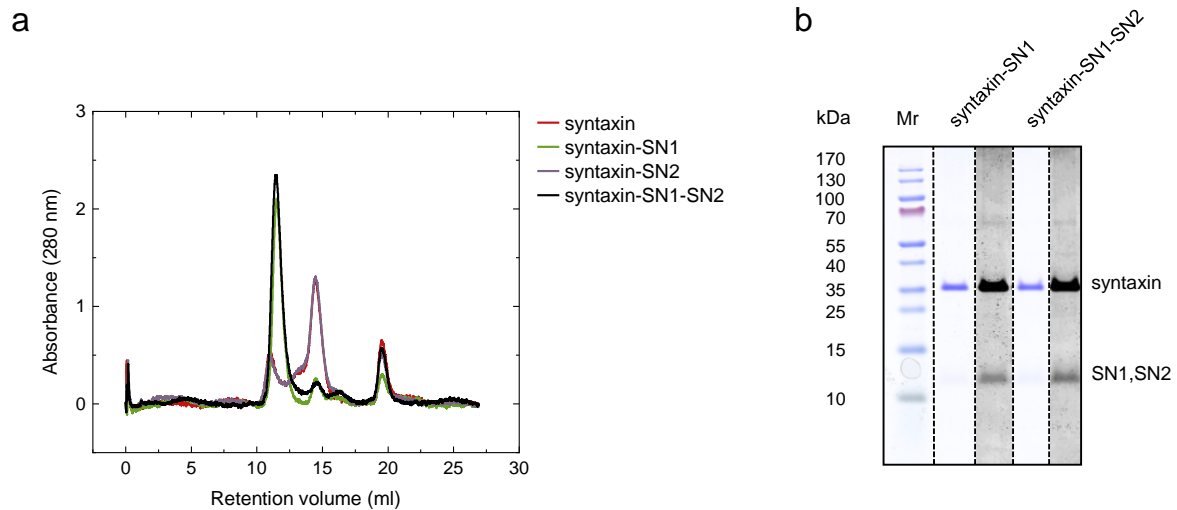


Figure 3.17. Size exclusion chromatography of the syntaxin-SN1, the syntaxin-SN2 syntaxin-SN1-SN2 complex. Size exclusion chromatography performed on overnight incubated syntaxin (red trace), syntaxin-SN1 (green trace), syntaxin-SN2 (purple trace) and syntaxin-SN1-SN2 (black trace) samples shows that the SN1 fragment of SNAP25 can form a complex with syntaxin alone or together with SN2 fragment (a). The peak fractions of the syntaxin-SN1 and the syntaxin-SN1-SN2 complexes were separated by SDS-PAGE and stained with Coomassie Brilliant Blue (b). Due to the low visibility of SN1 and SN2 band, the gel image was converted to a grayscale image and, after contrast adjustment, the presence of the SN1 and the SN1/SN2 bands was revealed. SN1 and SN2 fragments are of similar size making them indistinguishable on the SDS-PAGE.

3.2 PART II - INTERACTIONS INVOLVING ALL THREE SNARE PROTEINS

3.2.1 SNAP25 titration

Unlabeled SNAP25 was titrated over donor labeled syntaxin and acceptor labeled synaptobrevin. The concentration of both syntaxin and synaptobrevin in the reaction cell was 0,125 μ M, while SNAP25 was in 10-, 20-, 30-, 40- and 50-times concentration excess. The constant concentration and 1:1 ratio between the labeled proteins in all of the titration traces implies that any change in the fluorescent signal will be due to the change in the concentration of the unlabeled protein. Two of the proteins had to be premixed because of the difference between the number of proteins and the number of stopped flow syringes (three SNARE proteins and two syringes). In this case, syntaxin and synaptobrevin were

Results

premised since it was shown in Part I that these two proteins do not interact. The scheme of the experimental arrangement is shown in Figure 3.18a.

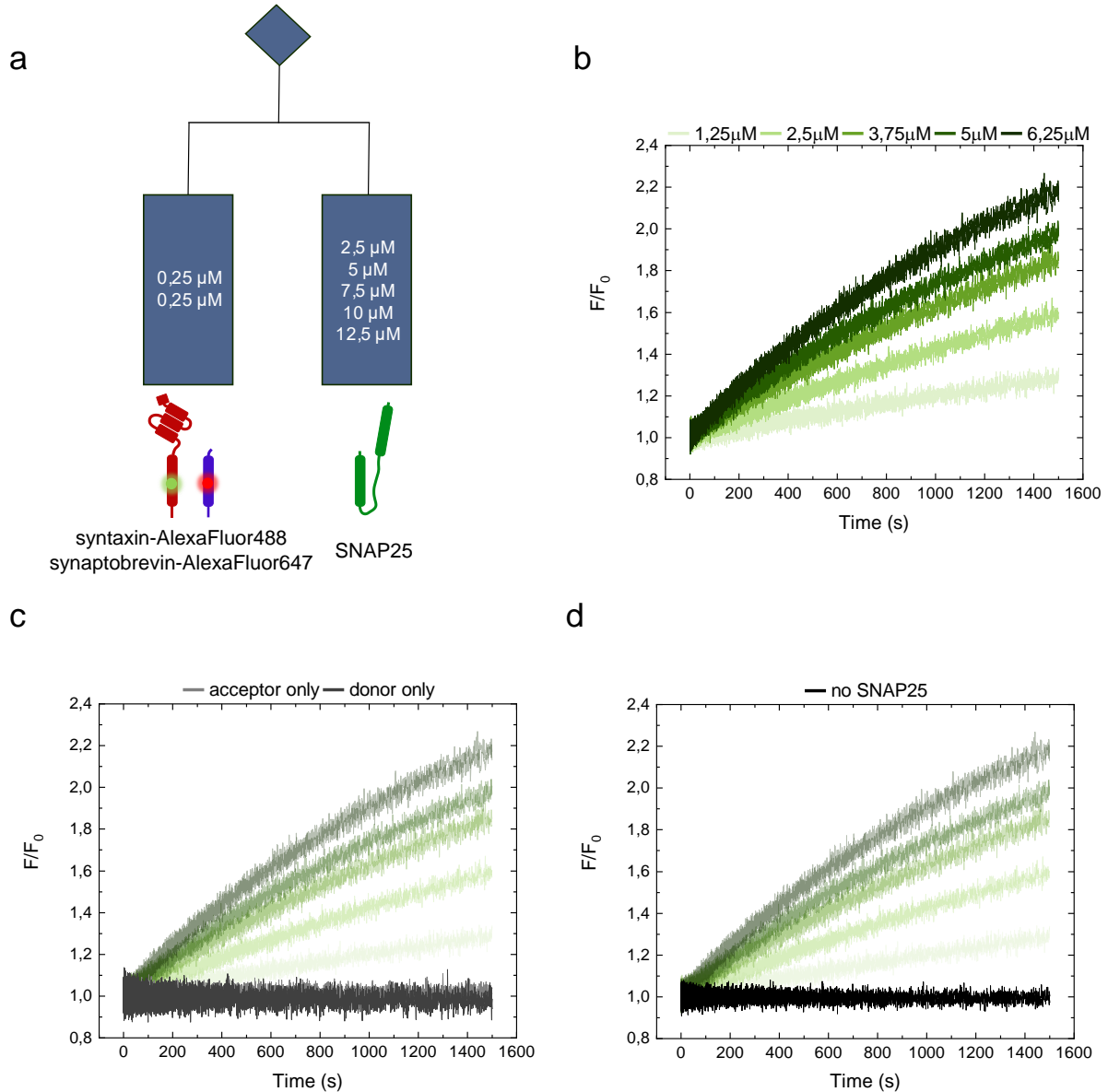


Figure 3.18. SNAP25 titration experiment. Schematic representation of the arrangement of the SNAP25 titration experiment. Donor labeled syntaxin and acceptor labeled synaptobrevin were placed in one syringe, both at a concentration of 0.25 μM (syringe on the lefthand side) while unlabeled SNAP25 was placed in a separate syringe at excess concentrations (syringe on the righthand side) (a). SNAP25 was titrated in 10-, 20-, 30-, 40- and 50-times molar excess over syntaxin and synaptobrevin. The donor dye was excited at 470 nm, and the change in the acceptor fluorescence was monitored over 1500 seconds. Acceptor fluorescence increased over time and with increasing SNAP25

Results

concentrations **(b)**. Omission of the acceptor (light grey) or the donor dye (dark grey) **(c)**, as well as the absence of SNAP25 (black) **(d)** did not show any change in fluorescence. The relative fluorescence change (F/F_0) is a ratio between the measured fluorescence intensity (F) and the average fluorescence intensity of the first 100 data points (F_0).

The recorded fluorescence increase indicates SNARE complex formation (Figure 3.18b). The amplitude and the observed rate constant were increasing with increasing SNAP25 concentration. Exclusion of the acceptor or the donor dye (Figure 3.18c), as well as the absence of SNAP25 (Figure 3.18d), did not show any change in fluorescence.

Titration traces were successfully fit to the monoexponential curve (1) to obtain k_{obs} (Figure 3.19). Setting the initial SNAP25 concentration much higher than the initial concentrations of syntaxin and synaptobrevin, $[SNAP25]_0 \gg [syntaxin]_0, [synaptobrevin]_0$ leads to the following relationship between k_{obs} and k_1, k_{-1} :

$$k_{obs} = k_1[SNAP25]_0 + k_{-1} \quad (3)$$

(modified from Bernasconi, 2012; Czerlinski, 1966)

Equation (3) is a linear equation and the plot of k_{obs} versus $[SNAP25]_0$ gives a straight line with the slope of k_1 and the intercept of k_{-1} (Figure 3.20).

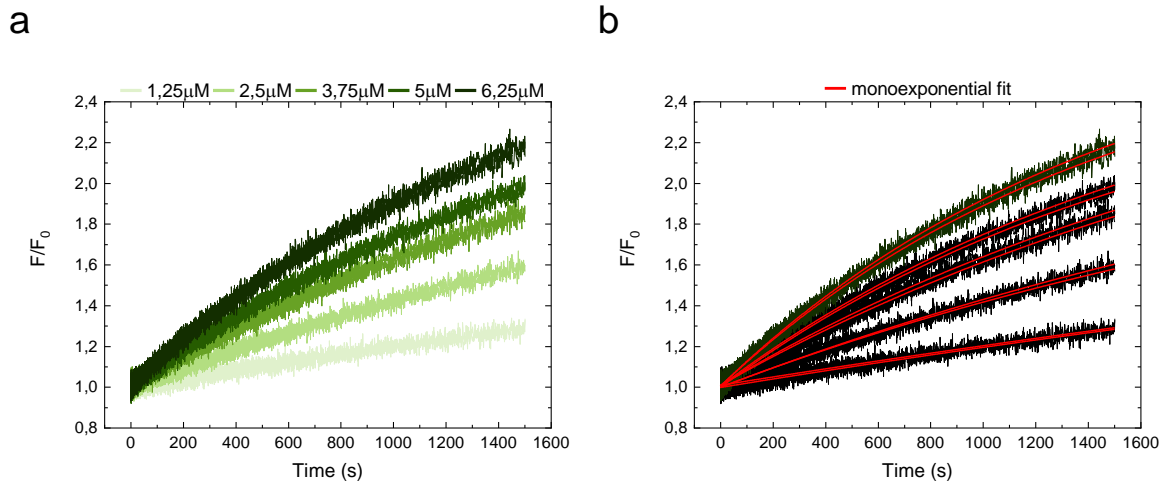


Figure 3.19. Fitting of the SNAP25 titration traces. The SNAP25 titration traces **(a)** were fit to a monoexponential equation. The fitted traces (red) are superimposed to the titration traces (now in black) **(b)**. The relative fluorescence change (F/F_0) is a ratio between the measured fluorescence intensity (F) and the average fluorescence intensity of the first 100 data points (F_0).

Results

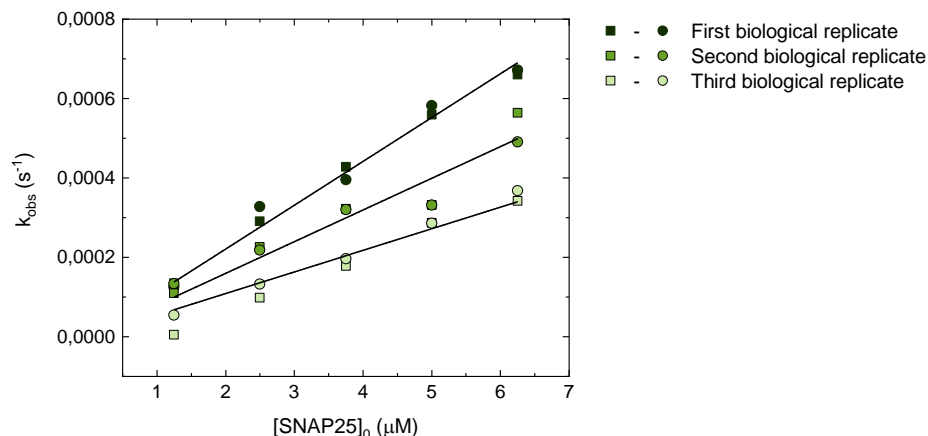


Figure 3.20. Concentration dependence of the k_{obs} for the SNAP25 titration experiment. The SNAP25 titration experiment was performed in three biological replicates (indicated with different shades of green) and two technical repeats (indicated with squares for the first and circles for the second repeat). The observed rate constants (k_{obs}) obtained from the monoexponential fit of the titration traces are plotted against initial concentrations of SNAP25 ($[SNAP25]_0$). The slope of the fitted lines (in black) gives the average k_1 value of $8,15 \times 10^{-5} \pm 2,89 \times 10^{-5}$, while the intercept value is close to zero, indicating that the reaction is irreversible.

The slope, which is equal to k_1 , was determined individually for all three biological replicates. The average obtained value for k_1 was $8,15 \times 10^{-5} \pm 2,89 \times 10^{-5}$, while the intercept, which represents k_{-1} , was close to zero, implying that the reaction is irreversible. Until the reaction steps that the obtained rate constants describe in the SNARE assembly model are known, the units of the rate constants are not defined and are presented at values as determined by the fitting. This caution is applied throughout the following text.

Identification of one k_{obs} for a reaction that, without a doubt, consists of more than one step means simply that at experimental conditions in which $[SNAP25]_0$ is in excess, individual steps could not be resolved. In Part I it was shown that only syntaxin and SNAP25 are able to form a stable complex. When SNAP25 is in excess, the reaction between syntaxin and SNAP25 will be “pushed” to the formation of the syntaxin-SNAP25 complex that would then be available for synaptobrevin binding. The signal from complex formation could only be detected once syntaxin and synaptobrevin come close. The only change that can be measured in this experiment comes from the varying concentrations of SNAP25. The obtained k_1 will thus most likely be the rate of formation of the syntaxin-SNAP25 complex multiplied by a number representing the binding of synaptobrevin.

3.2.2 Syntaxin titration

Donor labeled SNAP25 and acceptor labeled synaptobrevin, both at a concentration of 0,25 μM , were placed together in one stopped flow syringe. The other syringe contained unlabeled syntaxin in excess (Figure 3.21a) that was then titrated over SNAP25 and synaptobrevin.

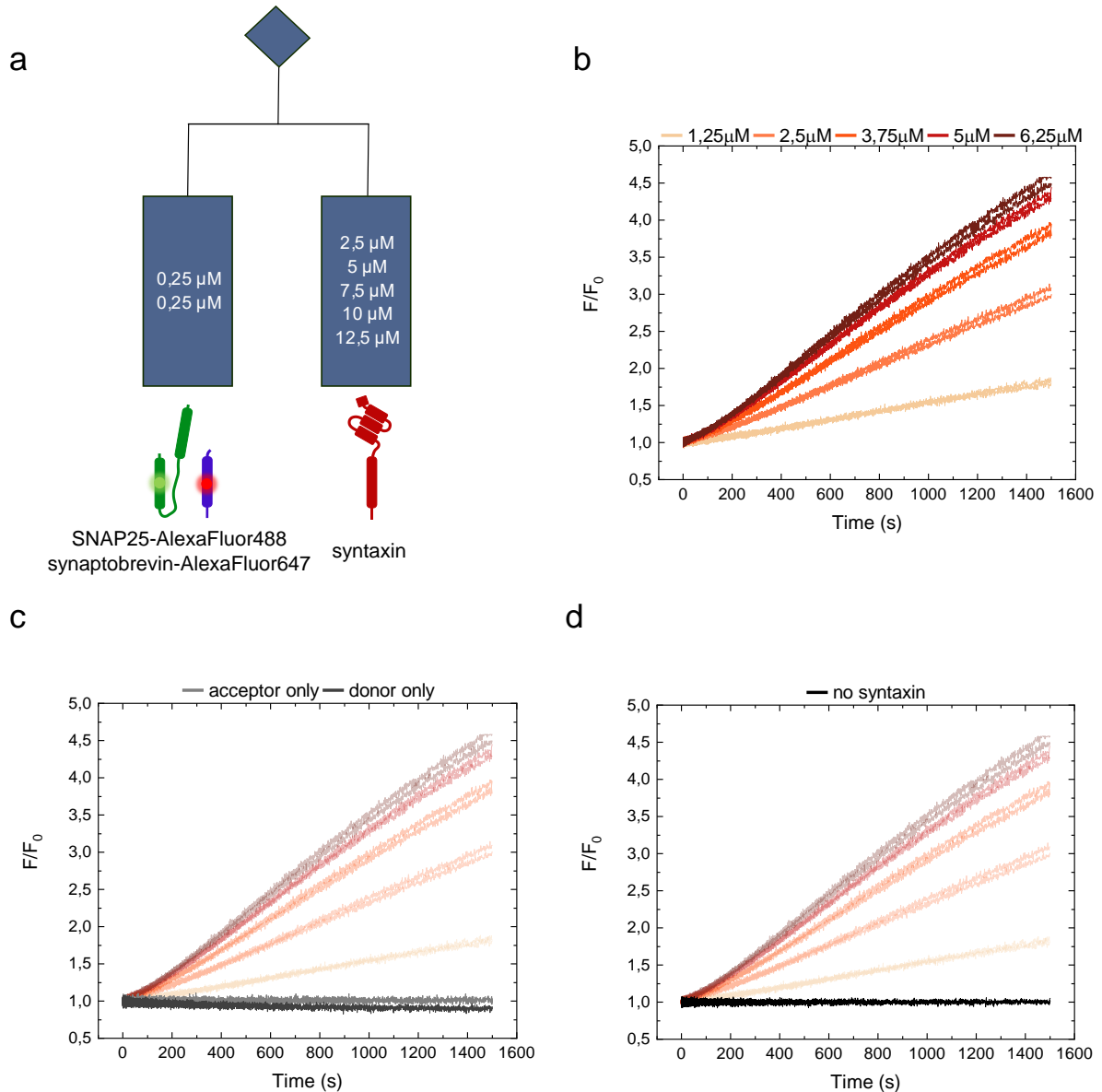


Figure 3.21. Syntaxin titration experiment. Schematic representation of the arrangement of the syntaxin titration experiment is shown. Donor labeled SNAP25 and acceptor labeled synaptobrevin, 0,25 μM each, were placed together in one syringe (the syringe on the lefthand side), while the unlabeled syntaxin, at excess concentrations, was

Results

placed in a separate syringe (syringe on the righthand side) (a). Syntaxin was titrated over SNAP25 and synaptobrevin in a 10-, 20-, 30- 40-, 50-times molar excess. The donor dye was excited and the change in fluorescence of the acceptor dye was monitored over 1500 seconds. The change in the acceptor fluorescence showed two distinct phases (b). The acceptor only (light grey) and donor only (dark grey) controls (c) as well as the omission of syntaxin (black) (d) remained flat. The biological replicates are indicated by different shades of red, while the technical repeats are shown as different shapes (squares and circles). The relative fluorescence change (F/F_0) is a ratio between the measured fluorescence intensity (F) and the average fluorescence intensity of the first 100 data points (F_0).

The titration of syntaxin over SNAP25 and synaptobrevin showed two distinct phases that could be fit with the biexponential equation (Figure 3.22):

$$y = A_1 e^{(-k_{1obs}x)} + A_2 e^{(-k_{2obs}x)} + C \quad (4)$$

where y represents the fluorescence intensity (F), x is the time, A_1 is the change in fluorescence amplitude governed by the first observed rate constant, k_{1obs} the first observed rate constant, A_2 is the change in the fluorescence amplitude governed by the second observed rate constant, k_{2obs} the second observed rate constant and C the starting point of the fit.

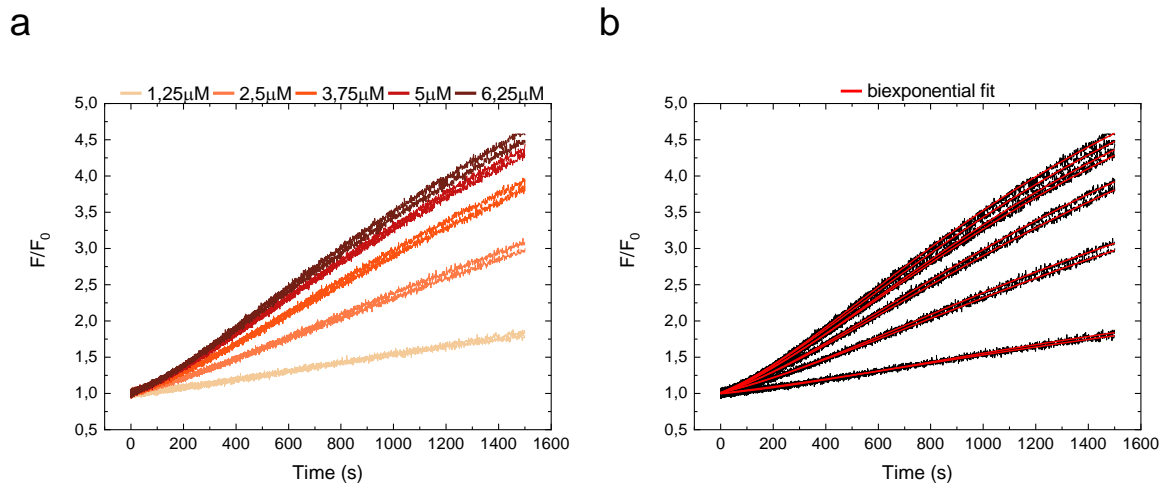


Figure 3.22. Fitting of the syntaxin titration traces. Syntaxin titration traces (a) were fitted to the biexponential equation. The resulting fitted curve was overlayed with the titration traces (in black) (b). The relative fluorescence change (F/F_0) is a ratio between the measured fluorescence intensity (F) and the average fluorescence intensity of the first 100 data points (F_0).

Results

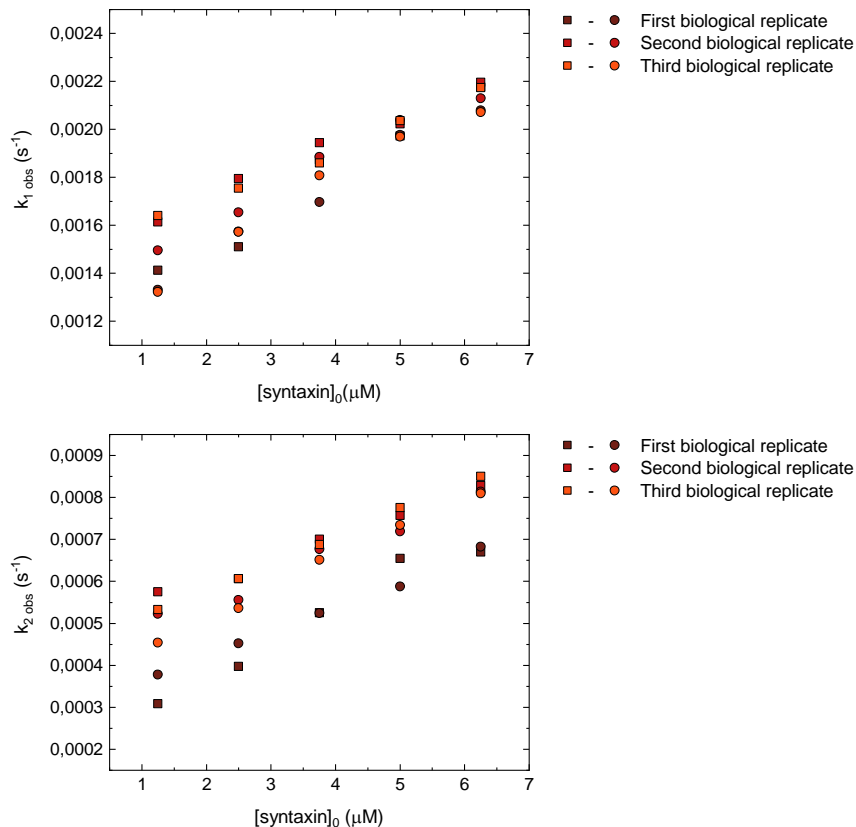


Figure 3.23. Concentration dependence of the k_{1obs} and k_{2obs} for the syntaxin titration experiment. The syntaxin titration experiment was performed in three biological replicates (indicated with different shades of red) and two technical repeats (indicated with squares for the first and circles for the second repeat). The observed rate constants, k_{1obs} (upper graph) and k_{2obs} (lower graph), obtained from the biexponential fitting of the syntaxin titration traces, were plotted against the initial concentration of syntaxin, $[syntaxin]_0$. Both observed rates change with the changing concentration of syntaxin showing that both observed processes depend on this protein.

Fitting the titration traces with the biexponential fit provided values for k_{1obs} and k_{2obs} . As shown in Figure 3.23, both of the obtained observed rates were dependent on syntaxin concentration and their similar magnitudes implied that there is a strong coupling between the two reaction steps (Bernasconi, 2012). As a result of this coupling, the expression that relates the observed rate constants with the real rate constants will, for both k_{1obs} and k_{2obs} , be a complex expression that includes all four processes involved in the reaction.

Determining the reaction steps that these four rate constants describe requires a closer look at the fitted traces. The biexponential fitting equation (4) provides, apart from k_{1obs} and k_{2obs} , values for the amplitudes, A_1 and A_2 . These amplitudes represent a part of the total change in fluorescence amplitude of the reaction that is described by the

Results

corresponding observed rate constants: A_1 is the change in the amplitude related to the process described by k_{1obs} , and A_2 is the change in the amplitude related to the process described by k_{2obs} . The sign of the amplitude, whether it is positive or negative, reveals whether the fluorescence is decreasing or increasing. The amplitudes obtained with biexponential fitting of the syntaxin titration data are of opposite signs, which shows that there is an initial decrease in fluorescence, followed by an increase. The initial decrease in fluorescence could be interpreted as the interaction between donor labeled SNAP25 and acceptor labeled synaptobrevin that is disrupted or otherwise modified by the arrival of unlabeled syntaxin. However, in Part I, it was shown by stopped-flow (Figure 3.3) and gel filtration (Figure 3.4) that SNAP25 and synaptobrevin do not interact even at concentrations 10-50 times higher than the ones used in this experiment. Careful examination of the control traces (Figure 3.24) shows that the donor only control, in which the acceptor dye is omitted, decreases at the observed rate constant similar to the k_{1obs} of the titration trace with the equal syntaxin concentration (namely, the middle titration concentration of 3,75 μ M). Acceptor only and no syntaxin controls do not change, indicating that the observed decrease in fluorescence comes from the interaction of the donor labeled SNAP25 and unlabeled syntaxin. This leads to a conclusion that k_{1obs} describes the formation of syntaxin-SNAP25 complex, while k_{2obs} describes binding of synaptobrevin to syntaxin-SNAP25 complex.

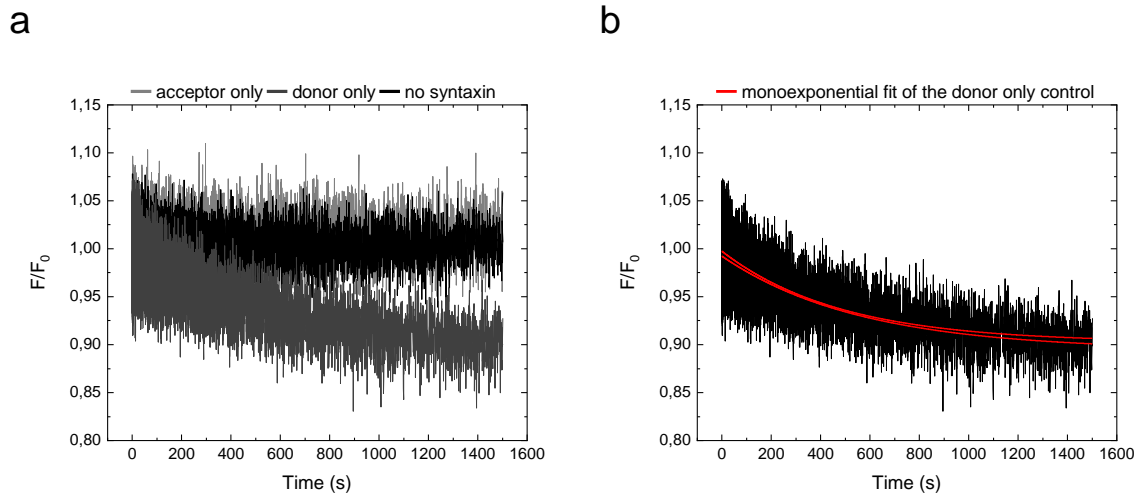


Figure 3.24. Isolated view of the syntaxin titration control traces. Controls of the syntaxin titration experiment: acceptor only in gray, donor only in dark gray and no syntaxin in black, show that the initial decrease in fluorescence of the titration traces comes from donor labeled SNAP25 interacting with unlabeled syntaxin (a). Donor only control could be fit to a monoexponential equation with the obtained observed rate constant matching the k_{1obs} obtained from the corresponding titration trace (b).

Results

The detailed derivation for the k_{1obs} and k_{2obs} , that can be found in Bernasconi, 2012, was modified in order to accommodate the two-step reaction at hand (syntaxin + SNAP25 \leftrightarrow syntaxin-SNAP25 + synaptobrevin \rightarrow SNARE) and the conditions at which the experiment was performed (excess syntaxin). The final conclusion of these derivations is that k_1 , k_{-1} , k_2 and k_{-2} can be estimated from the sum and the multiplication of the two observed rate constants:

$$k_{1obs} + k_{2obs} = k_1[syntaxin]_0 + k_{-1} + k_2(\bar{C}' + \overline{synaptobrevin}) + k_{-2} \quad (5)$$

$$k_{1obs} \times k_{2obs} = [k_1 k_2(\bar{C}' + \overline{synaptobrevin})][syntaxin]_0 + k_{-1} k_{-2} \bar{C}' + k_{-1} k_{-2} \quad (6)$$

$$\bar{C}' = \overline{syntaxin - SNAP25} - \Delta syntaxin$$

(modified from Bernasconi, 2012)

In expressions (5) and (6), $[syntaxin]_0$ represents the initial concentration of syntaxin, $\Delta syntaxin$ the change in syntaxin concentration, $\overline{syntaxin - SNAP25}$ the equilibrium concentration of syntaxin-SNAP25 complex and $\overline{synaptobrevin}$ the equilibrium concentration of synaptobrevin.

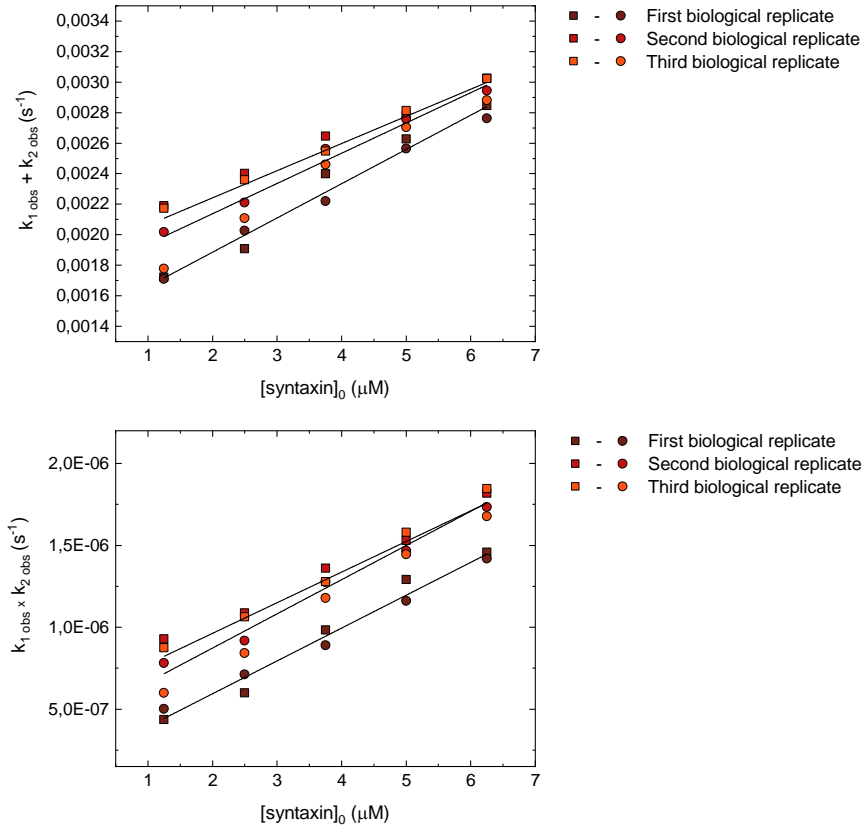


Figure 3.25. Concentration dependence of the sum and the multiplication of k_{1obs} and k_{2obs} for the syntaxin titration experiment. The sum (upper graph) and the multiplication (lower graph) of k_{1obs} and k_{2obs} were plotted against initial syntaxin concentration, $[syntaxin]_0$. The data was fit to a linear equation providing values for the slope and the intercept that were used for calculating of the rate constants.

Although seemingly complicated, equations (5) and (6) are linear equations. Plotting the sum and the multiplication of k_{1obs} and k_{2obs} versus the initial concentration of syntaxin, $[syntaxin]_0$, and fitting to a linear equation will provide slopes and intercepts that can be used to calculate the values of the rate constants (Figure 3.25).

The application of the previously described approach, together with the assumption that synaptobrevin binding is irreversible ($k_{-2} = 0$), yielded $k_1 = 2,23 \times 10^{-4} \pm 0,09 \times 10^{-4}$, $k_{-1} = 7,8 \times 10^{-4} \pm 1,24 \times 10^{-4}$ and $k_2 = 4,7 \times 10^{-4} \pm 2,15 \times 10^{-4} / \overline{synaptobrevin}$. The value for k_2 could not be determined further. The high uncertainty arises from uncertainty propagation during calculation.

3.2.3 Synaptobrevin titration

Unlabeled synaptobrevin was titrated over donor labeled syntaxin and acceptor labeled SNAP25. The experimental arrangement was slightly different to previously described stopped flow experiments involving the three SNARE proteins. Specifically, the labeled proteins were placed in separate syringes to avoid complex formation between syntaxin and SNAP25 (Figure 3.26a). As shown in section 3.1.3, syntaxin and SNAP25 interact to form a likely 2:1 complex, and previous reports have suggested that formation of this complex is a dead-end pathway in the reaction of SNARE complex formation (Fasshauer and Margittai, 2004; Wiederhold and Fasshauer, 2009). To ensure the progression of SNARE complex assembly, syntaxin and SNAP25 were kept separate before triggering the reaction.

As before, the acceptor fluorescence emission was monitored for 1500 seconds. The increase in the acceptor fluorescence was less prominent compared to the increase observed during SNAP25 and syntaxin titrations. Titration traces showed two phases which fit best to the following exponential-linear equation (Figure 3.27):

$$y = A_1 e^{(-k_{1obs}x)} + k_{2obs}x + C \quad (7)$$

Results

where y is the change in fluorescence intensity (F), A_1 is the change in fluorescence amplitude of the process described by k_{1obs} , k_{1obs} is the first observed rate constant, k_{2obs} is the second observed rate constant, x is the time of the observation and C is the starting point of the fit. The appearance of a linear part in the fitting equation means that the observed process is so slow that only a linear portion of the exponential increase could be observed.

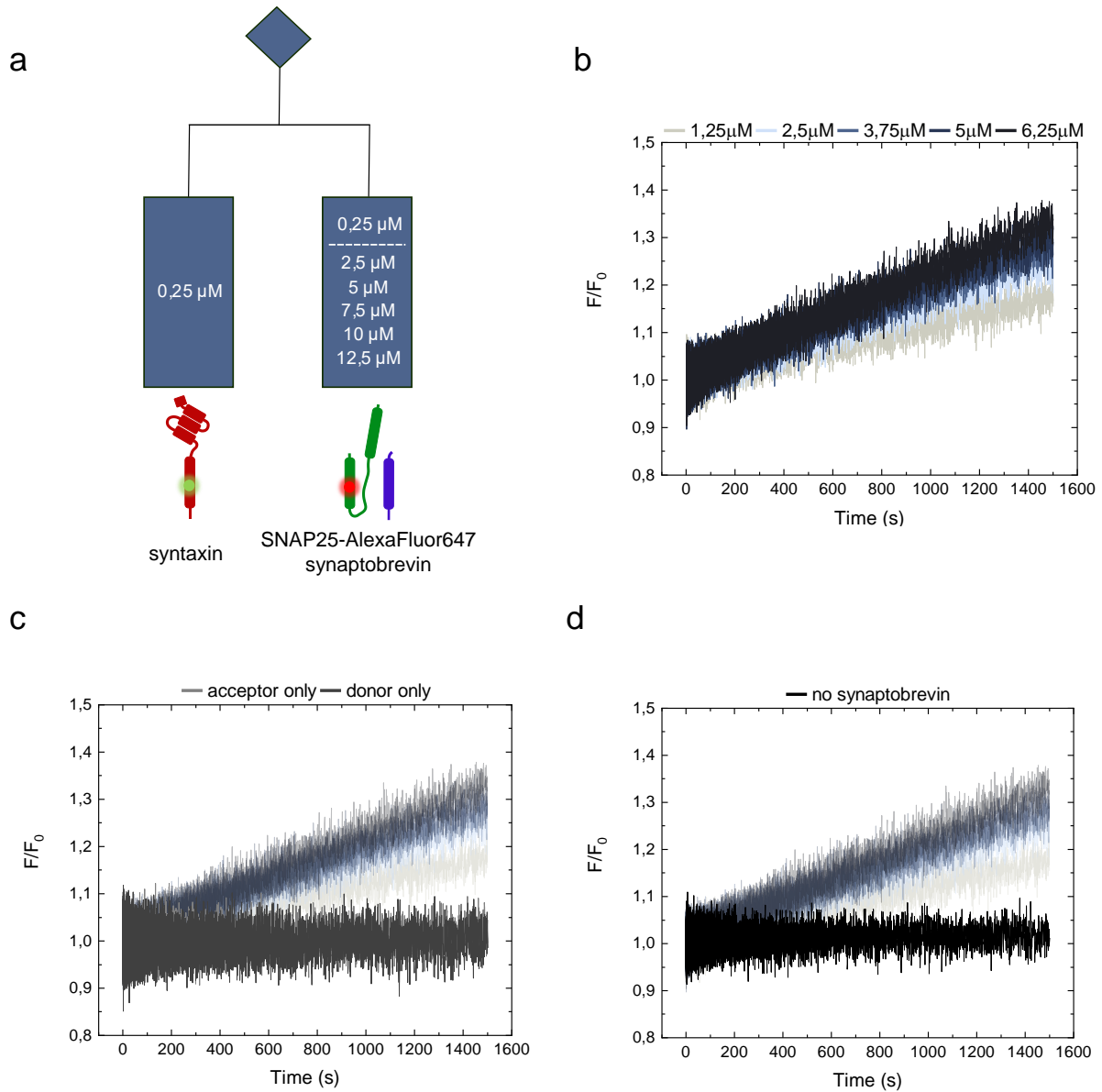


Figure 3.26. Synaptobrevin titration experiment. Schematic representation of the synaptobrevin titration experimental arrangement. Donor labeled syntaxin was placed in the lefthand syringe, while acceptor labeled SNAP25 and excess of unlabeled synaptobrevin were mixed and placed in the righthand syringe at concentrations indicated on the scheme

Results

(a). Synaptobrevin was titrated in 10- 20- 30- 40- and 50-times molar excess to both syntaxin and SNAP25. The acceptor fluorescence increased over the observed time of 1500 seconds and with increasing synaptobrevin concentrations (b). Acceptor only (light grey) and donor only (dark grey) controls did not show any change in fluorescence (c), while no synaptobrevin control (black) showed a slight increase in the first 200 seconds, reflecting the syntaxin-SNAP25 interaction, and then continues to be flat for the rest of the observed time (d). The relative fluorescence change (F/F_0) is a ratio between the measured fluorescence intensity (F) and the average fluorescence intensity of the first 100 data points (F_0).

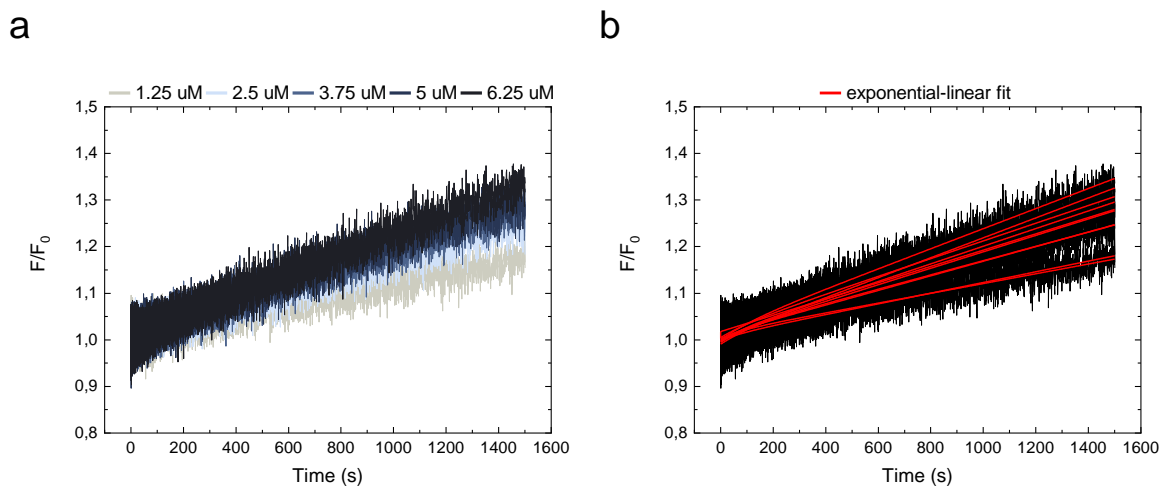


Figure 3.27. Fitting of the synaptobrevin titration traces. Synaptobrevin titration traces (a) were fit with the exponential-linear equation. The curve obtained from the fit (red) was overlayed with the titration traces (in black) (b). The relative fluorescence change (F/F_0) is a ratio between the measured fluorescence intensity (F) and the average fluorescence intensity of the first 100 data points (F_0).

Plotting the k_{1obs} versus the initial concentration of synaptobrevin, $[synaptobrevin]_0$, showed that the k_{1obs} is independent of the synaptobrevin concentration (Figure 3.28, upper graph). Since the increase in fluorescence reflects the close apposition between the donor labeled syntaxin and the acceptor labeled SNAP25, this result indicates that the formation of syntaxin-SNAP25 complex occurs first, even in the presence of high concentrations of synaptobrevin. In contrast, k_{2obs} showed hyperbolic dependence of synaptobrevin concentration (Figure 3.28, lower graph). Considering the conditions under which titration was performed, $[synaptobrevin]_0 \gg [syntaxin]_0, [SNAP25]_0$, the following equation can describe the relationship between k_{2obs} and the rate constants:

Results

$$k_{2obs} = \frac{k_1 k_2 [\text{synaptobrevin}]_0}{k_{-1} + k_2 [\text{synaptobrevin}]_0} \quad (\text{Connors, 1990}) \quad (8)$$

Based on the notion that the SNARE complex formation is irreversible, k_{-2} was considered to be 0 and for that reason it does not appear in equation (8). Fitting of the k_{2obs} - $[\text{synaptobrevin}]_0$ data was done with a formula for rectangular hyperbola:

$$y = a \times \frac{bx}{1+bx} \quad (9)$$

where a and b correspond to the vertical and the horizontal asymptotes, respectively. Combining equation (8) with equation (9) results in a corresponding to k_1 , and b to k_2/k_{-1} . The results of the fit are: $a = k_1 = 5,59 \times 10^{-4} \pm 0,46 \times 10^{-4}$, $b = k_2/k_{-1} = 0,39 \pm 0,11$. The values for k_2 and k_{-1} could not be further determined from the fitting.

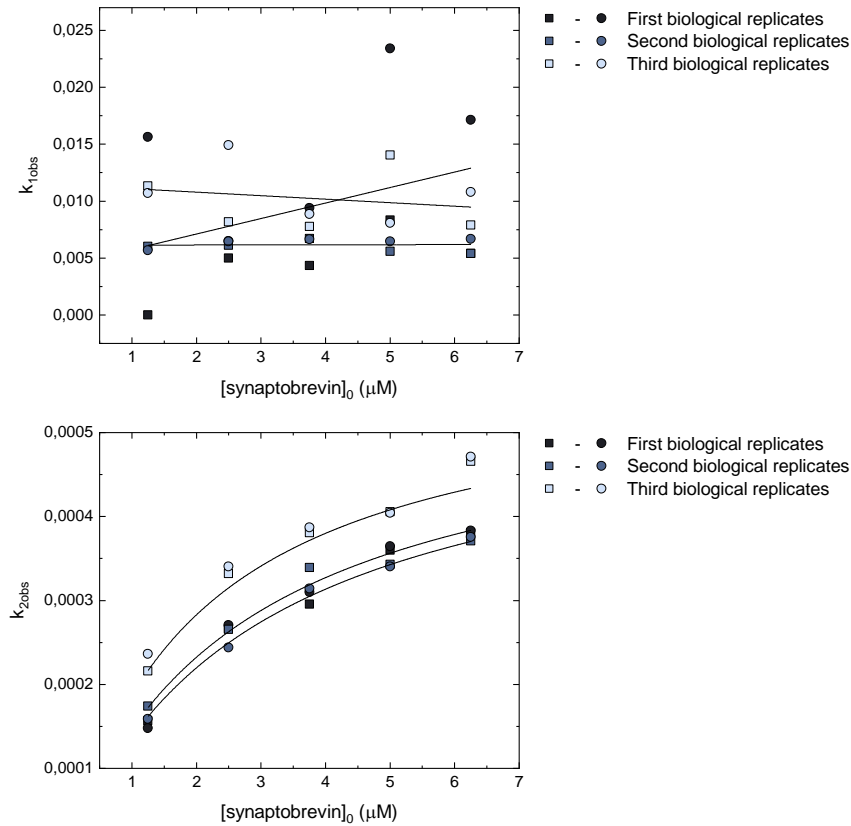


Figure 3.28. Concentration dependence of the k_{1obs} and k_{2obs} for the synaptobrevin titration experiment. The observed rate constants, k_{1obs} and k_{2obs} , obtained from the exponential-linear fitting of the titration traces, were plotted against the initial concentration of synaptobrevin, $[\text{synaptobrevin}]_0$. The first observed rate constant, k_{1obs} , changed independently of the synaptobrevin concentration (upper graph). The second observed rate constant, k_{2obs} , showed a hyperbolic dependence of synaptobrevin concentration (lower graph). The biological replicates are represented by different colors, while the technical repeats are shown as different shapes (squares and circles).

Results

All of the previously performed experiments, including this one, pointed to the syntaxin-SNAP25 complex as the first step of the SNARE assembly reaction. To be able to directly measure the rate of the synaptobrevin binding, syntaxin and SNAP25 were combined in an attempt to pre-form the syntaxin-SNAP25 complex to which then synaptobrevin can bind. As before, syntaxin was labeled with the donor and SNAP25 with the acceptor dye, while unlabeled synaptobrevin was titrated in excess. Figure 3.29a shows schematically the experimental arrangement.

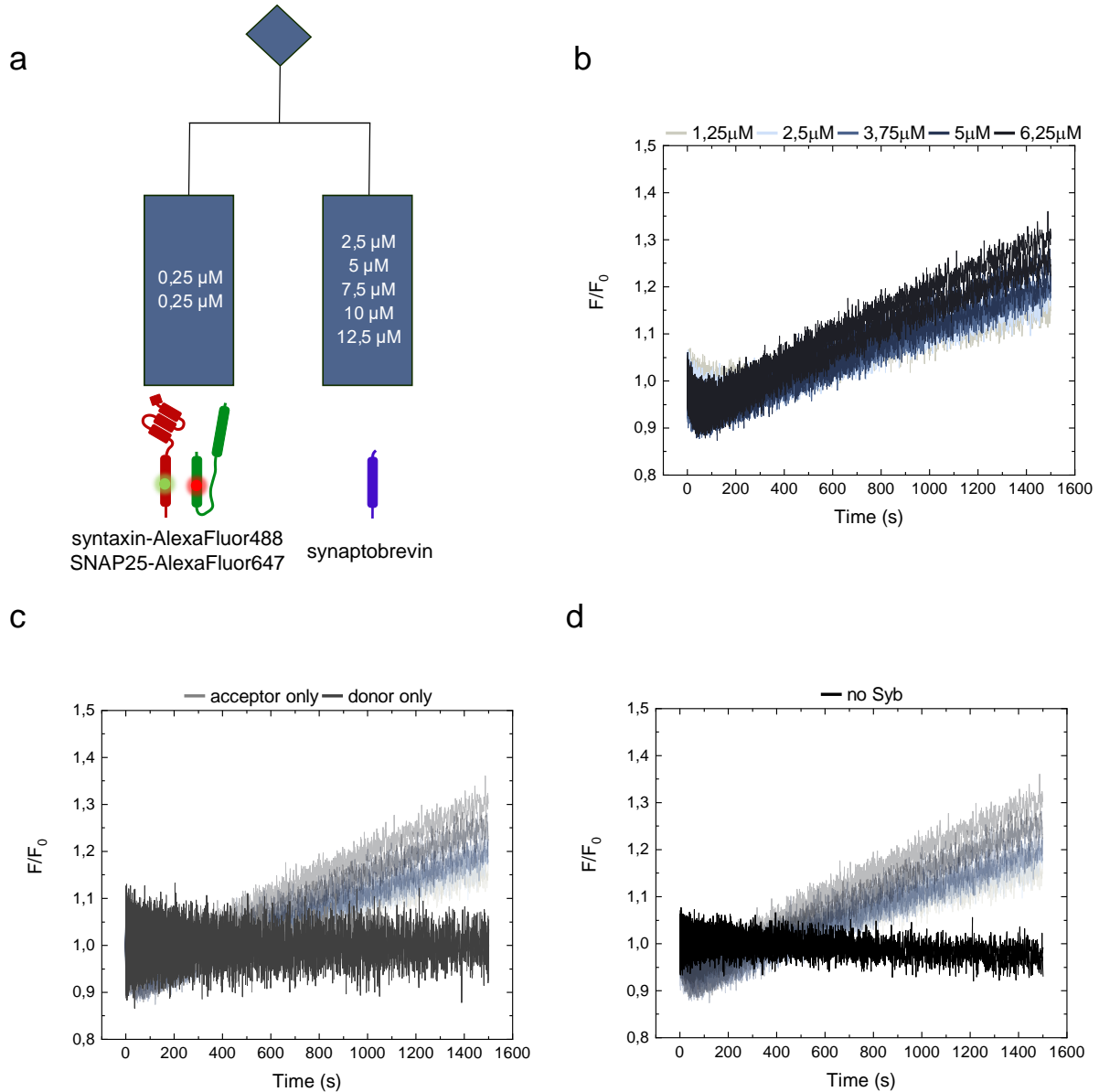


Figure 3.29. *The second synaptobrevin titration experiment. Schematic representation of the second unlabeled synaptobrevin titration (a). Donor labeled syntaxin and acceptor labeled SNAP25 were mixed and placed in the lefthand syringe, while the*

righthand syringe contained increasing concentrations of unlabeled synaptobrevin. Titration traces of synaptobrevin over premixed syntaxin and SNAP25 (b). The first 100 seconds show a surprising decrease in the acceptor fluorescence followed by an increase over the remaining 1400 seconds. Absence of the acceptor or of the donor dye did not show any fluorescence change (c). When synaptobrevin was omitted, there was a slight decrease in fluorescence that could potentially be caused by photobleaching or by the dilution-prompted disassembly of the syntaxin-SN25 complex (d). The relative fluorescence change (F/F_0) is a ratio between the measured fluorescence intensity (F) and the average fluorescence intensity of the first 100 data points (F_0).

Titration traces show two obvious phases with a surprising initial decrease in the acceptor fluorescence that is absent from all controls (Figure 3.29c,d). Fitting of the traces with exponential-linear equation (7) (Figure 3.30) and subsequent plotting of acquired k_{1obs} and k_{2obs} to initial synaptobrevin concentration (Figure 3.31) revealed that both observed rate constants depend on synaptobrevin. Considering that the fluorescent labels are on syntaxin and SNAP25, this experiment suggests that syntaxin and SNAP25 alone form a complex, most likely 2:1, that is dissociated or otherwise rearranged by the arrival of synaptobrevin.

Given that the k_{1obs} was more than 10-fold higher than k_{2obs} , the first process, described by k_{1obs} , will reach equilibrium before the second one makes any meaningful progress and can be monitored in isolation (Bernasconi, 2012). Fitting the graph of k_{1obs} -[synaptobrevin]₀ (Figure 3.31, the upper graph) to equation (3), replacing [SNAP25]₀ with [synaptobrevin]₀, gave k_1 of $7,75 \times 10^{-3} \pm 0,47 \times 10^{-3}$ and k_{-1} of ~ 0 . Consistent with the preceding experiment, k_{2obs} again showed hyperbolic dependence on synaptobrevin (Figure 3.31, the lower graph). Fitting of the k_{2obs} -[synaptobrevin]₀ graph to equation (8) and subsequent combination with equation (9) gave similar results: k_1 of $6,07 \times 10^{-4} \pm 0,82 \times 10^{-4}$ and k_2/k_{-1} of $0,34 \pm 0,08$. It is quite evident that k_1 and k_{-1} obtained through the k_{1obs} -[synaptobrevin]₀ graph do not correspond to k_1 and k_{-1} obtained from k_{2obs} -[synaptobrevin]₀. To avoid confusion, k_1 and k_{-1} calculated from k_{2obs} will be labeled as k_1' and k_{-1}' .

One possible explanation for the k_1 , k_{-1} and k_1' , k_{-1}' discrepancy is that they describe different processes. In that case, the first observed process, described by k_{1obs} , would not directly precede and influence the second process described by k_{2obs} .

Results

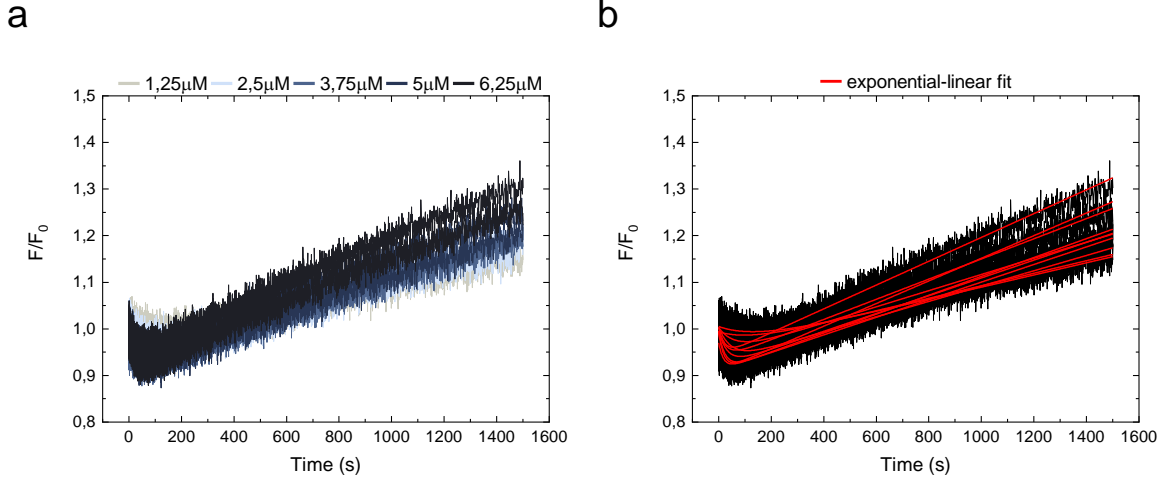


Figure 3.30. Fitting of the second synaptobrevin titration traces. The titration traces of the second unlabeled synaptobrevin titration experiment (a) were fit to an exponential-linear equation (b, red line) to obtain the observed rate constants. The relative fluorescence change (F/F_0) is a ratio between the measured fluorescence intensity (F) and the average fluorescence intensity of the first 100 data points (F_0).

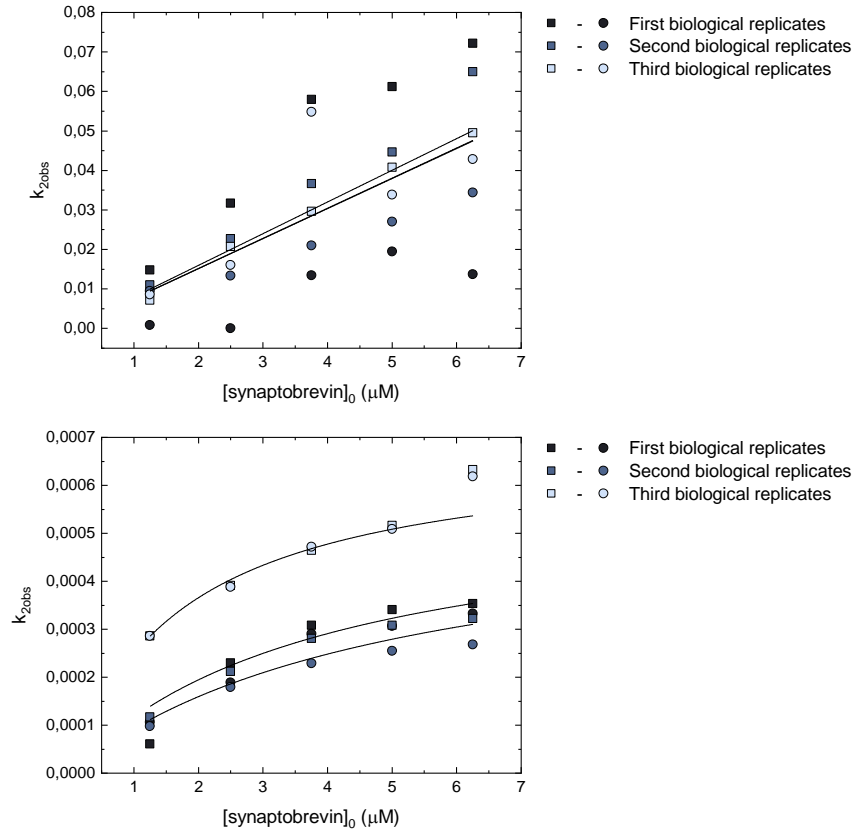


Figure 3.31. Concentration dependence of the k_{1obs} and k_{2obs} for the second

synaptobrevin titration experiment. The two observed rate constants, k_{1obs} and k_{2obs} , obtained by exponential-linear fitting of the second synaptobrevin titration traces, were plotted against the initial concentration of synaptobrevin, $[synaptobrevin]_0$. The first observed rate constant, k_{1obs} , shows linear dependence of $[synaptobrevin]_0$ (upper graph) and was fit to a linear equation yielding a slope of $7,75 \times 10^{-3} \pm 0,47 \times 10^{-3}$ and an intercept of ~ 0 . The second observed rate constant, k_{2obs} , showed a hyperbolic dependence of $[synaptobrevin]_0$ (lower graph) and was fit to an equation for rectangular hyperbola, giving $6,07 \times 10^{-4} \pm 0,82 \times 10^{-4}$ and $0,34 \pm 0,08$ as horizontal and vertical asymptote, respectively. The biological replicates are indicated by different shades of red, while the technical repeats are shown as different shapes (squares and circles).

3.2.4 Testing for stable subcomplexes

Titration experiments showed that SNARE complex formation occurs in at least two steps with the first step being the formation of the syntaxin-SNAP25 complex. SNAP25 brings two SNARE domains to the SNARE complex, unlike syntaxin and synaptobrevin that bring only one. During the titration experiments, only the SN1 SNARE domain of SNAP25 was fluorescently labeled. This means that all titration experiments show the point at which SN1 interacts with either syntaxin or synaptobrevin, while SN2 remains practically invisible. More detailed gel filtration experiments testing SN1 and SN2 interactions with syntaxin showed that SN2 does not bind to syntaxin in the absence of SN1 (section 3.1.3.1). SN2 is tightly bound in the assembled SNARE complex (Sutton et al., 1998), but it is not clear at what point it enters the complex and whether synaptobrevin binding precedes its binding. To get a better understanding of the order in which SN2 and synaptobrevin assemble in the SNARE complex, I examined the possibility of stable subcomplex formation. To this end, I incubated 5 μ M of syntaxin, SN1, SN2 and synaptobrevin in different combinations overnight and performed size exclusion chromatography. Both incubation and size exclusion were performed at 4°C. Temperature changes were avoided in order to preserve the equilibrium that was established overnight.

Results of the size exclusion chromatography show that both SN1 (Figure 3.32) and SN2 (Figure 3.33) are able to form a complex with syntaxin and synaptobrevin. The complex formed by syntaxin, SN1 and synaptobrevin appeared as a prominent peak at $\sim 8,8$ ml (Figure 3.32a) and SDS-PAGE of the peak fraction showed the presence of all three proteins (Figure 3.32b). As with the syntaxin-SN1 complex, the bands of SN1 and synaptobrevin were of much lower intensity compared to the syntaxin band. Additionally, the chromatogram of the complex showed a high amount of unbound synaptobrevin, while almost all of syntaxin seemed to migrate to the complex. Together, these data suggest that syntaxin, SN1 and synaptobrevin form a stable complex, and that the number of syntaxin, SN1 and synaptobrevin molecules present in the complex are not equal.

Results

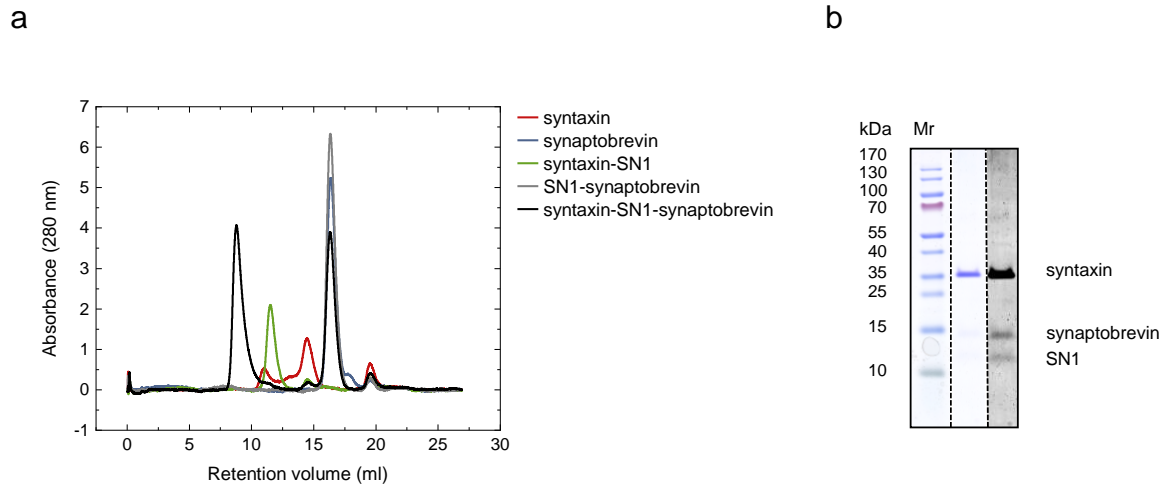


Figure 3.32. Size exclusion chromatography of the syntaxin-SN1-synaptobrevin subcomplex. Size exclusion chromatography was performed on overnight-incubated syntaxin (red), synaptobrevin (blue), syntaxin-SN1 (green), SN1-synaptobrevin (gray) and syntaxin-SN1-synaptobrevin (black) samples. The chromatogram (a) shows that syntaxin-SN1 and syntaxin-SN1-synaptobrevin form complexes with peaks at 11,6 ml and 8,8 ml, respectively. The peak fraction of syntaxin-SN1-synaptobrevin sample showed the presence of all three proteins (b). Due to different molecular masses and an unequal number of molecules of the three proteins in the peak, bands of SN1 and synaptobrevin appear markedly fainter than the band of syntaxin. For better visualization, the image of the gel was put in gray scale and the contrast was increased. These modifications revealed the clear presence of SN1 and synaptobrevin.

Experiments performed in sections 3.1.3.1 and 3.1.1, and presented again in Figure 3.33, demonstrate that SN2 and synaptobrevin alone do not bind to syntaxin. When present together, these three proteins seem to be able to interact and form a complex that appears as two distinct peaks at 9,5 ml and 11,2 ml. The presence of the two peaks was unexpected and might arise from two different conformations of the syntaxin-SN2-synaptobrevin complex with a more tightly bound complex eluting later. Another possible explanation is weak binding between the molecules in the complex that would fall apart during the size exclusion run. In that case, the two peaks would correspond to two syntaxin-SN2-synaptobrevin complexes that differ in the number of syntaxin, SN2 and synaptobrevin molecules contained in those complexes. SDS-PAGE of the two peak fractions shows the presence of all three proteins in the contrast-adjusted image, with the bands of SN2 and synaptobrevin being barely noticeable (Figure 3.33b). This might suggest that syntaxin molecules far outnumber SN2 and synaptobrevin molecules in both of the peaks.

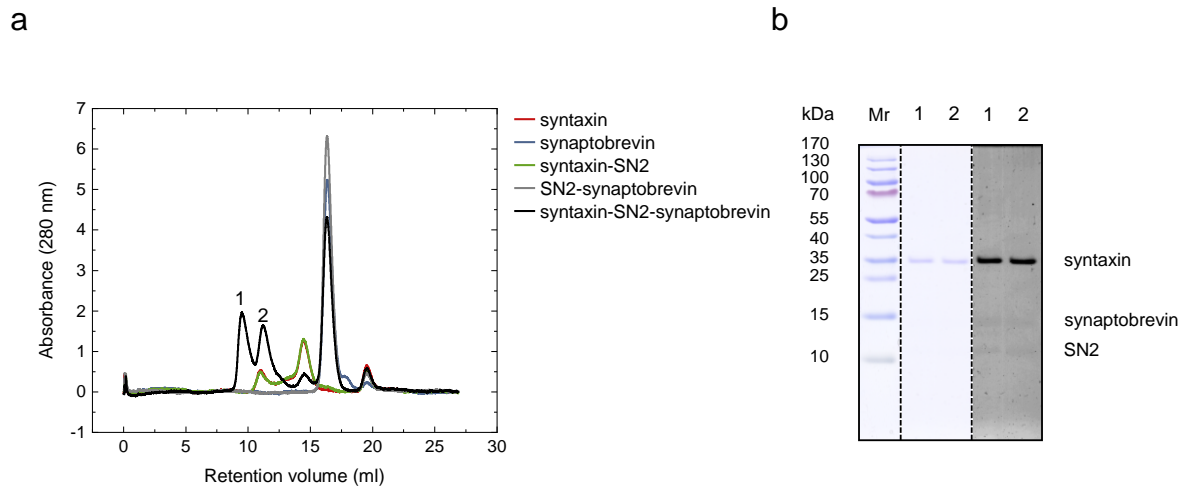


Figure 3.33. Size exclusion chromatography of syntaxin-SN2-synaptobrevin subcomplex. Size exclusion chromatography was performed on overnight incubated syntaxin (red), synaptobrevin (blue), syntaxin-SN2 (green), SN2-synaptobrevin (gray) and syntaxin-SN2-synaptobrevin (black) samples. The chromatogram (a) shows that only syntaxin-SN2-synaptobrevin forms a complex that elutes in two peaks at 9,5 ml and 11,2 ml. Both peak fractions show the presence of all three proteins (b). Bands of SN2 and synaptobrevin on the SDS-PAGE are barely noticeable even in the grayscale image with adjusted contrast and have substantially lower intensity compared to the syntaxin band. This difference in the band intensity most likely arises from different molecular mass and an unequal number of molecules of the three proteins in the complex.

Size exclusion experiment demonstrated that SN1 has a higher propensity for forming a complex with syntaxin and synaptobrevin compared to SN2. The higher stability of the syntaxin-SN1-synaptobrevin complex and the inability of SN2 to bind to syntaxin in the absence of SN1 or synaptobrevin indicates that the order in which SNARE domains enter the complex is likely the following: syntaxin and SN1 bind first, synaptobrevin binds second and SN2 arrives last.

As shown in section 3.1.3.1 and plotted again in Figure 3.34, overnight incubated syntaxin-SN1-SN2 sample forms a complex that elutes at 11,5 ml (Figure 3.34, peak 1). SDS-PAGE of the peak fraction cannot distinguish between SN1 and SN2 because of their similar molecular mass, and it is therefore not certain if the observed complex forms only between syntaxin and SN1 or between syntaxin, SN1 and SN2 (also discussed in section 3.1.3.1). Incubation of syntaxin, SN1 and SN2 with synaptobrevin leads to the formation of the SNARE complex, as expected (Figure 3.34, peak 2). The complex band elutes at 9,5 ml and in this experiment contains a shoulder that elutes very close the void volume and might

Results

arise from aggregation. It is known that SNARE complexes can oligomerize, and that is reflected on the size exclusion run. SDS-PAGE of the SNARE complex peak fraction shows the characteristic SDS-resistant band of at ~60 kDa, confirming that the proteins are functional and able to form the SNARE complex.

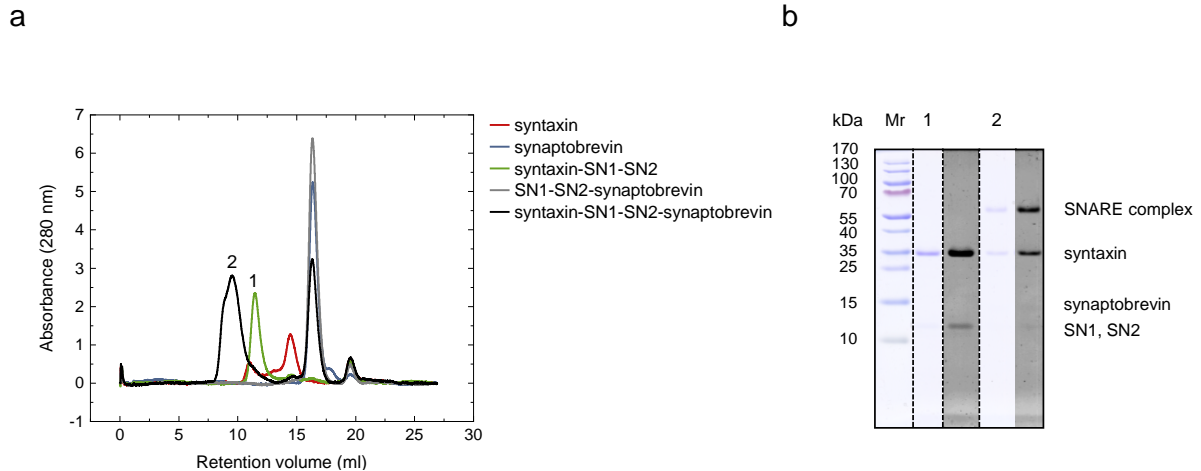


Figure 3.34. Size exclusion chromatography of the syntaxin-SN1-SN2-synaptobrevin complex. Size exclusion chromatography was performed on overnight incubated syntaxin (red), synaptobrevin (blue), syntaxin-SN1-SN2 (green), SN1-SN2-synaptobrevin (gray) and syntaxin-SN1-SN2-synaptobrevin (black) samples. The chromatogram (a) shows that syntaxin-SN1-SN2 and syntaxin-SN1-SN2-synaptobrevin form complexes that elute at 11,5 ml (peak 1) and 9,5 ml (peak 2), respectively. The SDS-PAGE of the peak fractions show the presence of syntaxin and SN1/SN2 band for peak 1 and syntaxin, synaptobrevin, SN1/SN2 and the SNARE complex band for peak 2 (b). As before, the gel image was converted to grayscale and the contrast was adjusted for better visualization of the bands present in the sample.

3.3 SUMMARY OF THE DATA

The presented stopped-flow and size exclusion experiments lead to the following conclusions: (i) syntaxin alone forms oligomers; (ii) syntaxin and SNAP25 are the only two SNARE proteins that are able to form a binary complex; (iii) the binary complex of syntaxin and SNAP25 consists of two syntaxin and one SNAP25 molecules; (iv) synaptobrevin binds to the syntaxin-SNAP25 complex; (v) out of the two SNARE domains of SNAP25, only SN1 is able to stably bind to syntaxin alone; (vi) syntaxin, SN1 and synaptobrevin can form a stable complex; (vii) syntaxin, SN2 and synaptobrevin can form a stable complex; (viii) SN2 cannot bind to syntaxin in the absence of SN1 or/and synaptobrevin. Based on these

conclusions and the uncertain mechanism of syntaxin and SNAP25 association, two models for the assembly of soluble SNAREs were constructed (Figure 3.35 and 3.36). In both proposed models, syntaxin and SNAP25 initiate the SNARE interaction by forming a precomplex to which synaptobrevin can bind. Whether the 2:1 complex formation is considered part of the SNARE assembly pathway or a side reaction is the main difference between the two models.

3.3.1 Model 1 of the soluble SNARE complex formation

The first step of the SNARE assembly reaction is the dimerization of syntaxin. At this point, I do not have an estimation for the rate constants that control this process. It is, however, clear from the preliminary syntaxin-syntaxin titration experiment (Figure 3.10) that dimerization equilibrates quite fast.

The second step is the binding of SNAP25 to the syntaxin dimer. The association rate constant of this step was estimated to be $2,23 \times 10^{-4} \pm 0,09 \times 10^{-4}$ by the syntaxin titration experiment (Figure 3.21). Since this rate constant is dependent on syntaxin and SNAP25 concentration, it is a second-order rate constant with dimensions $[M^{-1}s^{-1}]$. Given that the titration was done at μM concentrations, the value of the syntaxin dimer-SNAP25 association rate constant will be $2,23 \times 10^{-4} \pm 0,09 \times 10^{-4} \mu M^{-1}s^{-1}$, and after converting micromoles to moles, $223 \pm 0,09 M^{-1}s^{-1}$. In the same experiment, the dissociation constant of the syntaxin-SNAP25 complex was determined to be $7,8 \times 10^{-4} \pm 1,24 \times 10^{-4} s^{-1}$. A direct measurement of SNAP25 dissociation (Figure 3.16) provided a value of $3,44 \times 10^{-3} \pm 0,02 \times 10^{-3} s^{-1}$, which is not much different from the value determined by syntaxin titration. In general, determining the dissociation rate constant from the intercept of the k_{obs} -concentration graph is often not precise, and it is therefore always better to measure it directly when possible (Goodrich and Kugel, 2007).

The first and the second synaptobrevin titration experiments (Figure 3.26 and Figure 3.29) provided values for the ratio k_2/k_{-1} , which was determined to be $0,39 \pm 0,11$ and $0,34 \pm 0,08$, respectively. In this case, the k_{-1} corresponds to the dissociation rate constant of SNAP25 ($3,44 \times 10^{-3} \pm 0,02 \times 10^{-3} s^{-1}$). The calculated values for k_2 are therefore $1,72 \times 10^{-3} \pm 0,38 \times 10^{-3}$ and $1,17 \times 10^{-3} \pm 0,27 \times 10^{-3}$ for the first and second synaptobrevin titration, respectively. Averaging these two values gave $1,44 \times 10^{-3} \pm 0,32 \times 10^{-3}$. This is again a second order rate constant, giving finally $1440 \pm 320 M^{-1}s^{-1}$.

Preincubation of syntaxin and SNAP25 and subsequent addition of synaptobrevin showed an initial decrease of fluorescence that was changing with synaptobrevin concentration (Figure 3.29). In Model 1, this process is presented provisionally as the displacement of syntaxin from the 2:1 complex with the second order rate constant of $7750 \pm 470 M^{-1}s^{-1}$. Another possibility can be that the arrival of synaptobrevin rearranges or even displaces SNAP25 from the 2:1 complex.

In this model, the slowest, and therefore the rate limiting step of SNARE assembly, is the syntaxin dimer-SNAP25 complex formation.

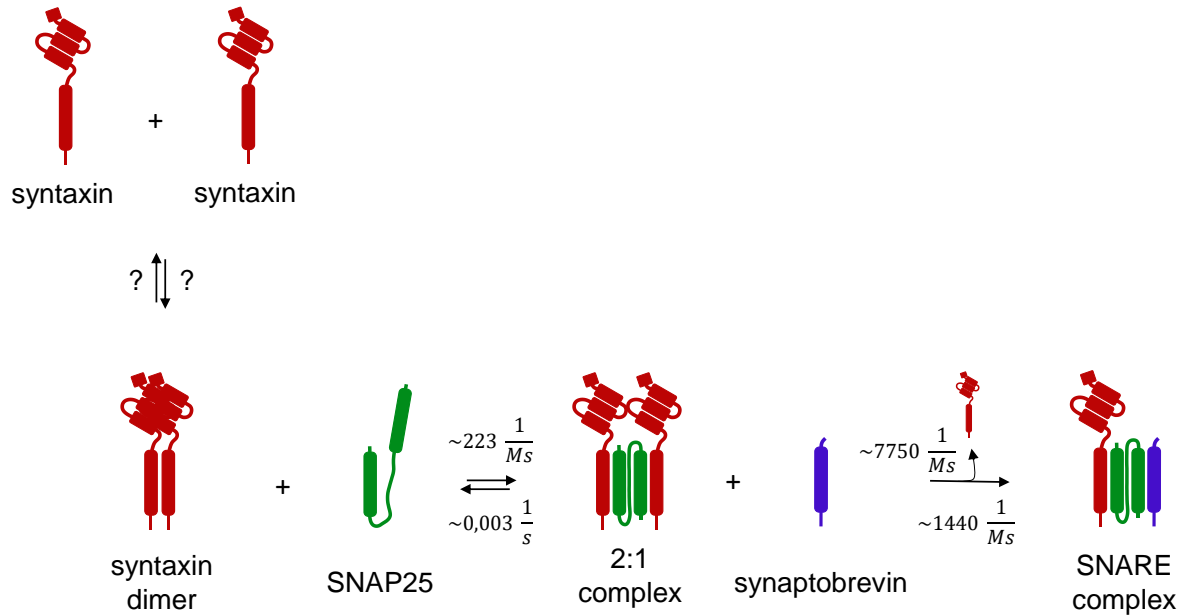


Figure 3.35. Model 1 of the soluble SNARE complex formation. Syntaxin molecules dimerize and bind SNAP25 to form a 2:1 complex. Synaptobrevin subsequently binds to the 2:1 complex, most likely displacing the second syntaxin and forming the SNARE complex. The estimated rate constants that govern each step are indicated on the scheme. The question marks indicate the unknowns.

3.3.2 Model 2 of the soluble SNARE complex formation

Model 2 corresponds to the accepted model for SNARE assembly in the literature (e.g. Wiederhold and Fasshauer, 2009). The first step of the reaction is an interaction between syntaxin and SNAP25 and a subsequent 1:1 heterodimer formation, with the association rate constant of $223 \pm 0,09 \text{ M}^{-1}\text{s}^{-1}$ and a dissociation rate constant of $3,44 \times 10^{-3} \pm 0,02 \times 10^{-3} \text{ s}^{-1}$. The heterodimer creates a binding site for both synaptobrevin and syntaxin. Binding of syntaxin forms a 2:1 complex with unknown rate constants. When synaptobrevin is present, it binds irreversibly to the 1:1 heterodimer with the association rate constant of $1440 \pm 320 \text{ M}^{-1}\text{s}^{-1}$. If a 2:1 complex is present, synaptobrevin is able to actively displace it at $7750 \pm 470 \text{ M}^{-1}\text{s}^{-1}$. A scheme of Model 2 is presented in Figure 3.36.

As with Model 1, the rate limiting step of Model 2 seems to be the formation of syntaxin-SNAP25 complex.

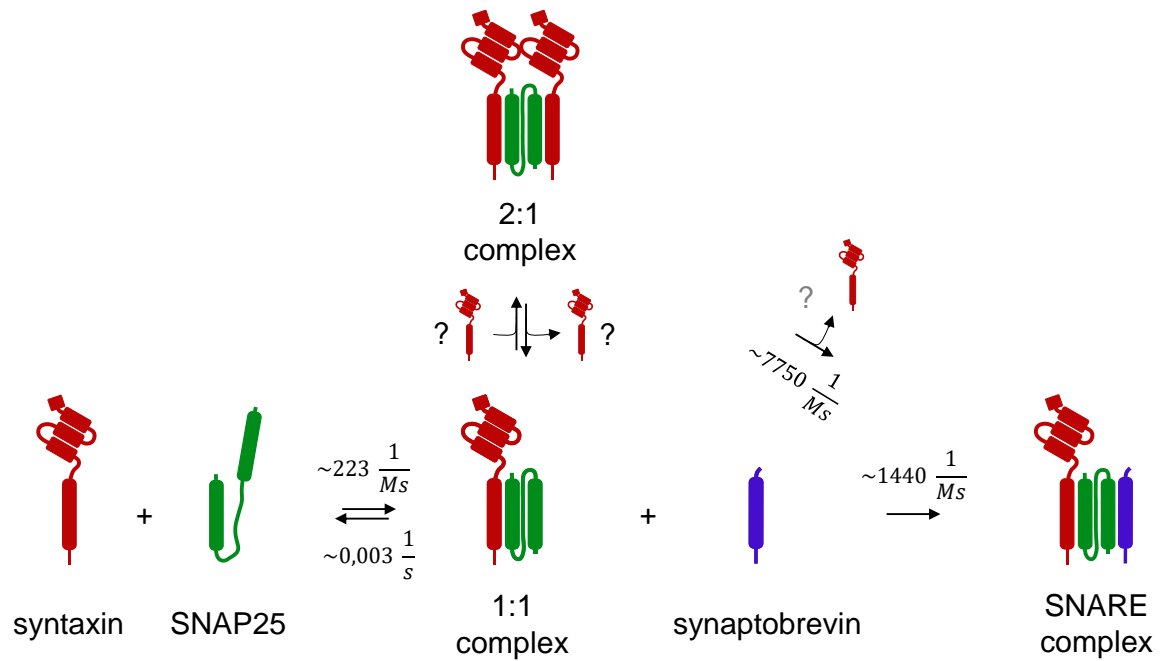


Figure 3.36. Model 2 of the SNARE complex formation in solution. Syntaxin and SNAP25 interact to form a 1:1 heterodimer to which both syntaxin and synaptobrevin can bind. Binding of syntaxin leads to the 2:1 complex formation. Binding of synaptobrevin to the 1:1 complex leads to the irreversible formation of the SNARE complex. The estimated rate constants that govern each step are indicated on the scheme. The question marks indicate the unknowns.

4 DISCUSSION

Previous research suggested two possible ways in which the neuronal SNARE proteins can enter the assembly reaction: (i) syntaxin and SNAP25 bind first, and are followed by synaptobrevin or (ii) syntaxin and synaptobrevin bind first, and are followed by SNAP25. My work confirms the first hypothesis, namely, that syntaxin and SNAP25 interaction represents the first step in the assembly reaction. Synaptobrevin subsequently binds to the syntaxin-SNAP25 complex to form the SNARE complex.

The proximity of syntaxin and SNAP25 in the presynapse and their localization to the plasma membrane makes the syntaxin-SNAP25 binding the logical first step in the assembly pathway. The majority of the conducted research that investigated the mechanism of SNARE zippering supports this notion (Fasshauer and Margittai, 2004; Pobbati et al., 2006; Wiederhold and Fasshauer, 2009). However, the acceptance of syntaxin-SNAP25 as a stable intermediate has been hampered by the complexity of its formation. Specifically, it has been postulated that for quick binding of synaptobrevin, syntaxin and SNAP25 need to be in 1:1 molar ratio. This is often not the case as syntaxin and SNAP25 readily form a complex in which two syntaxin molecules are bound to one SNAP25 molecule.

The 2:1 complex is mostly described in the literature as a dead-end of the assembly pathway and experimenters go out of their way to prevent its formation. The prevailing opinion is that syntaxin and synaptobrevin compete for the same binding site formed by the transient 1:1 syntaxin-SNAP25 complex (Fasshauer and Margittai, 2004). One of the most common ways in which experimenters prevent 2:1 complex formation is having an excess of SNAP25 in the reaction. An excess of SNAP25 is considered to bind all available syntaxin molecules, preventing them from binding to a 1:1 syntaxin-SNAP25 complex and consequently forming a 2:1 complex. It is worth noting that some authors claim that excess SNAP25 leads to the formation of a 1:2 complex that contains one syntaxin and two SNAP25 molecules and that also blocks synaptobrevin binding (Li et al., 2016). I, however, found that the excess of syntaxin, that should ensure the 2:1 complex formation, does not obstruct synaptobrevin binding. On the contrary, the interaction between SNAP25 and synaptobrevin was faster with the increasing syntaxin concentration. The same was true for the excess of SNAP25: increasing concentrations lead to faster syntaxin-synaptobrevin interaction. These results seem to contradict the previously reported data. However, they do not necessarily point to the absence of competition between syntaxin and synaptobrevin. With increasing syntaxin concentration, the formation of the 1:1 syntaxin-SNAP25 complex will be faster and the binding site for the second syntaxin or synaptobrevin will be available sooner. Whether syntaxin or synaptobrevin will bind first depends on their

affinity for the 1:1 complex and on their respective concentrations. Syntaxin will have a concentration advantage over synaptobrevin, however, ITC experiments determined that the affinity of the second syntaxin is much lower compared to synaptobrevin (Wiederhold and Fasshauer, 2009). Additionally, synaptobrevin binds irreversibly, leading to the formation of a stable SNARE complex. Overall, in the case of competition between syntaxin and synaptobrevin for the same binding spot on 1:1 syntaxin-synaptobrevin complex, in conditions of excess syntaxin, the higher affinity and the irreversibility can ensure that synaptobrevin binding prevails.

Higher affinity of synaptobrevin for the 1:1 syntaxin-SNAP25 complex also means that, unless syntaxin and SNAP25 are premixed, an excess of synaptobrevin in the reaction should not allow for 2:1 complex formation. Proper Q-SNARE nucleation is considered to be one of the limiting steps in SNARE assembly. Keeping syntaxin and SNAP25 separate before the addition of synaptobrevin can therefore delay synaptobrevin binding for the time it takes for the mentioned nucleation to take place. Premixing syntaxin and SNAP25 will circumvent this delay, but it will also allow for 2:1 complex formation, and it has been reported that synaptobrevin cannot actively displace the second syntaxin from the 2:1 complex (Fasshauer and Margittai, 2004). In this case, synaptobrevin binding will be delayed by the time it takes for the second syntaxin to dissociate from the 2:1 complex. The delay caused by the nucleation and the displacement of the second syntaxin should differ. Nonetheless, I found that whether syntaxin and SNAP25 were kept separate or were premixed did not seem to affect the rate of SNARE complex formation. Moreover, in the case of premixed syntaxin and SNAP25, synaptobrevin was able to actively rearrange the 2:1 complex and this rearrangement did not seem to directly relate to the rate of SNARE zippering.

So far, the assembly of the 2:1 complex was considered to be as follows: (i) syntaxin and SNAP25 form a 1:1 complex, (ii) the second syntaxin binds to the 1:1 complex forming a 2:1 syntaxin-SNAP25 complex. This order of events has been established almost as soon as the 2:1 complex was discovered (Fasshauer et al., 1997a) and is mainly supported by the fact that the ratio of syntaxin and SNAP25 in the SNARE complex is 1:1. Experimental conditions that supposedly prevent the formation of 2:1 complex have been shown to increase the rate of lipid mixing. It is therefore assumed that syntaxin and SNAP25 go through a 1:1 stage on their way to a 2:1 complex, and that this stage is captured by synaptobrevin. Results obtained in this work seem to provide support for an alternative hypothesis in which syntaxin dimers form first and SNAP25 binds to the syntaxin dimer, forming a 2:1 complex. As mentioned before, it has been observed that syntaxin can form dimers and tetramers in solution (Lerman et al., 2000; Margittai et al., 2001; Misura et al., 2001a). One interesting observation from the crystal structure of the tetramer of syntaxin H3 domain is that the two pairs of syntaxin molecules are in an antiparallel orientation. The antiparallel orientation is explained by phenylalanine 216 posing a steric hindrance

to a parallel tetramer. Even though this data is disputed by EPR experiments that claim a parallel tetramer orientation, it leads to an intriguing conclusion that syntaxin can only form dimers when present in the plasma membrane. It is then conceivable that SNAP25 binds to the already present dimers. In this sequence of events, a 2:1 complex would present a part of the assembly pathway and not a dead-end side reaction. To form a SNARE complex, synaptobrevin would have to displace or in some other way rearrange the 2:1 complex which is also supported by this work. The “syntaxin dimer first” hypothesis offers an answer to the mystery surrounding the existence of 2:1 complex. It can also explain some of the confusing data obtained when examining the syntaxin-SNAP25 interaction. At this point, there is not enough evidence to support this hypothesis, but it is my opinion that it should at least be put forward.

The values for the rate constants calculated in this work differ from the ones calculated previously (Fasshauer and Margittai, 2004; Wiederhold and Fasshauer, 2009). It needs to be kept in mind that in previous works, only the H3 domain of syntaxin was used, and it is known to have faster kinetics, presumably because of the absence of the closed conformation of syntaxin. The differences might also arise from the different assumptions for the interaction mechanism and, therefore, from different treatment of the data. Notably, treatment of the syntaxin-SNAP25 interaction as a single step reaction yielded the values for association rate constant similar to the ones reported before (Fasshauer and Margittai, 2004) when only the H3 domain of syntaxin was used. This could suggest that the differences in the assembly kinetics between the H3 and the entire cytoplasmic domain of syntaxin do not arise from the stalling of SNAP25 binding by the closed conformation of syntaxin, but from retarded synaptobrevin binding.

Evidence from vacuolar fusion lead to the formulation of an alternative hypothesis for SNARE assembly: syntaxin and synaptobrevin, with the help of Munc18, form a template complex to which SNAP25 binds (Baker et al., 2015; Jiao et al., 2018; Zhang and Hughson, 2021). This hypothesis avoids the problem of syntaxin-SNAP25 nucleation altogether. Additionally, it proposes that Munc18 introduces a new interaction between the SNARE proteins that changes the pathway of their assembly, which can explain the essential role of Munc18 in neuronal exocytosis. Munc18 was shown to bind to syntaxin and to synaptobrevin (Zhang and Hughson, 2021), but never at the same time. In order for the template complex to form, syntaxin needs to be “open” to allow Munc18 to take a conformation in which synaptobrevin binding can occur. The weakness of this model is that the data in support of it are obtained entirely through optical tweezer experiments. To be able to perform these experiments, SNARE proteins need to be crosslinked. In the case of experiments that support the template model, syntaxin and synaptobrevin are crosslinked at their N-terminus while their C-terminus is modified for attachment to the polystyrene beads (Jiao et al., 2018). Crosslinking of syntaxin and synaptobrevin and their attachment to beads restricts protein motion. Creating one protein molecule out of two decreases

rotational and translational entropies (Fersht, 2017) and changes configurational entropy, which are the critical components in molecular recognition, binding and interaction kinetics (Caro et al., 2017; Fersht, 2017). Any weak interaction that might exist between syntaxin and synaptobrevin could therefore be potentially stabilized and potentiated.

In my experiments, I did not detect an interaction between syntaxin and synaptobrevin. This does not provide evidence against the template complex formation, since it requires binding of Munc18. However, data obtained from PC12 cells show that syntaxin exists in ~20-fold excess over Munc18 (Schütz et al., 2005), suggesting that the majority of syntaxin in the cell is not occupied by Munc18. Considering that the amount of syntaxin and SNAP25 in isolated nerve terminals is comparable (Walch-Solimena et al., 1995), it follows that SNAP25 is also in excess over Munc18. Since the distribution of syntaxin and SNAP25 molecules in the membrane was shown to have substantial overlap (Rickman et al., 2010), it can be assumed that the syntaxin-SNAP25 complex forms. Furthermore, ultrahigh-resolution imaging showed that Munc18 colocalizes with syntaxin and SNAP25 at the plasma membrane (Pertsinidis et al., 2013). Taking all of this into account and considering that a wealth of evidence supports a Qabc-Munc18 complex formation (Dawidowski and Cafiso, 2013; Jakhanwal et al., 2017; Shen et al., 2007; Zhang et al., 2016), it is difficult to envision the mechanism of the template complex formation in the cell.

In general, it is very difficult to compare data from different work. The findings can be highly variable depending on the protein constructs used, purification protocols, salt concentrations, presence of absence of lipids, reconstitution protocols, size and curvature of liposomes etc. In many publications, protein interactions are measured indirectly, most commonly through lipid and content mixing experiments, in which protein interaction mechanisms are inferred from the kinetics of liposome docking and fusion (see Introduction, section 1.5.2).

The main advantage of the kinetics method employed in this work over the lipid and content mixing experiments is that the interactions of the SNARE proteins are measured directly. In order to determine the action of accessory proteins, it is necessary to first establish the interaction pathway in a system of minimal complexity, or in other words, when only the SNARE proteins are present. Once a pathway is established, other variables can be added and their influence can be deciphered.

This work dealt only with the cytoplasmic domains of the SNARE proteins in an effort to minimize the variability in the system. However, the SNARE proteins are transmembrane proteins, and their function is strongly coupled to their membrane anchorage. Membrane anchorage will introduce constraints in the motion of SNARE proteins and, through interaction with lipids (Bogaart et al., 2013; Gonzalo et al., 1999; Khuong et al., 2013; Williams et al., 2009), influence their conformation (Lakomek et al., 2019). These changes would most likely have a positive effect on the kinetics of individual steps in the SNARE

Discussion

assembly mechanism, but should not change the order in which the steps occur. Nevertheless, this claim remains to be experimentally verified.

In summary, in this PhD thesis I show that the steps through which the SNARE complex assembly occurs involve a formation of syntaxin-SNAP25 precomplex that subsequently binds synaptobrevin. The reaction mechanism with the estimated rate constants provides the first steps for a detailed understanding of the protein interactions responsible for synaptic vesicle fusion.

Bibliography

- Aghajanian, G.K., and Bloom, F.E. (1967). THE FORMATION OF SYNAPTIC JUNCTIONS IN DEVELOPING RAT BRAIN: A QUANTITATIVE ELECTRON MICROSCOPIC STUDY. *Brain Res.* 6, 716–727.
- Agilent Technologies (2011). QuikChange Lightning Site-Directed Mutagenesis Kit. Instr. Man. *Revision D*.
- Antonin, W., Fasshauer, D., Becker, S., Jahn, R., and Schneider, T.R. (2002). Crystal structure of the endosomal SNARE complex reveals common structural principles of all SNAREs. *Nat. Struct. Biol.* 2002 9, 107–111.
- Applied Photophysics (2012). User Manual SX20-LED Stopped Flow Spectrometer.
- Baker, R.W., and Hughson, F.M. (2016). Chaperoning SNARE assembly and disassembly. *Nat. Rev. Mol. Cell Biol.* 2016 17, 465–479.
- Baker, R.W., Jeffrey, P.D., Zick, M., Phillips, B.P., Wickner, W.T., and Hughson, F.M. (2015). A direct role for the Sec1/Munc18-family protein Vps33 as a template for SNARE assembly. *Science* (80-.). 349, 1111–1114.
- Balch, W.E., Dunphy, W.G., Braell, W.A., and Rothman, J.E. (1984). Reconstitution of the transport of protein between successive compartments of the golgi measured by the coupled incorporation of N-acetylglucosamine. *Cell* 39, 405–416.
- Bar-On, D., Wolter, S., Linde, S. van de, Heilemann, M., Nudelman, G., Nachliel, E., Gutman, M., Sauer, M., and Ashery, U. (2012). Super-resolution Imaging Reveals the Internal Architecture of Nano-sized Syntaxin Clusters *. *J. Biol. Chem.* 287, 27158–27167.
- Bark, I.C. (1993). Structure of the Chicken Gene for SNAP-25 Reveals Duplicated Exons Encoding Distinct Isoforms of the Protein. *J. Mol. Biol.* 233, 67–76.
- Bark, I.C., Hahn, K.M., Ryabinin, A.E., and Wilson, M.C. (1995). Differential expression of SNAP-25 protein isoforms during divergent vesicle fusion events of neural development. *Proc. Natl. Acad. Sci.* 92, 1510–1514.
- Bennett, M.V.L., and Zukin, R.S. (2004). Electrical Coupling and Neuronal Synchronization in the Mammalian Brain. *Neuron* 41, 495–511.
- Bennett, M.M.K., Calakos, N., and Scheller, R.R.H. (1992). Syntaxin: A synaptic protein implicated in docking of synaptic vesicles at presynaptic active zones. *Science* (80-.). 257, 255–259.
- Bernardino de la Serna, J., Schütz, G.J., Eggeling, C., and Cebecauer, M. (2016). There Is No Simple Model of the Plasma Membrane Organization. *Front. Cell Dev. Biol.* 0, 106.
- Bernasconi, C. (2012). Relaxation kinetics (Elsevier).
- Berridge, M.J., Lipp, P., and Bootman, M.D. (2000). The versatility and universality of calcium signalling. *Nat. Rev. Mol. Cell Biol.* 1, 11–21.

Bibliography

- Biederer, T., Kaeser, P.S., and Blanpied, T.A. (2017). Transcellular Nanoalignment of Synaptic Function. *Neuron* **96**, 680–696.
- Binotti, B., Jahn, R., and Angel Pérez-Lara, ´ (2021). An overview of the synaptic vesicle lipid composition. *Arch. Biochem. Biophys.* **709**, 108966.
- Blasi, J., Chapman, E.R., Link, E., Binz, T., Yamasaki, S., Camilli, P. De, Südhof, T.C., Niemann, H., and Jahn, R. (1993). Botulinum neurotoxin A selectively cleaves the synaptic protein SNAP-25. *Nat.* 1993 3656442 **365**, 160–163.
- Bogaart, G. van den, Holt, M.G., Bunt, G., Riedel, D., Wouters, F.S., and Jahn, R. (2010). One SNARE complex is sufficient for membrane fusion. *Nat. Struct. Mol. Biol.* 2010 173 **17**, 358–364.
- Bogaart, G. Van Den, Lang, T., and Jahn, R. (2013). Microdomains of SNARE Proteins in the Plasma Membrane (Elsevier Inc.).
- Brenner, S. (1974). THE GENETICS OF CENORABDITIS ELEGANS. *Genetics* **77**, 71–94.
- Brewer, K.D., Li, W., Horne, B.E., and Rizo, J. (2011). Reluctance to membrane binding enables accessibility of the synaptobrevin SNARE motif for SNARE complex formation. *Proc. Natl. Acad. Sci.* **108**, 12723–12728.
- Broadie, K., Prokop, A., Bellen, H.J., Kane, C.J.O., Schulze, K.L., and Sweeney, S.T. (1995). Syntaxin and Synaptobrevin Function Downstream of Vesicle Docking in *Drosophila*. **15**, 663–673.
- Burkhardt, P., Hattendorf, D.A., Weis, W.I., and Fasshauer, D. (2008). Munc18a controls SNARE assembly through its interaction with the syntaxin N-peptide. *EMBO J.* **27**, 923.
- Calakos, N., Bennett, M.K., Peterson, K.E., and Scheller, R.H. Protein-Protein Interactions Contributing to the Specificity of Intracellular Vesicular Trafficking.
- Caro, J.A., Harpole, K.W., Kasinath, V., Lim, J., Granja, J., Valentine, K.G., Sharp, K.A., and Wand, A.J. (2017). Entropy in molecular recognition by proteins. *Proc. Natl. Acad. Sci. U. S. A.* **114**, 6563.
- Catterall, W.A. (2011). Voltage-gated calcium channels. *Cold Spring Harb. Perspect. Biol.* **3**, 1–23.
- Chapman, E.R., Hanson, P.I., An, S., and Jahn, R. (1995). Ca²⁺ Regulates the Interaction between Synaptotagmin and Syntaxin 1 (*). *J. Biol. Chem.* **270**, 23667–23671.
- Chen, X., Tomchick, D.R., Kovrigin, E., Araç, D., Machius, M., Südhof, T.C., and Rizo, J. (2002). Three-dimensional structure of the complexin/SNARE complex. *Neuron* **33**, 397–409.
- Chen, X., Lu, J., Dulubova, I., and Rizo, J. (2008). NMR analysis of the closed conformation of syntaxin-1. *J. Biomol. NMR* 2008 411 **41**, 43–54.
- Chernomordik, L. V., and Kozlov, M.M. (2003). Protein-lipid interplay in fusion and fission of biological membranes. *Annu. Rev. Biochem.* **72**, 175–207.
- Chernomordik, L. V., and Kozlov, M.M. (2008). Mechanics of membrane fusion. *Nat.*

Struct. Mol. Biol. *15*, 675–683.

Chernomordik, L. V., Kozlov, M.M., Melikyan, G.B., Abidor, I.G., Markin, V.S., and Chizmadzhev, Y.A. (1985). The shape of lipid molecules and monolayer membrane fusion. *BBA - Biomembr.* *812*, 643–655.

Connell, E., Darios, F., Broersen, K., Gatsby, N., Peak-Chew, S.Y., and Rickman, C. (2007). Mechanism of arachidonic acid action on syntaxin - Munc18. *EMBO Rep.* *8*, 414–419.

Connors, K.A. (1990). Chemical kinetics: the study of reaction rates in solution (Wiley-VCH Verlag GmbH).

Connors, B.W., and Long, M.A. (2004). Electrical synapses in the mammalian brain. *Annu. Rev. Neurosci.* *27*, 393–418.

Cowan, W.M., Cowan, W.M., Südhof, T.C., and Stevens, C.F. (2003). Synapses (JHU Press).

Czerlinski, G.H. (1966). Chemical relaxation; an introduction to theory and application of stepwise perturbation.

Dawidowski, D., and Cafiso, D.S. (2013). Allosteric control of syntaxin 1a by munc18-1: Characterization of the open and closed conformations of syntaxin. *Biophys. J.* *104*, 1585–1594.

Delgado-Martínez, I., Nehring, R., and Sørensen, J. (2007). Differential Abilities of SNAP-25 Homologs to Support Neuronal Function. *J. Neurosci.* *27*, 9380–9391.

Dietrich, L.E.P., Boeddinghaus, C., LaGrassa, T.J., and Ungermann, C. (2003). Control of eukaryotic membrane fusion by N-terminal domains of SNARE proteins. *Biochim. Biophys. Acta - Mol. Cell Res.* *1641*, 111–119.

Dulubova, I., Sugita, S., Hill, S., Hosaka, M., Fernandez, I., Südhof, T.C., and Rizo, J. (1999). A conformational switch in syntaxin during exocytosis: Role of munc18. *EMBO J.* *18*, 4372–4382.

Dulubova, I., Khvotchev, M., Liu, S., Huryeva, I., Südhof, T.C., and Rizo, J. (2007). Munc18-1 binds directly to the neuronal SNARE complex. *Proc. Natl. Acad. Sci.* *104*, 2697–2702.

Eccles, J.C., and Jaeger, J.C. (1957). The relationship between the mode of operation and the dimensions of the junctional regions at the synapses and the motor end-organs. *Proc. R. Soc. Lond. B* *148*, 38–56.

Ellena, J.F., Liang, B., Wiktor, M., Stein, A., Cafiso, D.S., Jahn, R., and Tamm, L.K. (2009). Dynamic structure of lipid-bound synaptobrevin suggests a nucleation-propagation mechanism for trans-SNARE complex formation. *Proc. Natl. Acad. Sci.* *106*, 20306–20311.

Fasshauer, D., and Margittai, M. (2004). A Transient N-terminal Interaction of SNAP-25 and Syntaxin Nucleates SNARE Assembly *. *J. Biol. Chem.* *279*, 7613–7621.

Fasshauer, D., Bruns, D., Shen, B., Jahn, R., and Brunger, A.T. (1997a). A Structural

Bibliography

- Change Occurs upon Binding of Syntaxin to SNAP-25 *. *J. Biol. Chem.* **272**, 4582–4590.
- Fasshauer, D., Otto, H., Eliason, W.K., Jahn, R., Brünger, A.T., and Brünger, A.T. (1997b). Structural changes are associated with soluble N-ethylmaleimide- sensitive fusion protein attachment protein receptor complex formation. *J. Biol. Chem.* **272**, 28036–28041.
- Fasshauer, D., Sutton, R.B., Brunger, A.T., and Jahn, R. (1998a). Conserved structural features of the synaptic fusion complex: SNARE proteins reclassified as Q- and R-SNAREs. *Proc. Natl. Acad. Sci.* **95**, 15781–15786.
- Fasshauer, D., Eliason, W.K., Brünger, A.T., and Jahn, R. (1998b). Identification of a Minimal Core of the Synaptic SNARE Complex Sufficient for Reversible Assembly and Disassembly†. *Biochemistry* **37**, 10354–10362.
- Fasshauer, D., Antonin, W., Subramaniam, V., and Jahn, R. (2002). SNARE assembly and disassembly exhibit a pronounced hysteresis. *Nat. Struct. Biol.* **9**, 144–151.
- Fersht, A. (2017). *Structure and mechanism in protein science: a guide to enzyme catalysis and protein folding* (World Scientific Publishing Co. Pte. Ltd).
- Förster, T. (1946). Energiewanderung und Fluoreszenz. *Naturwissenschaften* **33**, 166–175.
- Gao, Y., Zorman, S., Gundersen, G., Xi, Z., Ma, L., Sirinakis, G., Rothman, J.E., and Zhang, Y. (2012). Single Reconstituted Neuronal SNARE Complexes Zipper in Three Distinct Stages. *Science* (80-.). **337**, 1340–1344.
- Gonzalo, S., and Linder, M.E. (1997). SNAP-25 Palmitoylation and Plasma Membrane Targeting Require a Functional Secretory Pathway. *Mol. Biol. Cell* **9**, 585–597.
- Gonzalo, S., Greentree, W.K., and Linder, M.E. (1999). SNAP-25 Is Targeted to the Plasma Membrane through a Novel Membrane-binding Domain *. *J. Biol. Chem.* **274**, 21313–21318.
- Goodrich, J.A., and Kugel, J.F. (2007). *Binding and kinetics for molecular biologists.* (CSH Laboratory Press, Cold Spring Harbor, NY).
- Greaves, J., Prescott, G.R., Fukata, Y., Fukata, M., Salaun, C., and Chamberlain, L.H. (2009). The Hydrophobic Cysteine-rich Domain of SNAP25 Couples with Downstream Residues to Mediate Membrane Interactions and Recognition by DHHC Palmitoyl Transferases. <https://doi.org/10.1091/mbc.E08-09-0944> **20**, 1845–1854.
- Hamm, M., and Kozlov, M.M. (1998). Tilt model of inverted amphiphilic mesophases.
- Hanahan, D. (1983). Studies on transformation of *Escherichia coli* with plasmids. *J. Mol. Biol.* **166**, 557–580.
- Hanson, P.I., Heuser, J.E., and Jahn, R. (1997). Neurotransmitter release-four years of SNARE complexes . *Curr. Opin. Neurobiol.* **7**, 310–315.
- Harris, K. m., and Sultan, P. (1995). Variation in the number, location and size of synaptic vesicles provides an anatomical basis for the nonuniform probability of release at hippocampal CA1 synapses. *Neuropharmacology* **34**, 1387–1395.

Bibliography

- Hazzard, J., Südhof, T.C., and Rizo, J. (1999). NMR analysis of the structure of synaptobrevin and of its interaction with syntaxin. *J. Biomol. NMR* 1999 143 14, 203–207.
- Hernandez, J.M., Stein, A., Behrmann, E., Riedel, D., Cypionka, A., Farsi, Z., Walla, P.J., Raunser, S., and Jahn, R. (2012). Membrane Fusion Intermediates via Directional and Full Assembly of the SNARE Complex. *Science* (80-.). 336, 1581–1584.
- Hernández, J.M., and Podbilewicz, B. (2017). The hallmarks of cell-cell fusion. *Dev.* 144, 4481–4495.
- Hess, S.D., Doroshenko, P.A., and Augustine, G.J. (1993). A functional role for GTP-binding proteins in synaptic vesicle cycling. *Science* (80-.). 259, 1169–1172.
- Hirano, T. (2018). Purkinje Neurons: Development, Morphology, and Function. *Cerebellum* 2018 176 17, 699–700.
- Hoekstra, D., and Düzgüneş, N. (1993). Lipid Mixing Assays to Determine Fusion in Liposome Systems. *Methods Enzymol.* 220, 15–32.
- Huang, K., Yanai, A., Kang, R., Arstikaitis, P., Singaraja, R.R., Metzler, M., Mullard, A., Haigh, B., Gauthier-Campbell, C., Gutekunst, C.A., et al. (2004). Huntingtin-Interacting Protein HIP14 Is a Palmitoyl Transferase Involved in Palmitoylation and Trafficking of Multiple Neuronal Proteins. *Neuron* 44, 977–986.
- Imig, C., Min, S.W., Krinner, S., Arancillo, M., Rosenmund, C., Südhof, T.C., Rhee, J.S., Brose, N., and Cooper, B.H. (2014). The Morphological and Molecular Nature of Synaptic Vesicle Priming at Presynaptic Active Zones. *Neuron* 84, 416–431.
- Jahn, R., and Scheller, R.H. (2006). SNAREs — engines for membrane fusion. *Nat. Rev. Mol. Cell Biol.* 7, 631–643.
- Jakhanwal, S., Lee, C.-T., Urlaub, H., and Jahn, R. (2017). An activated Q-SNARE/SM protein complex as a possible intermediate in SNARE assembly. *EMBO J.* 36, 1788–1802.
- Jiao, J., He, M., Port, S.A., Baker, R.W., Xu, Y., Qu, H., Xiong, Y., Wang, Y., Jin, H., Eisemann, T.J., et al. (2018). Munc18-1 catalyzes neuronal SNARE assembly by templating SNARE association. *Elife* 1–32.
- Johansson, J.U., Ericsson, J., Janson, J., Beraki, S., Stanić, D., Mandić, S.A., Wikström, M.A., Hökfelt, T., Ögren, S.O., Rozell, B., et al. (2008). An Ancient Duplication of Exon 5 in the Snap25 Gene Is Required for Complex Neuronal Development/Function. *PLOS Genet.* 4, e1000278.
- Johnson, K.A. (2010). KinTek Global Kinetic Explorer™ Manual. 175.
- Johnson, K.A., Simpson, Z.B., and Blom, T. (2009a). Global Kinetic Explorer: A new computer program for dynamic simulation and fitting of kinetic data. *Anal. Biochem.* 387, 20–29.
- Johnson, K.A., Simpson, Z.B., and Blom, T. (2009b). FitSpace Explorer: An algorithm to evaluate multidimensional parameter space in fitting kinetic data. *Anal. Biochem.* 387, 30–41.

Bibliography

- Kádková, A., Radecke, J., and Sørensen, J.B. (2019). The SNAP-25 Protein Family. *Neuroscience* *420*, 50–71.
- Kaksonen, M., and Roux, A. (2018). Mechanisms of clathrin-mediated endocytosis. *Nat. Rev. Mol. Cell Biol.* *19*, 313–326.
- KATZ, B., and MILEDI, R. (1965). The measurement of synaptic delay, and the time course of acetylcholine release at the neuromuscular junction. *Proc. R. Soc. London. Ser. B. Biol. Sci.* *161*, 483–495.
- Kee, Y., and Scheller, R.H. (1996). Localization of Synaptotagmin-Binding Domains on Syntaxin. *J. Neurosci.* *76*, 1975–1981.
- Khuong, T.M., Habets, R.L.P., Kuenen, S., Witkowska, A., Kasproicz, J., Swerts, J., Jahn, R., van den Bogaart, G., and Verstreken, P. (2013). Synaptic PI(3,4,5)P3 Is Required for Syntaxin1A Clustering and Neurotransmitter Release. *Neuron* *77*, 1097–1108.
- Khvotchev, M., Dulubova, I., Sun, J., Dai, H., Rizo, J., and Südhof, T.C. (2007). Dual Modes of Munc18-1/SNARE Interactions Are Coupled by Functionally Critical Binding to Syntaxin-1 N Terminus. *J. Neurosci.* *27*, 12147–12155.
- Kozlov, M.M., McMahon, H.T., and Chernomordik, L. V. (2010). Protein-driven membrane stresses in fusion and fission. *Trends Biochem. Sci.* *35*, 699–706.
- Kozlovsky, Y., and Kozlov, M.M. (2002). Stalk model of membrane fusion: Solution of energy crisis. *Biophys. J.* *82*, 882–895.
- Kreutzberger, A.J.B., Liang, B., Kiessling, V., and Tamm, L.K. (2016). Assembly and Comparison of Plasma Membrane SNARE Acceptor Complexes. *Biophys. J.* *110*, 2147–2150.
- Lakomek, N.-A., Yavuz, H., Jahn, R., and Pérez-Lara, Á. (2019). Structural dynamics and transient lipid binding of synaptobrevin-2 tune SNARE assembly and membrane fusion. *Proc. Natl. Acad. Sci.* *116*, 8699–8708.
- Lakowicz, J.R. (2013). *Principles of fluorescence spectroscopy* (Springer science & business media).
- Lang, T., Bruns, D., Wenzel, D., Riedel, D., Holroyd, P., Thiele, C., and Jahn, R. (2001). SNAREs are concentrated in cholesterol-dependent clusters that define docking and fusion sites for exocytosis. *20*, 2202–2213.
- Latham, C.F., Osborne, S.L., Cryle, M.J., and Meunier, F.A. (2007). Arachidonic acid potentiates exocytosis and allows neuronal SNARE complex to interact with Munc18a. *J. Neurochem.* *100*, 1543–1554.
- Leikin, S., Parsegian, V.A., Rau, D.C., and Rand, R.P. (1993). HYDRATION FORCES. *Annu. Rev. Phys. Chem.* *44*, 369–395.
- Leikin, S.L., Kozlov, M.M., Chernomordik, L. V., Markin, V.S., and Chizmadzhev, Y.A. (1987). Membrane fusion: Overcoming of the hydration barrier and local restructuring. *J. Theor. Biol.* *129*, 411–425.

Bibliography

- Lerman, J.C., Robblee, J., Fairman, R., and Hughson, F.M. (2000). Structural Analysis of the Neuronal SNARE Protein Syntaxin-1A †, ‡. *Biochemistry* 39, 41.
- Li, F., Pincet, F., Perez, E., Eng, W.S., Melia, T.J., Rothman, J.E., and Tareste, D. (2007). Energetics and dynamics of SNAREpin folding across lipid bilayers. *Nat. Struct. Mol. Biol.* 2007 1410 14, 890–896.
- Li, F., Tiwari, N., Rothman, J.E., and Pincet, F. (2016). Kinetic barriers to SNAREpin assembly in the regulation of membrane docking/priming and fusion. *Proc. Natl. Acad. Sci. U. S. A.* 113, 10536–10541.
- Liang, B., Kiessling, V., and Tamm, L.K. (2013). Prefusion structure of syntaxin-1A suggests pathway for folding into neuronal trans-SNARE complex fusion intermediate. *Proc. Natl. Acad. Sci. U. S. A.* 110, 19384–19389.
- Liang, B., Dawidowski, D., Ellena, J.F., Tamm, L.K., and Cafiso, D.S. (2014). The SNARE Motif of Synaptobrevin Exhibits an Aqueous–Interfacial Partitioning That Is Modulated by Membrane Curvature. *Biochemistry* 53, 1485–1494.
- Ma, C., Li, W., Xu, Y., and Rizo, J. (2011). Munc13 mediates the transition from the closed syntaxin–Munc18 complex to the SNARE complex. *Nat. Struct. Mol. Biol.* 2011 185 18, 542–549.
- Ma, C., Su, L., Seven, A.B., Xu, Y., and Rizo, J. (2013). Reconstitution of the Vital Functions of Munc18 and Munc13 in Neurotransmitter Release. *Science* (80-.). 339, 421–425.
- Macherey-Nagel (2011). Plasmid DNA Purification. User Man.
- Margittai, M., Fasshauer, D., Pabst, S., Jahn, R., and Langen, R. (2001). Homo- and Heterooligomeric SNARE Complexes Studied by Site-directed Spin Labeling *. *J. Biol. Chem.* 276, 13169–13177.
- Margittai, M., Widengren, J., Schweinberger, E., Schrö, G.F., Felekyan, S., Haustein, E., Kö, M., Fasshauer, D., Grubmü, H., Jahn, R., et al. (2003). Single-molecule fluorescence resonance energy transfer reveals a dynamic equilibrium between closed and open conformations of syntaxin 1.
- Markin, V.S., Kozlov, M.M., and Borovjagin, V.L. (1984). On the Theory of Membrane Fusion. The Stalk Mechanism. *Gen. Physiol. Biophys* 5, 361–377.
- Milovanovic, D., Honigmann, A., Koike, S., Göttfert, F., Pähler, G., Junius, M., Müller, S., Diederichsen, U., Janshoff, A., Grubmüller, H., et al. (2015). Hydrophobic mismatch sorts SNARE proteins into distinct membrane domains. *Nat. Commun.* 2015 61 6, 1–10.
- Misura, K.M.S., Scheller, R.H., and Weis, W.I. (2001a). Self-association of the H3 region of syntaxin 1A. Implications for intermediates in SNARE complex assembly. *J. Biol. Chem.* 276, 13273–13282.
- Misura, K.M.S., Gonzalez, L.C., May, A.P., Scheller, R.H., and Weis, W.I. (2001b). Crystal Structure and Biophysical Properties of a Complex between the N-terminal SNARE Region of SNAP25 and Syntaxin 1a. *J. Biol. Chem.* 276, 41301–41309.
- Mondal Roy, S., and Sarkar, M. (2011). Membrane Fusion Induced by Small Molecules

and Ions. *J. Lipids* 2011, 1–14.

Montecucco, C. (1986). How do tetanus and botulinum toxins bind to neuronal membranes? *Trends Biochem. Sci.* 11, 314–317.

Motulsky, H., and Christopoulos, A. (2004). Fitting models to biological data using linear and nonlinear regression: a practical guide to curve fitting (Oxford University Press).

Mueller, V.J., Wienisch, M., Nehring, R.B., and Klingauf, J. (2004). Monitoring Clathrin-Mediated Endocytosis during Synaptic Activity. *J. Neurosci.* 24, 2004–2012.

Murthy, V.N., and Stevens, C.F. (1998). Synaptic vesicles retain their identity through the endocytic cycle. *Nature* 392, 497–501.

Nagy, G., Milosevic, I., Mohrmann, R., Wiederhold, K., Walter, A.M., and Sørensen, J.B. (2008). The SNAP-25 Linker as an Adaptation Toward Fast Exocytosis. <https://doi.org/10.1091/mbc.E07-12-1218> 19, 3769–3781.

Nagy, J.I., Pereda, A.E., and Rash, J.E. (2018). Electrical synapses in mammalian CNS: Past eras, present focus and future directions. *Biochim. Biophys. Acta - Biomembr.* 1860, 102–123.

New England Biolabs (2020). IMPACT Kit. Instr. Man. 1–19.

Nichols, B.J., Ungermann, C., Pelham, H.R.B., Wickner, W.T., and Haas, A. (1997). Homotypic vacuolar fusion mediated by t- and v-SNAREs. *Nat.* 1997 3876629 387, 199–202.

Novick, P., Field, C., and Schekman, R. (1980). Identification of 23 Complementation Groups Required for Post-translational Events in the Yeast Secretory Pathway. *Cell* 21, 205–215.

O'Brien, J. (2019). Design principles of electrical synaptic plasticity. *Neurosci. Lett.* 695, 4–11.

Parisotto, D., Pfau, M., Scheutzw, A., Wild, K., Mayer, M.P., Malsam, J., Sinning, I., and Söllner, T.H. (2014). An Extended Helical Conformation in Domain 3a of Munc18-1 Provides a Template for SNARE (Soluble N-Ethylmaleimide-sensitive Factor Attachment Protein Receptor) Complex Assembly *. *J. Biol. Chem.* 289, 9639–9650.

Pereda, A.E. (2014). Electrical synapses and their functional interactions with chemical synapses. *Nat. Rev. Neurosci.* 15, 250–263.

Perin, M.S., Fried, V.A., Mignery, G.A., Jahn, R., and Südhof, T.C. (1990). Phospholipid binding by a synaptic vesicle protein homologous to the regulatory region of protein kinase C. *Nat.* 1990 3456272 345, 260–263.

Pertsinidis, A., Mukherjee, K., Sharma, M., Pang, Z.P., Park, S.R., Zhang, Y., Brunger, A.T., Südhof, T.C., and Chu, S. (2013). Ultrahigh-resolution imaging reveals formation of neuronal SNARE/Munc18 complexes in situ. *Proc. Natl. Acad. Sci. U. S. A.* 110, E2812–E2820.

Petty, K.J. (1996). Metal-Chelate Affinity Chromatography. *Curr. Protoc. Protein Sci.* 4, 9.4.1-9.4.16.

Bibliography

- Pobbat, A. V., Stein, A., and Fasshauer, D. (2006). N- to C-Terminal SNARE Complex Assembly Promotes Rapid Membrane Fusion. *Science* (80-.). *313*, 673–676.
- Ramón y Cajal, S. (1888). Sobre las fibras nerviosas de la capa molecular del cerebelo.
- Richmond, J.E., Davis, W.S., and Jorgensen, E.M. (1999). UNC-13 is required for synaptic vesicle fusion in *C. elegans*. *Nat. Neurosci.* 1999 211 *2*, 959–964.
- Richmond, J.E., Weimer, R.M., and Jorgensen, E.M. (2001). An open form of syntaxin bypasses the requirement for UNC-13 in vesicle priming. *Nat.* 2001 4126844 *412*, 338–341.
- Rickman, C., and Davletov, B. (2003). Mechanism of Calcium-independent Synaptotagmin Binding to Target SNAREs *. *J. Biol. Chem.* *278*, 5501–5504.
- Rickman, C., Medine, C.N., Dun, A.R., Moulton, D.J., Mandula, O., Halemani, N.D., Rizzoli, S.O., Chamberlain, L.H., and Duncan, R.R. (2010). t-SNARE Protein Conformations Patterned by the Lipid Microenvironment *. *J. Biol. Chem.* *285*, 13535–13541.
- Rizo, J., and Südhof, T.C. (2012). The Membrane Fusion Enigma: SNAREs, Sec1/Munc18 Proteins, and Their Accomplices—Guilty as Charged? *Annu. Rev. Cell Dev. Biol.* *28*, 279–308.
- Rosenmund, C., and Stevens, C.F. (1996). Definition of the Readily Releasable Pool of Vesicles at Hippocampal Synapses. *Neuron* *16*, 1197–1207.
- Saheki, Y., and De Camilli, P. (2012). Synaptic vesicle endocytosis. *Cold Spring Harb. Perspect. Biol.* *4*.
- Schägger, H., and von Jagow, G. (1987). Tricine-sodium dodecyl sulfate-polyacrylamide gel electrophoresis for the separation of proteins in the range from 1 to 100 kDa. *Anal. Biochem.* *166*, 368–379.
- Schaub, J.R., Lu, X., Doneske, B., Shin, Y.-K., and McNew, J.A. (2006). Hemifusion arrest by complexin is relieved by Ca^{2+} —synaptotagmin I. *Nat. Struct. Mol. Biol.* 2006 138 *13*, 748–750.
- Schiavo, G. (1992). Tetanus and botulinum-B neurotoxins block neurotransmitter release by proteolytic cleavage of synaptobrevin. *Nature* *359*, 832–835.
- Schiavo, G., Rossetto, O., Catsicas, S., De Laureto, P.P., DasGupta, B.R., Benfenati, F., and Montecucco, C. (1993). Identification of the nerve terminal targets of botulinum neurotoxin serotypes A, D, and E. *J. Biol. Chem.* *268*, 23784–23787.
- Schoch, S., Deák, F., Königstorfer, A., Mozhayeva, M., Sara, Y., Südhof, T., and Kavalali, E. (2001). SNARE Function Analyzed in Synaptobrevin/VAMP Knockout Mice. *Science* (80-.). *294*, 1117–1122.
- Schütz, D., Zilly, F., Lang, T., Jahn, R., and Bruns, D. (2005). A dual function for Munc-18 in exocytosis of PC12 cells. *Eur. J. Neurosci.* *21*, 2419–2432.
- Shah, N., Colbert, K.N., Enos, M.D., Herschlag, D., and Weis, W.I. (2014). Three SNAP and 10 ATP Molecules Are Used in SNARE Complex Disassembly by N-ethylmaleimide-

Bibliography

sensitive Factor (NSF) *.

Shen, J., Tareste, D.C., Paumet, F., Rothman, J.E., and Melia, T.J. (2007). Selective Activation of Cognate SNAREpins by Sec1/Munc18 Proteins. *Cell* *128*, 183–195.

Sieber, J.J., Willig, K.I., Kutzner, C., Gerding-Reimers, C., Harke, B., Donnert, G., Rammner, B., Eggeling, C., Hell, S.W., Grubmüller, H., et al. (2007). Anatomy and Dynamics of a Supramolecular Membrane Protein Cluster. *Science* (80-.). *317*, 1072–1076.

Sitarska, E., Xu, J., Park, S., Liu, X., Quade, B., Stepien, K., Sugita, K., Brautigam, C.A., Sugita, S., and Rizo, J. (2017). Autoinhibition of munc18-1 modulates synaptobrevin binding and helps to enable munc13-dependent regulation of membrane fusion. *Elife* *6*.

Snead, D., and Eliezer, D. (2019). Intrinsically disordered proteins in synaptic vesicle trafficking and release. *J. Biol. Chem.* *294*, 3325–3342.

Sørensen, J.B., Wiederhold, K., Müller, E.M., Milosevic, I., Nagy, G., De Groot, B.L., Grubmüller, H., and Fasshauer, D. (2006). Sequential N- To C-terminal SNARE complex assembly drives priming and fusion of secretory vesicles. *EMBO J.* *25*, 955–966.

Soreq, H., and Seidman, S. (2001). Acetylcholinesterase — new roles for an old actor. *Nat. Rev. Neurosci.* 2001 *24* 2, 294–302.

Sprong, H., Sluijs, P. Van Der, and Meer, G. Van (2001). Review: How Proteins Move Lipids. *Nat. Mol. Cell Biol.* *2*, 504–513.

Stein, A., Weber, G., Wahl, M.C., and Jahn, R. (2009). Helical extension of the neuronal SNARE complex into the membrane. *Nature* *460*, 525–528.

Südhof, T.C. (2012). The presynaptic active zone. *Neuron* *75*, 11–25.

Sutton, R.B., Fasshauer, D., Jahn, R., and Brunger, A.T. (1998). Crystal structure of a SNARE complex involved in synaptic exocytosis at 2.4 Å resolution. *Nat.* 1998 *395*6700 *395*, 347–353.

Takamori, S., Holt, M., Stenius, K., Lemke, E.A., Grønborg, M., Riedel, D., Urlaub, H., Schenck, S., Brügger, B., Ringler, P., et al. (2006). Molecular Anatomy of a Trafficking Organelle. *Cell* *127*, 831–846.

Trimbuch, T., and Rosenmund, C. (2016). Should I stop or should I go? The role of complexin in neurotransmitter release. *Nat. Rev. Neurosci.* *17*, 118–125.

Vardar, G., Chang, S., Arancillo, M., Wu, Y.-J., Trimbuch, T., and Rosenmund, C. (2016). Distinct Functions of Syntaxin-1 in Neuronal Maintenance, Synaptic Vesicle Docking, and Fusion in Mouse Neurons. *J. Neurosci.* *36*, 7911–7924.

Veit, M., Söllner, T.H., and Rothman, J.E. (1996). Multiple palmitoylation of synaptotagmin and the t-SNARE SNAP-25. *FEBS Lett.* *385*, 119–123.

Verhage, M., and Sørensen, J.B. (2008). Vesicle Docking in Regulated Exocytosis. *Traffic* *9*, 1414–1424.

Verhage, M., Maia, A.S., Plomp, J.J., Brussaard, A.B., Heeroma, J.H., Vermeer, H., Toonen, R.F., Hammer, R.E., den, T.K. van, Berg, et al. (2000). Synaptic Assembly of the

Bibliography

- Brain in the Absence of Neurotransmitter Secretion. *Science* (80-.). *287*, 864–869.
- Walch-Solimena, C., Blasi, J., Edelman, L., Chapman, E.R., von Mollard, G.F., and Jahn, R. (1995). The t-SNAREs syntaxin 1 and SNAP-25 are present on organelles that participate in synaptic vesicle recycling. *J. Cell Biol.* *128*, 637–645.
- Washbourne, P., Cansino, V., Mathews, J.R., Graham, M., Burgoyne, R.D., and Wilson, M.C. (2001). Cysteine residues of SNAP-25 are required for SNARE disassembly and exocytosis, but not for membrane targeting. *Biochem. J* *357*, 625–634.
- Watanabe, S., and Boucrot, E. (2017). Fast and ultrafast endocytosis. *Curr. Opin. Cell Biol.* *47*, 64–71.
- Watanabe, S., Trimbuch, T., Camacho-Pérez, M., Rost, B.R., Brokowski, B., Söhl-Kielczynski, B., Felies, A., Davis, M.W., Rosenmund, C., and Jorgensen, E.M. (2014). Clathrin regenerates synaptic vesicles from endosomes. *Nat.* *2014 5157526 515*, 228–233.
- Weber, P., Batoulis, H., Rink, K.M., Dahlhoff, S., Pinkwart, K., Söllner, T.H., and Lang, T. (2017). Electrostatic anchoring precedes stable membrane attachment of SNAP25/SNAP23 to the plasma membrane. *Elife* *6*.
- Weber, T., Zemelman, B. V., McNew, J.A., Westermann, B., Gmachl, M., Parlati, F., Söllner, T.H., and Rothman, J.E. (1998). SNAREpins: Minimal machinery for membrane fusion. *Cell* *92*, 759–772.
- Weber, T., Parlati, F., McNew, J.A., Johnston, R.J., Westermann, B., Söllner, T.H., and Rothman, J.E. (2000). Snarepins Are Functionally Resistant to Disruption by Nsf and α SNAP. *J. Cell Biol.* *149*, 1063–1072.
- Weninger, K., Bowen, M.E., Chu, S., and Brunger, A.T. (2003). Single-molecule studies of SNARE complex assembly reveal parallel and antiparallel configurations. *Proc. Natl. Acad. Sci.* *100*, 14800–14805.
- Wiederhold, K., and Fasshauer, D. (2009). Is assembly of the SNARE complex enough to fuel membrane fusion? *J. Biol. Chem.* *284*, 13143–13152.
- Williams, D., Vicôgne, J., Zaitseva, I., McLaughlin, S., and Pessin, J.E. (2009). Evidence that Electrostatic Interactions between Vesicle-associated Membrane Protein 2 and Acidic Phospholipids May Modulate the Fusion of Transport Vesicles with the Plasma Membrane. <https://doi.org/10.1091/Mbc.E09-04-0284> *20*, 4910–4919.
- Witkowska, A., Spindler, S., Mahmoodabadi, R.G., Sandoghdar, V., and Jahn, R. (2020). Differential Diffusional Properties in Loose and Tight Docking Prior to Membrane Fusion. *Biophys. J.* *119*, 2431–2439.
- Witkowska, A., Heinz, L.P., Grubmüller, H., and Jahn, R. (2021). Tight docking of membranes before fusion represents a metastable state with unique properties. *Nat. Commun.* *2021 121 12*, 1–7.
- Xiao, W., Poirier, M.A., Bennett, M.K., and Shin, Y.-K. (2001). The neuronal t-SNARE complex is a parallel four-helix bundle. *Nat. Struct. Biol.* *2001 84 8*, 308–311.
- Xu, M.Q., and Evans, T.C. (2001). Intein-mediated ligation and cyclization of expressed proteins. *Methods* *24*, 257–277.

Bibliography

- Xu, Y., Su, L., and Rizo, J. (2010). Binding of Munc18-1 to Synaptobrevin and to the SNARE Four-Helix Bundle. *Biochemistry* **49**, 1568–1576.
- Xue, M., Craig, T.K., Xu, J., Chao, H.-T., Rizo, J., and Rosenmund, C. (2010). Binding of the complexin N terminus to the SNARE complex potentiates synaptic-vesicle fusogenicity. *Nat. Struct. Mol. Biol.* **2010** *175* **17**, 568–575.
- Yang, L., and Huang, H.W. (2002). Observation of a Membrane Fusion Intermediate Structure. *Science* (80-.). **297**, 1877–1879.
- Yang, B., Gonzalez, L., Prekeris, R., Steegmaier, M., Advani, R.J., and Scheller, R.H. (1999). SNARE interactions are not selective. Implications for membrane fusion specificity. *J. Biol. Chem.* **274**, 5649–5653.
- Yang, X., Wang, S., Sheng, Y., Zhang, M., Zou, W., Wu, L., Kang, L., Rizo, J., Zhang, R., Xu, T., et al. (2015). Syntaxin opening by the MUN domain underlies the function of Munc13 in synaptic-vesicle priming. *Nat. Struct. Mol. Biol.* **2015** *227* **22**, 547–554.
- Yavuz, H. (2014). In vitro investigation of trans SNARE complexes arrested between artificial membranes. Georg-August-Universität Göttingen.
- Yavuz, H., Kattan, I., Hernandez, J.M., Hofnagel, O., Witkowska, A., Raunser, S., Walla, P.J., and Jahn, R. (2018). Arrest of trans-SNARE zippering uncovers loosely and tightly docked intermediates in membrane fusion. *J. Biol. Chem.* **293**, 8645–8655.
- Yoon, T.-Y., Lu, X., Diao, J., Lee, S.-M., Ha, T., and Shin, Y.-K. (2008). Complexin and Ca²⁺ stimulate SNARE-mediated membrane fusion. *Nat. Struct. Mol. Biol.* **2008** *157* **15**, 707–713.
- Yu, H., Crisman, L., Stowell, M.H.B., and Shen, J. (2019). Functional reconstitution of intracellular vesicle fusion using purified SNAREs and Sec1/Munc18 (SM) proteins. In *SNAREs*, (Springer), pp. 237–249.
- Zhang, Y., and Hughson, F.M. (2021). Chaperoning SNARE Folding and Assembly. *Annu. Rev. Biochem.* **90**, 581–603.
- Zhang, X., Rebane, A.A., Ma, L., Li, F., Jiao, J., Qu, H., Pincet, F., Rothman, J.E., and Zhang, Y. (2016). Stability, folding dynamics, and long-range conformational transition of the synaptic t-SNARE complex. *Proc. Natl. Acad. Sci.* **113**, E8031–E8040.
- Zhou, Q., Zhou, P., Wang, A.L., Wu, D., Zhao, M., Südhof, T.C., and Brunger, A.T. (2017). The primed SNARE-complexin-synaptotagmin complex for neuronal exocytosis. *Nature* **548**, 420–425.

Curriculum vitae**Sonja Pribićević**

M.Sc. in Neurosciences
 Am Faßberg, 11
 37077 Göttingen
 e-mail: sonja.pribicevic@mpibpc.mpg.de

Personal Details

Gender: Female
 Date of Birth: 21. March 1991
 Place of Birth: Belgrade, Serbia
 Nationality: Serbian

Education

June, 2017-	Ph.D. in Neuroscience <i>Georg-August University, Göttingen, Germany</i>
October, 2015-March, 2017	M.Sc. in Neuroscience <i>Georg-August University, Göttingen, Germany</i> Average grade: 1.6 (good) ECTS: 120
January, 2014-May, 2014	B.Sc. – semester <i>Paris Descartes University, Paris, France</i> Average grade: 14,5 (good) ECTS: 30
October, 2010-July, 2015	B.Sc. in Molecular Biology <i>University of Belgrade, Belgrade, Serbia</i> Average grade: 9.12 (excellent) ECTS: 240
September, 2006-June, 2010	High school diploma <i>Ninth Belgrade High School “Mihailo Petrović-Alas”, Belgrade, Serbia</i> Average grade: 4.55 (excellent) Graduation exam grade: 5.00 (excellent)
September, 2006-June, 2010	Musical high school diploma <i>Musical High School “Kosta Manojlović”, Belgrade, Serbia</i>